Development of hemodynamic targeted theranostic nanoparticles for the prevention of atherosclerosis

By

Lucas Hudson Hofmeister

Dissertation

Submitted to the Faculty of the

Graduate School of Vanderbilt University

in partial fulfillment of the requirements

for the degree of

DOCTOR OF PHILOSOPHY

In

Biomedical Engineering

May, 2015

Nashville, Tennessee

Approved:

Prof. Hak-Joon Sung

Prof. David G. Harrison

Prof. Todd D. Giorgio

Prof. Craig L. Duvall

Prof. Kasey C. Vickers

In loving memory of my best friend Cory “Eddie” Ebbert

May 31, 1988 – March 8, 2015

ACKNOWLEDGEMENTS

First and foremost, I would like to thank my advisor Dr. Hak-Joon Sung. Dr. Sung, who gave me with the opportunity to pursue my Ph.D. For his acceptance and support I will be forever grateful. Without Dr. Sung's guidance, insight and friendship this work would not be possible. I would also like to thank Dr. David Harrison for his mentorship, insight, patience and guidance that made this project possible. The members of my thesis committee, Dr. Criag Duvall, Dr. Todd Giorgio, and Dr. Kasey Vickers deserve special acknowledgment for their contribution to this work. They were always willing to lend me their time and immense knowledge and always kept me going in the right direction.

I would also like to give a special thanks to Dr. John Wikswo. I worked with Dr. Wikswo during high school, and without his inspiration and support I would not be where I am today. I also owe a special thanks Dr. Christina Marasco, Dr. Kevin Seale for supporting my ambitions in teaching and research by allowing me to participate in the SyBBURE Searle program. Their friendship and moral support have been invaluable in my pursuit of this degree. I would also like to thank the undergraduate students who patiently allowed me to mentor them and who were always willing to help with my experiments.

I would like to thank my fellow lab members from the Sung, Duvall, Giorgio and Harrison labs: Dr. Mukesh Gupta, Dr. Xintong Wang, Dr. Jun Bok Lee, Daniel Balikov, Dr. Angela Zachman, Dr. Shann Yu, Dr. Spencer Crowder, Sue Lee, Tim Boire, Dr. Chris Nelson, Kelsey Beavers, Brian Evans, John Martin, Kameron Kilchrist, Thomas Werfel, Dr. Jing Wu, Dr. Hana Itani, Dr. Mohamed Saleh, Dr. Liang Xiao, Dr. Dan Trott, Dr. Danielle Michell, Dr. Alfiya Bikineyeva, Dr. William McMaster, Roxanna Lopreda, Alli Norlander,

Kim Montaniel, Dr. Wei Chen, and Dr. Annet Kirabo for their valuable insight, help with experiments, day to day lab work, and support through the past five years.

I would like to acknowledge the support and help I got from my friends and family. Thank you to my parents, Mandy and William Hofmeister, who support me in all of my efforts, and gave me every opportunity to succeed. They encouraged me to pursue research from a young age, and always kept me grounded with a shared passion for sailing, travel, and the outdoors. Thank you to my sister, Rebecca, and to my brothers Richard and Matthew for their love and support. Thank you to my friends who provided support, new experiences, and welcome distractions from my research and studies. Finally, thank you to my girlfriend Francesca Solinas. Francesca's encouragement, support, patience and boundless love kept me grounded and focused through the last two years of my studies. I will be forever indebted to the village of people who contributed to my studies.

TABLE OF CONTENTS

Page

LIST OF TABLES

LIST OF FIGURES

Chapter I

Chapter II

LIST OF ABBREVIATIONS

Nitric oxide (NO)

Prostacyclin (PGI2)

Endothelin (ET)

Cardiovascular disease (CVD)

nicotinamide adenine dinucleotide phosphate (NADPH)

NADPH oxidase (NOX)

Reactive oxygen species (ROS)

Nitric oxide synthase (NOS)

Flavin mononucleotide (FMN)

Flavin adenine dinucleotide (FAD)

low-density lipoprotein (LDL)

(6R-),6,7,8-tetrahydrobiopterin (BH_4)

Michaelis constant (K_m)

dihydrobiopterin (BH_2)

Guanine nucleotide binding proteins (G proteins)

Adenosine triphosphate (ATP)

Extracellular matrix (ECM)

Platelet endothelial cell adhesion molecule-1 (PECAM1)

Vascular endothelial (VE)-cadherin,

Vascular endothelial growth factor receptor 2 (VEGFR2).

Phosphoinositide 3-kinase (PI3K)

Endothelial nitric oxide synthase (eNOS)

Nuclear factor kappa light chain enhancer of activated B cells (NF□B)

Superoxide dismutase (SOD)

Guanosine-5’-triphosphate cyclohydrolase 1 (GTPCH-1)

Ultrasmall superparamagnetic iron oxides (USPIOs)

Enhanced permeability and retention effect (EPR)

Poly(ethylene glycol) (PEG)

Apolipoprotein E knockout (ApoE$^{-/-}$)

Human aortic endothelial cells (hAECs)

Tris buffered saline (TBS)

Tris buffered saline containing 0.1% tween 20 (TBST)

Escherichia coli (*E-coli)*

β-galactosidase (β-gal)

Lysogeny broth (LB)

Left common carotid artery (LCA)

Right common carotid artery (RCA)

External carotid artery (ECA)

Internal carotid artery (ICA)

Occipital artery (OA)

Fluorenylmethyloxycarbonyl chloride (Fmoc)

N-methylpyrrolidone (NMP)

Electrospray ionization mass spectrometry (ESI-MS)

High performance liquid chromatography (HPLC)

SLSSYNGSALAS (DistL12)

GSPREYTSYMPH (PREY)

5(6)-Carboxyfluorescein (FAM)

N-Hydroxysuccinimide ester (NHS)

Fluorescence minus one (FMO)

Phosphate buffered saline (PBS)

Fluorescence assisted cell sorting (FACS)

Fluorescein isothiocyanate (FITC)

Epithelial growth factor-like module-containing mucin-like horomone receptor-like 1 (F4/80)

Protein tyrosine phosphatase receptor type C (CD45)

Platelet endothelial cell adhesion molecule (CD31)

Stem cell antigen-1, Ly-6A/E (Sca1)

7-aminoactinomycin-D (7-AAD)

5-(Biotinamido)pentylamine (pentylamine-biotin)

1-Ethyl-3-(3-dimethylaminopropyl)carbodiimide (EDC)

N-hydroxysulfosuccinimide (sulfoNHS)

Tandem mass spectra (MS/MS)

Sodium dodecyl sulfate polyacrylamide gel electrophoresis (SDS-PAGE),

polyvinylidene fluoride (PVDF)

Optimum cutting temperature medium (OCT)

Bovine serum albumin (BSA)

4’,6-diamidino-2-phenylindole (DAPI)

THRPMSSYEPGYGSGS-COOH (scrambled PREY)

Poly(propylene sulfide) (PPS)

Poly(ethylene glycol)-b-poly(propylene sulfide) (PEG-PPS)

Magnetic resonance imaging (MRI)

1,8-Diazabicyclo[5.4.0]undec-7-ene (DBU)

PPS-phthalamide (PPS-Phth)

Nuclear magnetic resonance (NMR)

Gel permeation chromatography (GPC)

Polydispersity (PDI)

Dimethylformamide (DMF)

dimethylsulfoxide (DMSO)

Dynamic light scattering (DLS)

Transmission electron microscopy (TEM)

Dicyclohexylcarbodiimide (DCC)

N-Methyl-2-pyrrolidone (NMP)

1,2-Dipalmitoyl-sn-Glycero-3-Phosphoethanolamine-N-(hexanoylamine) (DPHE)

1,2-dipalmitoyl-sn-glycero-3-phosphocholine (DPPC)

1,1'-Dioctadecyl-3,3,3',3'-Tetramethylindodicarbocyanine Perchlorate (DiD)

1,1'-Dioctadecyl-3,3,3',3'-Tetramethylindotricarbocyanine Iodide (DiR)

Hanks buffered saline (HBS)

Fast Low Angle Shot (FLASH)

Dihydroethidium (DHE)

High density lipoprotein (HDL)

CHAPTER I

INTRODUCTION

BACKGROUND

Cardiovascular anatomy

Mammals have a closed pressurized vascular system that is responsible for transporting nutrients to and removing waste products from every cell in the body. The vascular system has three major components: the heart, the arterial, and the venous systems. The arterial system begins proximal to the heart with the largest vessel in the body, the aorta. Distal to the aorta, each branch of the arterial system reduces diameter in a pattern described by Murray's law [1, 2]. Murray's law states that at any point in the circulation, blood flows through arteries whose radii cubed are summed to a constant value. Large arteries are highly elastic with three distinct layers: the intima, media, and adventitia. The intima, the innermost layer, consists of the vascular endothelium, a single layer of cells on top of a thin layer of basement membrane. The media is the next concentric layer and is comprised of alternating layers of smooth muscle and elastic lamina. The adventitia, the outermost layer, consists of connective tissue and is rich in fat. The adventitial also contains the *vasa vasorum*, which provides nutrients and oxygen to outer layers of large vessels, is innervated, and is home to resident immune cells. As arteries become smaller in more distal branches, they generally have fewer layers of elastic lamina, and become more contractile and less elastic. This is reflected by the requirements of Laplace's law, which states that vessel wall thickness is

proportional to vessel radius at a constant pressure. Therefore, capillaries, the smallest arteries, may have only one or two cell layers to facilitate nutrient transport. The venous system is responsible for transporting deoxygenated blood back to the heart for re-oxygenation in the pulmonary circulation. Postcapillary venules are the venous system corollary to capillaries, are largely responsible for immune infiltration into tissue and connect the venous system to the arterial system. The venous system operates at lower pressure and has thinner walls and higher compliance to match these requirements.

The vascular endothelium

Originally, endothelial cells were thought to be an inert barrier on the inside of blood vessels and lymphatics [3]. However, endothelial cells are diverse in phenotype and function and are master regulators of vascular homeostasis [4]. Endothelial cells are responsible for regulating vascular permeability to allow transport of nutrients into tissue and transport of waste away from tissue. Vascular permeability can be modulated by factors such as local inflammation and circulating factors such as lipoproteins. Endothelial cells are also responsible for regulating blood pressure and vascular tone in response to changes in cardiac output, for example as a response to exercise or stress. Endothelial cells release vasodilators such as nitric oxide (NO) and prostacyclin (PGI2) and vasoconstrictors such as endothelin (ET) and platelet activating factor [5].

Endothelial cells also regulate the interaction of blood and blood cells with tissue. For example, endothelial cells are critical for hemostasis. Normally, endothelial cells are anticoagulant. However, in the case of injury or activation, endothelial cells become procoagulant by producing tissue factor, fibrinogen, and thrombomodulin regulating the coagulation of blood. In addition, endothelial cells are responsible for regulating

inflammation by recruiting leukocytes from the blood to fight infection in tissue. When injured, endothelial cells express selectins, cell adhesion molecules, and chemokines, which recruit immune cells into the vessel wall and promote proliferation of resident immune cells.

Cardiovascular disease

Cardiovascular disease (CVD) is the leading cause of death in the developed world. In 2015, 85.6 million American adults have at least one type of cardiovascular disease, and CVD is responsible for over 30% of deaths globally [6]. Hypertension is the most common form of CVD in adults, afflicting approximately 80 million adults in the US. While hypertension is the most common form of CVD, complications from atherosclerosis such as heart attack and stroke are responsible for the majority of CVD related deaths [6]. CVD is an enormous economic burden on the health care system, and costs are expected to rise as the incidence of diseases such as obesity and diabetes continues to increase. The risk factors that are currently recognized for CVD include family history and genetics, hyperlipidemia, hypertension, diabetes mellitus, metabolic syndrome, obesity, physical inactivity, nutrition, chronic kidney disease, and smoking.

Atherosclerosis is a chronic disease of the vessel wall and predominantly forms in medium and large sized arteries. Atherosclerosis can develop from early in life beginning with, “fatty streaks,” which are purely inflammatory lesions rich in macrophages and T lymphocytes and are common in infants and young children [7]. At all stages, atherosclerosis can be considered a chronic inflammatory disease [8]. Starting with a response-to-injury hypothesis, an initial insult disrupts the normal

homeostatic properties of the vascular endothelium. The so-called, “dysfunctional endothelium,” initiates a series of events after damage, which can result in chronic inflammation and gradual development of atherosclerosis. Some examples of injurious stimuli include elevated cholesterol, specifically elevated low-density lipoprotein, increased free radicals, diabetes, elevated homocysteine, and bacterial or viral infection. These damaging stimuli lead to increased adhesiveness of the endothelium to platelets and immune cells and increased vascular permeability. At the onset of inflammation immune cells infiltrate and release chemokines and growth factors, causing smooth muscle cell proliferation and migration, which thickens the artery wall. In intermediate atherosclerotic lesions, this proliferation process is accompanied by outward remodeling so that the lumen remains patent. If inflammation persists, more cells migrate from the blood and proliferate in lesions, promoting smooth muscle proliferation, fibrous tissue formation and lipid accumulation. In advanced lesions the vessel can no longer outwardly remodel, resulting in narrowing or occlusion of the artery.

Cardiovascular risk factors are associated with oxidative stress

Oxidative stress is a major cause of endothelial dysfunction in diseases such as atherosclerosis, hypertension and diabetes [9, 10]. Oxidative stress is the overproduction of oxidants or reactive oxygen species (ROS) from the redox reaction of molecular oxygen to water. Examples include the free radicals superoxide, hydroxyl, nitric oxide and nonradicals such as hydrogen peroxide, peroxynitrite, and hypochlorous acid. Overproduction of these forms of ROS, specifically superoxide, can lead to the formation of other ROS by radical chain reactions, formation of damaging products such as lipid peroxides and oxidized proteins, activate pathological signaling pathways, and

further drive production of ROS by enzyme activation and expression (positive feedback). In the vasculature there are several enzymatic sources of ROS including nicotinamide adenine dinucleotide phosphate (NADPH) oxidases, xanthine oxidase, cyclooxygenase, lipoxygenase, mitochondrial enzymes, P450 mono-oxygenase, and uncoupled nitric oxide synthase [11]. The three best studied enzymes responsible for oxidative stress in vascular disease are NADPH oxidases, xanthine oxidase, and uncoupled nitric oxide synthase.

NADPH oxidases were originally identified in phagocytic cells such as neutrophils, however they are expressed in all tissues, and are important for many biological responses. NADPH oxidase has been identified as a major source of superoxide in vasculature. Cardiovascular risk factors cause increased expression and activity of NADPH oxidases. This has been validated in animal models of hypertension, diabetes, and atherosclerosis. Risk factors such as hypercholesterolemia are associated with increased activation of NADPH oxidases; for example, catalytic subunits Nox2 and Nox4 are overexpressed in atherosclerotic arteries. Xanthine oxidase is another potential source of superoxide and oxidant stress in cardiovascular disease, however there are conflicting reports of the impact of xanthine oxidase inhibitors such as purinol on development of cardiovascular disease [12]. These studies also show little evidence that other enzyme systems such as cyclooxegnase, or cytochrome P450 are pathologically important sources of superoxide.

Nitric oxide synthase (NOS)

NO is produced by a class of enzymes called nitric oxide synthases (NOS). There are three isoforms of NOS that share a common reaction mechanism to generate NO [13].

NOS are modular enzymes that require dimerization to produce NO through a tightly regulated transfer of electrons. Each monomer of NOS has a C-terminal reductase domain and an N-terminal oxygenase domain. The C-terminal reductase domain of NOS binds to NADPH, flavin mononucleotide (FMN) and Flavin adenine dinucleotide (FAD) [13]. NOS monomers are linked together at the N-terminal oxygenase domains through a structurally important zinc-thiolate cluster [14]. The oxygenase domain also carries a prosthetic heme group and binds to the enzyme substrates, L-arginine, molecular oxygen (O_2), and (6R-),6,7,8-tetrahydrobiopterin (BH_4) [15-18]. In the functioning enzyme, an increase of intracellular calcium leads to calmodulin binding to NOS, which catalyzes electron transfer from NADPH and the flavins in the C-terminus reductase domain to the heme center where the electrons reduce O_2 [19]. To produce NO, the enzyme cycles twice. The first cycle hydroxylates L-arginine to N^{ω}-hydroxy-L-arginine. In the second step NOS oxidizes the N^{ω}-hydroxy-L-arginine to L-citrulline and NO [20].

Role of nitric oxide (NO) in vascular disease

NO was first identified as endothelium-derived relaxing factor in 1987 by Palmer et al. [21, 22]. In this role, NO causes blood vessel dilation by stimulating soluble guanylyl cylcase and increasing cyclic guanosine monophosphate in smooth muscle cells thereby reducing vasomotor tone [23, 24]. Aside from directly causing smooth muscle relaxation, NO has broad regulatory and signaling functions including suppressing inflammation, inhibiting platelet aggregation, reducing leukocyte adhesion to endothelium, and reducing smooth muscle cell proliferation [25, 26].

Almost all risk factors for cardiovascular disease have been shown to reduce vascular NO. Reduced bioavailability of NO could be due to decreased expression of NOS, decreased availability of NOS substrate L-arginine due to overexpression of arginases or oxidation, decreased NOS cofactors, increased NOS inhibitor asymmetric dimethyl-L-arginine, and increased superoxide [27, 28]. Superoxide reacts with NO to form the strong oxidant peroxynitrite ($OONO^-$) and eliminates the beneficial actions of NO [29, 30]. This reaction is extremely avid, occurring a rate ten times faster than the enzyme superoxide dismutase converts superoxide to hydrogen peroxide (K_m = 6.7 x 10^9, or nearly diffusion limited) [31, 32]. This means that NO production and availability is modulated by superoxide production, therefore the balance of the two is critical for vascular homeostasis. Reduced vascular NO is associated with dysfunction of homeostatic signaling pathways, leading to vascular disease. Notably, this effect cannot be rescued by increasing enzymatic production of NO, or supplementation with nitrovasodilators, which raise systemic NO [33, 34]. In the United States, there are two classes of nitrovasodilators used, organic nitrates such as nitroglycerin, and nitroprusside [35]. A primary concern of use of these drugs is the development of nitrate tolerance, which leaves patients vulnerable to acute ischemia [36]. Also, Long term treatment with nitrovasodilators is associated with endothelial dysfunction and overproduction of superoxide by the endothelium of tolerant vessels, leading to the breakdown of NO and other deleterious effects [37-39]. Consequently, systemic administration of nitrovasodilators has led to worsened prognosis for patients with coronary artery atherosclerosis [37]. The harmful result of NO supplementation is likely due to the avid reaction of NO with superoxide forming $ONOO^-$ [29]. Therefore, it is of greater facility to focus therapies on reducing superoxide rather than donating excess

nitric oxide. Another proposed mechanism for nitric oxide's contribution to oxidative stress in cardiovascular disease is dysfunction of the enzyme that produces NO [40].

Production of ROS by NOS

Studies with hypertensive mice demonstrated that treatment with NOS inhibitor NG-nitro-L-arginine reduced oxidative stress in vessels, demonstrating a significant contribution of the NOS enzymes to oxidative stress in vascular disease [41]. In the absence of enzyme substrate L-arginine or the cofactor BH_4, the flow of electrons in NOS is disrupted and the oxygenase domain of NOS produces superoxide instead of NO [42-44]. This is called NOS uncoupling. NOS uncoupling is a primary candidate for vascular ROS production and therefore oxidative stress in vascular disease [28, 45, 46]. NOS uncoupling has been observed in cells treated with low-density lipoprotein (LDL), cells treated with peroxynitrite and vessels from animals experimentally induced hypertension and diabetes [27, 47, 48]. NOS uncoupling has also been observed in patients with diabetes, hypertension, hypercholesterolemia, and in chronic smokers [49-52]. There are several mechanisms by which NOS can become uncoupled. One explanation could be deficiency of the enzyme substrate L-arginine. However, L-arginine levels are normally several times higher than the Michaelis constant of the NOS enzyme, cells can recycle L-citrulline to L-arginine, and obtain L-arginine from breakdown of proteins in the urea cycle, and supplementation with L-arginine does not decrease NOS uncoupling [53]. In association with low levels of L-arginine, the presence of dimethyl-L-arginine could also inhibit the NOS enzyme and reduce availability of NO [54, 55]. However, elevated dimethyl-L-arginine levels are more likely to be a result of elevated ROS rather than a cause. Another explanation for NOS uncoupling and production of ROS in disease is that NOS monomers are unable to form

dimers. However, the efficiency of electron transfer by NADPH is much higher in NOS dimers, therefore dissociated NOS monomers are unlikely to be a significant source of ROS [56].

A major cause for NOS uncoupling is reduced concentration of the cofactor BH_4 [28, 57, 58]. Studies have demonstrated that reduced intracellular BH_4 correlates directly with NOS dysfunction. BH_4 level depends on the balance of production and oxidation of pterins [59]. Because BH_4 is one of the most potent naturally occurring reducing agents, it is readily oxidized to inactive forms such as dihydrobiopterin (BH_2). Therefore, oxidative stress may result in the excessive oxidation of BH_4 and reduction of the availability of the cofactor. Reduced BH_4 has been reported in animal models of cardiovascular disease, and in human patients with cardiovascular disease [60, 61]. In addition, supplementation of BH_4 has been shown to reduce production of superoxide by NOS, suggesting that BH_4 plays the central role in NOS uncoupling [48-50, 52, 53, 62].

Production of radicals by xanthane oxidase, NADPH oxidase, mitochondrial electron transport, and uncoupled NOS in response to pathological stimuli can be “kindling” radicals. These radicals oxidize or modify other enzymes, leading to an increase in ROS formation by these other enzymes or “bonfire” radicals. Many examples exist in the literature of this interaction [63, 64].

Hemodynamics

The vascular system is constantly exposed to hemodynamic mechanical stimulation. During each cardiac cycle, blood pressure fluctuates and causes pulsatile fluid flow and

cyclic expansion of blood vessels. The propagation of this pressure wave exerts both hoop stress and fluid shear stress on blood vessels.

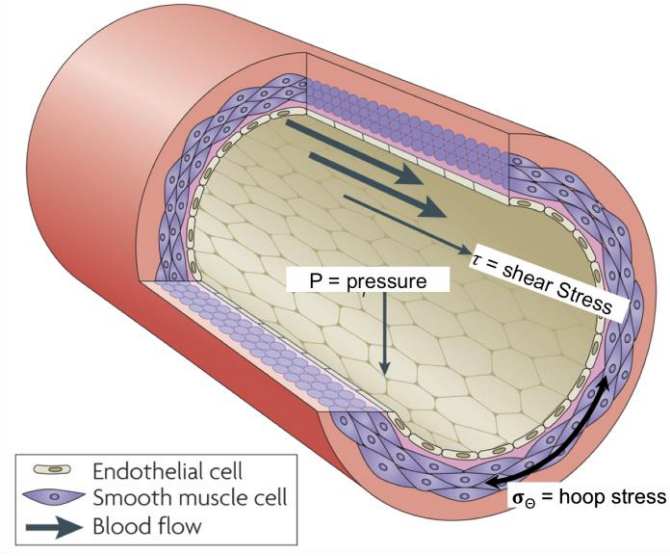

Figure 1. Hemodynamic forces acting on the vasculature. The two major stresses are hoop stress from cyclic changes in blood pressure, and shear stress, the tangential frictional force of blood flowing across the vascular wall. Figure adapted from Hahn et. al. [65].

Fluid shear stress a force tangential to the inner surface of the blood vessel caused by viscous drag from fluid flow. Fluid shear stress at the endothelium is loosely approximated by modeling blood as a Newtonian fluid flowing through a straight rigid pipe of constant diameter using Poiseuille's law derived from the Navier-Stokes equations. This model describes a parabolic flow profile, where the maximum velocity of fluid flow is in the center of the channel, and the velocity at the wall is zero (no slip condition). The gradient of fluid velocity in the radial dimension is the fluid shear stress, and is approximated by the Hagen-Poiseuille equation (Figure 2). Poiseuille's law is dependent on laminar flow, and the Reynolds number of the system can be used to

approximate the presence of laminar flow. The Reynolds number is defined as the ratio between the inertial forces and viscous forces in the system and is dependent on the mean velocity of fluid flow, the kinematic viscosity, and the length scale of the system (the diameter for a pipe). In Poiseuille flow in a straight pipe, transition from laminar to turbulent flow occurs at Reynolds numbers above 2040 [66].

$$\boldsymbol{Re = \frac{inertial\ forces}{viscous\ forces} = \frac{\rho v L}{\eta}},$$

$$\boldsymbol{where: \rho = density, v = mean\ velocity, L = characteristic\ length, \eta = dynamic\ viscosity}$$

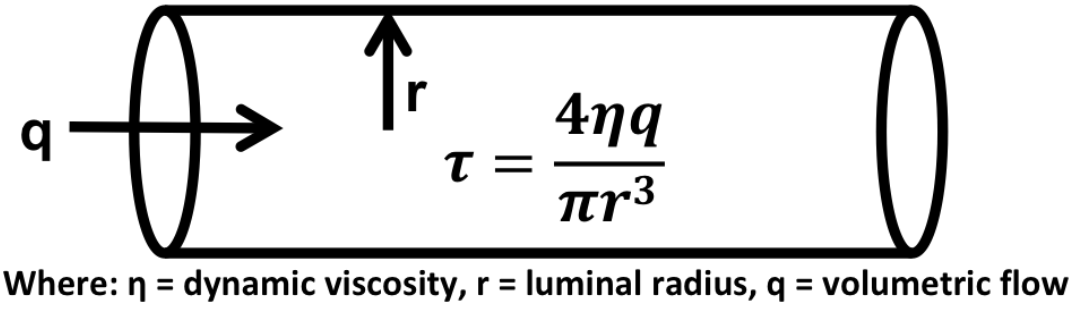

Where: η = dynamic viscosity, r = luminal radius, q = volumetric flow

Figure 2. Reynolds number and Fluid shear stress calculated assuming Hagen-Poiseuille flow in a rigid pipe.

There are many factors that lead to disruption of laminar flow *in vivo*. Blood is a heterogeneous, multicomponent, thixotropic non-Newtonian fluid. Shear thinning behavior means that blood viscosity is least during peak systole, and greatest during peak diastole. In addition, blood vessels are not rigid but distensible; flow rate varies with cardiac cycle and arterial geometry changes rapidly.

Arterial geometry affects the blood flow pattern in the cardiovascular system. In straight, un-branched vascular segments blood flow is approximately unidirectional and laminar and time average fluid shear stress is high. At branch points, sites of curvature and distal to stenoses blood flow becomes disturbed. Such regions can display flow separation, vortical shedding and low and oscillatory fluid shear stresses [67]. These phenomena are indicative of transition from laminar flow to turbulent flow and breakdown of the Poiseuille model. Transition away from laminar flow is induced by changes in geometry. This is observed with Newtonian fluids in models of the human carotid bulb where Reynolds number is as low as 400. An example of this phenomenon at Reynolds number 800 is depicted below.

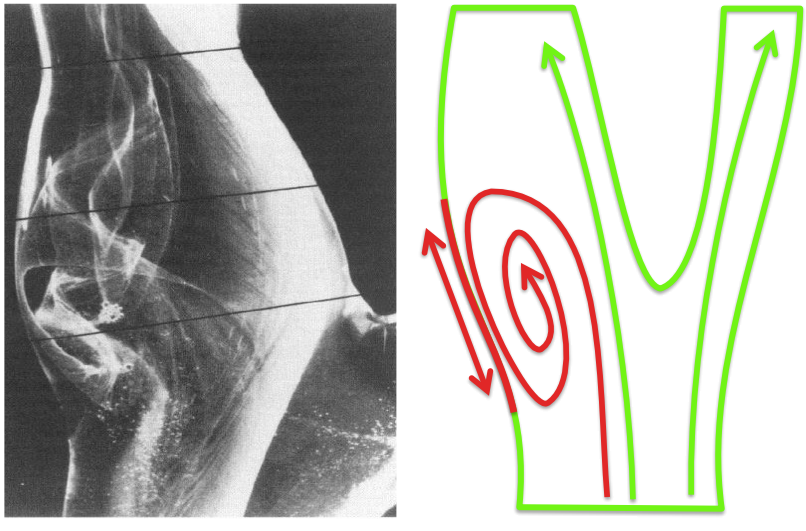

Figure 3. Glass model of blood flow in the human carotid artery bulb. This image was captured by Zarins et al. by modeling a human carotid artery bulb in glass, and flowing hydrogen bubbles in a viscous solution to visualize flow patterns [68]. This demonstrates the formation of disturbed flow in response to arterial geometry.

In vitro *and* in vivo *models for studying shear stress*

To study the effects of variations in blood flow, model systems are required that recapitulate the flow patterns observed in these naturally occurring locations of altered flow. *In vitro* models are useful because they allow a reductionist approach that eliminates variables such as the non-Newtonian nature of blood and unpredictable changes in geometry. There are several useful *in vitro* models for the study of the effects of altered shear stress on cellular phenotype [69]. Cone-in-plate cell culture, pioneered by C. Forbes Dewey, has become a well-established method to subject living cells to fluid shear stress [70, 71]. The system works in much the same manner as a cone-in-plate viscometer, were cells can be cultured in a dish, and fluid flow induced by rotating a cone in the culture media above the cells. This system makes it possible to recapitulate either laminar unidirectional fluid shear stress or oscillatory fluid shear stress at physiologically relevant fluid shear stresses. However, due to the length scale of the device, and the use of culture media that is more similar to a Newtonian fluid, these devices are unlikely to achieve disturbed flows as observed *in vivo*. Another common approach for *in vitro* cell culture under fluid shear conditions is a parallel plate flow chamber. In this apparatus, cells are grown in a rectangular channel, and flow is provided either by hydrostatic pressure, or by pumps. These systems are also capable of achieving laminar unidirectional flow, as well as oscillatory flow, but are subject to the same limitations imposed by Reynolds number and transition to turbulent flow.

In vivo models are more likely to accurately capture dynamics of the complex variations in blood flow patterns. One option for studying variations in fluid shear stress is to simply observe locations that are known to develop disturbed flow such as the branches of the coronary arteries, where the iliac arteries branch from the distal aorta, and where

the aorta curves sharply proximal to the heart. There are also *in vivo* models available that can recapitulate variations in shear in a more controlled manner. A first example is the implantation of perivascular cuffs that can constrict arteries creating a sort of artificial stenosis [72, 73]. Rapid changes in geometry such as constrictions result in development of disturbed flow downstream of the restriction. This model is best suited for use in larger animals, and its limited utility in murine models prone to atherosclerosis prompted the more recent development of the murine partial carotid artery ligation model. In this model, three of the four ascending branches of the left carotid artery are surgically ligated. With each cardiac cycle, blood flows up the common carotid artery and encounters resistance from the ligations causing retrograde flow [74]. This leads to the rapid formation of advanced atherosclerotic lesions in mice prone to develop atherosclerosis [74]. Both of these models create flow patterns that are characteristic of disturbed flow observed pathophysiological sites.

Endothelial mecahnotransduction

The vascular endothelium is in direct contact with flowing blood and displays remarkable plasticity in response varying fluid shear stresses [75]. Endothelial response to fluid shear stress is likely an adaptive mechanism designed to maintain sufficient blood flow to body tissues. For example, fluid shear stress acutely regulates blood vessel diameter by maintaining endothelial signaling for smooth muscle cell relaxation by nitric oxide production, prostacyclin, and arachidonic acid [25, 26, 76]. These changes serve to normalize fluid shear stress in response to sudden increases in cardiac output, for example during exercise [77, 78]. Over time, increased flow can result in permanent vascular remodeling [79-81]. It is interesting to note that the cyclic hoop stress on endothelial cells from oscillating pressure is four orders of magnitude

larger than the fluid shear stress from blood flow, but shear stress is still believed to be the major determinant of endothelial response [82].

There are numerous proposed mechanisms for mecahnotransduction of fluid shear stress in endothelial cells. For example, endothelial cells may sense forces and transduce them to downstream chemical signals through the cytoskeleton, ion channels, integrins, receptor tyrosine kinases, primary cilia, the apical glycocalyx, heterodymeric guanine nucleotide binding proteins (G proteins), and caveolins. The cytoskeleton is responsible for maintaining the shape and morphology of endothelial cells, and plays important roles in cellular response to forces [83-86]. The cytoskeleton has several components: actin, microtubules, and intermediate filaments. In experiments studying mecahnotransduction, pharmacological or genetic inhibition of cytoskeletal components block endothelial responses to shear [87-89]. However, there is little evidence that suggests that the cytoskeleton is solely responsible for transduction of shear stress. Some putative mechanosensors reside on the cell surface and are in direct contact with flowing blood making them logical candidates for transduction of fluid shear signals. For example, fluid shear modulates the fluidity of cell membranes, which could implicate caveolins or other membrane components [90-94]. In addition, changes in membrane fluidity affect the activity of G proteins, which could be involved in flow sensing in either ligand dependent or independent roles [95-98]. Considering the profound effects of changes in intracellular potassium and calcium on downstream signals associated with shear sensing, mechanosensitive ion channels are also implicated as mechanotransducers [99-102]. In addition, these channels can control the release of adenosine triphosphate (ATP) and ATP synthesis [103-108]. Also present on the surface of endothelial cells is a dense glycocalyx [109-111]. This covering of

proteoglycans may protect the actual cell membrane surface from directly experiencing shear from flowing blood, and suggests that force may be transmitted through the glycocalyx [112-114]. Some studies have shown that digestion of proteoglycans blunts response to shear, however it is unclear if this is due to disruption of the apical glycocalyx or the basal lamina, which would affect integrin signaling through extracellular matrix (ECM) proteins [115, 116]. Endothelial cells also express primary cilia, and genetic deletion of primary cilia protein results in vascular defects in mice [117-119]. However, their role in fluid shear sensing *in vivo* is unclear, although they may be responsible for sensing low levels of fluid shear stress [120-122].

The major mechanosensing mechanism is likely receptors between cells, namely a three-protein complex of platelet endothelial cell adhesion molecule-1 (PECAM1), vascular endothelial (VE)-cadherin, and vascular endothelial growth factor receptor 2 (VEGFR2) [123]. Within this complex, increased tension on PECAM1 leads to the activation of a Src family kinase which acts on VEGFR2 to recruit and activate Phosphoinositide 3-kinase (PI3K) by a ligand independent receptor activation process. PI3K activation is the effector of downstream shear stress activation including NOS phosphorylation and increased integrin recruitment. VE-cadherin appears to mediate VEGFR2 association with PECAM1 [25]. While this integrin mediated signaling is responsible for downstream endothelial activation, the upstream activator of PECAM1 in response to shear stress is still unclear. The role of cyclic hoop stress in endothelial mecahnotransduction is also unclear, as it is impossible to decouple the two phenomenon *in vivo*.

Endothelial response to shear stress waveforms

In the setting of unidirectional laminar fluid shear stress, endothelial cells elongate and align in the direction of flow and develop an anti-inflammatory and anti-thrombotic phenotype [65]. These effects are associated with acute changes in endothelial cell signaling and marked changes in gene expression over the long term [75, 124]. As examples, in response to laminar shear endothelial cells increase NO and prostacyclin production, increase mRNA and protein expression of kruppel like factor 4 and endothelial nitric oxide synthase (eNOS), and exhibit decreases in inflammatory mediators such as nuclear factor kappa light chain enhancer of activated B cells (NF**κ**B) and adhesion molecules [10].

In striking contrast, endothelial cells exposed to disturbed flow do not align and elongate, and become pro-inflammatory and pro-thrombotic. Disturbed flow causes the same transient changes in endothelial cells, however, exposure to disturbed flow is associated with sustained activation of pro-inflammatory signals such as NFκB, JUN N-terminal kinase, p21-activated kinase, and increased expression of inflammatory mediators including vascular cell adhesion molecule-1, intracellular adhesion molecule-1 and chemokines such as the monocyte chemoattractant peptide-1 [65, 74, 125-127].

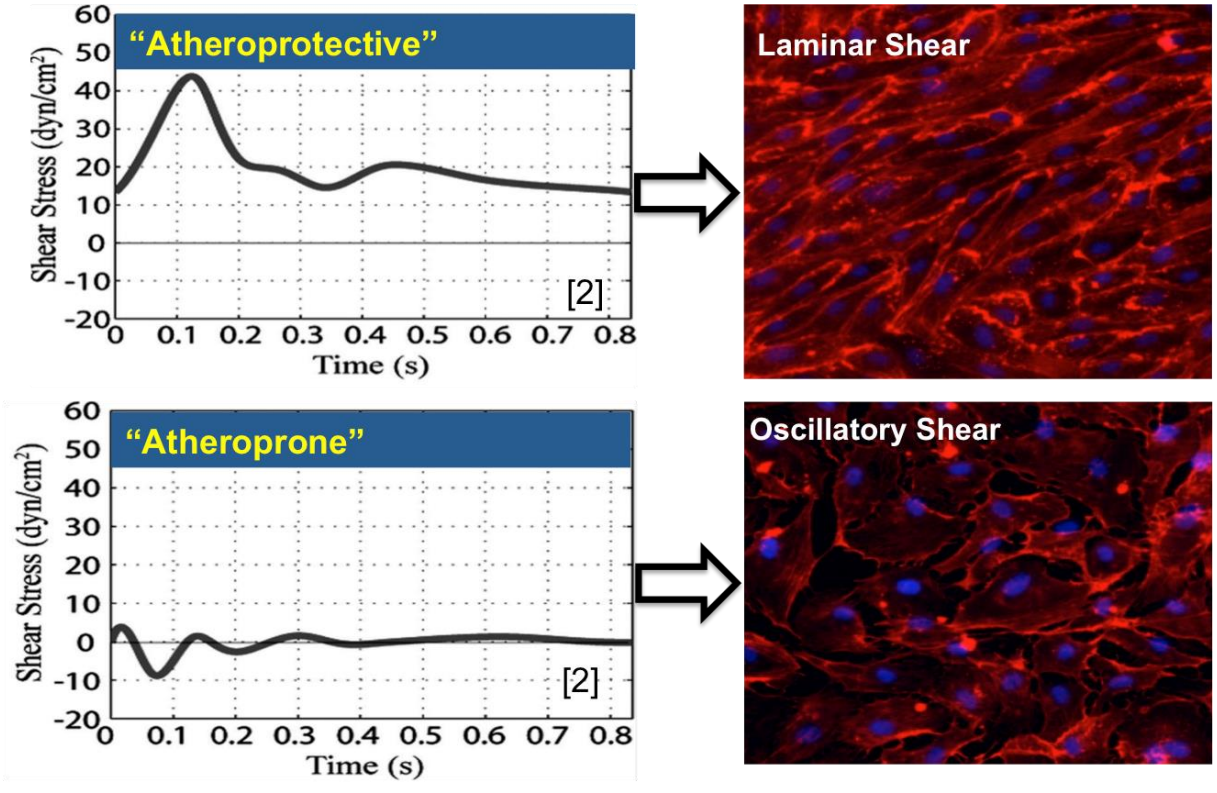

Figure 4. Shear stress waveforms measured by MRI in healthy human patients corresponding to atheroprotective and atheroprone flow adapted from Dai et al. [128]. Endothelial morphology changes when exposed to atheroprotective versus atheroprone fluid shear waveforms.

Focal Development of atherosclerosis

The changes in endothelial cell phenotype caused by disturbed flow predispose these regions to local lipid deposition, inflammation and the focal development of atherosclerosis. This is exemplified by the fact that endothelial function nearly directly correlates with risk factor profiles [48]. In a seminal paper, Ku et al. observed that atherosclerosis correlates with sites of disturbed flow *in vivo* [67]. Atherosclerotic lesions predominantly occur at sites known to have disturbed flow such as branch points, the proximal coronary arteries and the distal aorta [48, 125, 126].

Effect of shear stress profiles on vascular NO

The most abundant source of NO in vasculature is the endothelial NOS isoform (eNOS). When exposed to atheroprotective shear stress, *in vitro* there is a transient increase in intracellular calcium in endothelial cells, which causes calmodulin binding to eNOS and increases eNOS activity [129]. Simultaneously, phosphorylation by protein kinase B increases eNOS activity [130-133]. Over the course of several hours, shear stress causes an increase in eNOS protein, mRNA, and mRNA stability through the canonical MAP kinase pathway [10, 126]. eNOS transcription is increased by NFκB binding to the eNOS promoter [134]. After this acute effect, increased NO inhibits NFκB by nitrosylation of p50, decreasing activation of pro-inflammatory pathways, and returning eNOS transcription to the basal rate [135, 136]. In addition to increasing eNOS production and activity, atheroprotective flow also increases production of reactive oxygen species through NADPH oxidase, which is balanced by increased expression of enzymes that scavenge harmful ROS such as Cu/Zn superoxide dismutase (SOD), extracellular SOD, and glutathione peroxidase [137-142].

Tetrahydrobiopterin (BH_4) and atherosclerosis

It has been shown that a major source of reactive oxygen species in endothelial cells exposed to disturbed flow is uncoupled eNOS [28]. Oscillatory fluid shear stress on endothelial cells results in an uncoupling of the eNOS enzyme. The mechanism of oscillatory fluid shear stress induced eNOS uncoupling is a combination of fluid shear effects on production of BH_4 and destruction of BH_4 by increased oxidative stress. Three enzymes coordinate the de-novo synthesis of BH_4. First, Guanosine-5'-triphosphate cyclohydrolase 1 (GTPCH-1), cleaves GTP to 7,8-dihydroneopterin triphosphate. Next,

6-pyruvoyl-tetrahydropterin synthase (PTPS) converts 7,8-dihydroneopterin triphosphate to 6-pyruvoyl-tetrahydropterin. In a final NADPH-dependent step sepiapterin reductase (SR) reduces 6-pyruvoyl-tetrahydropterin to BH_4. GTPCH-1 is the rate-limiting enzyme in the de-novo synthesis pathway of BH_4. Hydrogen peroxide stimulation can lead to an upregulation of GHPCH-1 protein levels, and increased BH_4 production [143-145]. Laminar shear causes a 2 fold increase GTPCH-1 phosphorylation at serine 81 by the α' subunit of casein kinase 2 (CK2) and increases its activity 30 fold compared to static culture *in vitro* [33, 127]. Shear stress does not regulate PTPS or SR, and does not change the protein levels of GTPCH-1, PTPS, SR, or CK2, indicating that shear stress regulates BH_4 synthesis by phosphorylation of GTPCH-1. BH_4 oxidation to inactive BH_2 is also increased in disturbed flow due to oxidative stress, which further depletes intracellular stocks of BH_4. While stocks of the critical cofactor are depleted, electron transfer from NADPH continues to form the heme-oxygen intermediate at the oxygenase domain prosthetic heme group of the NOS enzyme. However, without BH_4 to reduce the heme-oxygen intermediate NOS is not coupled to L-arginine and therefore produces superoxide rather than NO.

Need for targeted cardiovascular disease treatments

Most of the current treatments for atherosclerosis focus treatment of systemic risk factors. However, none of these therapies completely prevent cardiovascular events resulting from atherosclerosis. As an example, HMG Co-A reductase inhibitors reduce cardiovascular events by approximately 40 to 50% indicating that there are residual risks that persist after lipid lowering [146, 147]. This outcome indicates that there may be additional, underappreciated risk factors of cardiovascular disease that are not addressed with current therapies. One explanation for this residual risk is that current

treatments do not specifically target atheroprone vasculature. Such regions might require a high local concentration of drug not achieved by systemic administration.

A common complication of atherosclerosis is thrombosis. Systemic administration of antithrombotic drugs increases the risk for hemorrhage. Fibrinolytic drugs such as streptokinase and tissue plasminogen activator are inactivated rapidly in plasma and may fail to reach effective concentrations [148-151]. Targeted administration of antithrombotic treatments is an example of the need for targeted cardiovascular disease treatments [152]. However, the focus of this thesis is prevention of atherosclerosis, and thrombosis is an end stage complication of atherosclerosis.

Other therapeutic approaches target oxidative stress in cardiovascular disease. For example, supplementation with exogenous BH_4 can rescue the uncoupled state of eNOS and prevent atherosclerosis in experimental animals [153]. However, there are barriers to using BH_4 as a therapeutic for cardiovascular disease. Major challenges associated with delivery of exogenous BH_4 include oxidation and poor cellular uptake in endothelial and parenchymal cells [62]. While already oxidized forms of BH_4 such as BH_2 have better pharmacokinetics, the salvage pathway that converts BH_2 to BH_4 is downregulated where fluid shear stress is oscillatory [127]. This potentially negates the benefit of delivering BH_2 to atheroprone endothelium. In addition, BH_4 is also a cofactor for the synthesis of catecholamines, which could lead to unanticipated neurological effects if the co-factor is not delivered in a targeted fashion [33]. Nanomedicine is an attractive platform for targeting cardiovascular disease therapies such as BH_4, anti-inflammatory drugs, statins, and antithrombotic therapies to regions of the circulation at risk for atherosclerosis

Nanomedicine

Nanomaterials are of particular interest for drug delivery because they offer advantages over traditional molecular drugs [154]. For instance, nanomaterials can be used to extend drug activity, deliver drugs to specific cells or tissues, deliver poorly soluble drugs, facilitate imaging and drug delivery simultaneously, deliver multiple therapeutics simultaneously, deliver macromolecular drugs, and bypass delivery barriers [154, 155]. Nanomedicine is also ideal for targeted intravascular drug delivery. Several nanoparticle approaches have been explored for cardiovascular disease diagnosis and therapy. Examples include polymer micelles, polymer nanospheres, ultrasound-sensitive materials such as nano and microbubbles, gold nanoparticles such as rods and shells, polymer dendrimers, quantum dots, magnetically sensitive nanoparticles such as ultrasmall superparamagnetic iron oxides (USPIOs), radiolabeled particles, and naturally occurring nanoparticles such as high density lipoprotein. However, the best-studied nanoparticle for vascular delivery applications is the liposome.

Liposomes for drug delivery

Liposomes were the first nanotechnology drug delivery platform and were developed in the 1960s [156]. Liposome formulations are diverse and flexible. The most basic characterization of liposomes is based on their size, surface charge, and lamellarity (number of layers). Basic classifications of liposomes are uni- or multi-lamellar, small (<100 nm), intermediate (100 – 250 nm), large (> 250nm), and either cationic, anionic, or neutral charge [157]. Since their inception, liposomes have been widely used due to their biocompatibility, ease of use, versatility and facile chemistry. Liposomes can encapsulate hydrophilic, hydrophobic and amphiphilic drugs, and there are numerous

lipid modifications available with different physical and chemical characteristics. Because of the versatility of chemistries available, liposomes are generally considered to be more easily scalable for production. In addition, the lipids used to form liposomes are of natural origin and are therefore inherently biocompatible, and limit the toxic effects that can be encountered with synthetic nanoparticles.

Nanotherapeutic targeting

The first targeted liposomes were developed in the early 1980s [158, 159]. Nanomedicine has been applied most often to the fields of cancer and vascular pathologies. Targeting is highly important for these fields due to the focal nature of both diseases, and the need for high local concentrations of drugs of effectively combat the pathologies. Particularly in the field of cancer therapies, there is a significant effort to use nanomaterials that are targeted to tumor sites to reduce off target potentially toxic effects of cytotoxic drugs and increase concentrations in tumor cells.

Passive targeting

The most common method to achieve targeted drug delivery is passive targeting to tumors through the enhanced permeability and retention effect (EPR) [160]. This is achieved by nanoparticle-encapsulated drugs passively extravasating through leaky vasculature and the irregular lymphatic system of tumors. The EPR method relies on tuning the size, charge, and circulation time of nanoparticles to optimize uptake in permeable tissues. A common method to increase circulation time is addition of a highly hydrophilic corona, usually by conjugation with a polymer such as poly(ethylene glycol) (PEG). PEG also serves to shield the surface charge of cationic nanoparticles, for example those used to condense negatively charged DNA. While this effectively

increases circulation half-life of these drugs, and therefore improves passive targeting, disadvantages of using PEGylation include changes in pharmacokinetic behavior, immunological reactions, biodegradability, and toxicity of degradation products [161]. PEGylated nanoparticles have increased the incidence of stomatitis in clinical trials [157]. Tailoring the surface charge of nanoparticles can further enhance passive targeting. For example, inclusion of positive charge in the nanoparticle corona can enhance targeting to tumor vasculature [162]. While there are some reports of increased permeability in the setting of cardiovascular disease, specifically targeted approaches are more attractive for diagnosis and treatment of cardiovascular disease with nanoparticles.

Targeting nanomaterials to vascular disease sites

The molecular mechanisms of vascular disease both necessitate and provide exciting opportunities for disease site specific targeting of nanomaterials. Nanoparticles can be functionalized to home to specific vascular regions affected by inflammation, thrombosis, lipid accumulation or oxidative injury. Table 1 shows a list of targeting strategies that have been employed to target nanomaterials to sites of vascular disease.

Table 1. Potential targets for cardiovascular disease nanotherapeutics.

Target	**Cell/mechanisms targeted**
VCAM	Endothelial cells
ICAM	Endothelial cells
PECAM	Endothelial cells
E-Selectin	Endothelial cells
P-Selectin	Endothelial cells/ platelets
L-Selectin	Endothelial cells
Integrin αVβ3	Platelets
Integrin GPIIb-IIIa	Platelets
Integrin GPIa-IIa	Platelets
Integrin GPVI	Platelets

Integrin GPIb-IX-V	Platelets
Scavenger Receptors	Macrophages
Oxidized LDL receptors	Macrophages
Lipoproteins	Hyperlipidemia
Annexins	Coagulation/ inflammation
Fibrin	Coagulation
Collagen	Coagulation/ tissue remodeling
MMPs	Tissue remodeling
Tissue factor	Coagulation

Liposomes in cardiovascular disease targeting

Liposomes have been studied extensively utilizing the potential targets listed in table 1. By far the most common targets for liposomes and other nanomaterials are cell adhesion molecules such as PECAM, ICAM-1, and VCAM-1 [155]. Liposomes functionalized with anti VCAM-1 antibodies have been used for imaging and to deliver prostaglandins to lesion sites [163]. Liposomes decorated with anti-ICAM-1 antibodies have been used to deliver ultrasound contrast enhancement to sites of atheroma [164]. Liposomes have also been utilized for anti-thrombotic treatments by targeting to platelets through surface receptors such as P-selectin and integrin BPIIb-IIIa and RGD peptides [165, 166]. Several thrombolytic approaches have also relied on nonspecific uptake at areas of clotting [167, 168]. Another targeting approach for molecular imaging of atherosclerosis is indirectly targeting lesions through macrophages. Adding charged membrane components such as phosphatidylserine and decadeoxyguanine to the liposomes induces uptake in macrophages through scavenger receptors [169-172].

Shortcomings of current targeting strategies

While there are clinically approved nanomedicines, most notably liposome-encapsulated doxorubicin; in the 35 years since the development of the first targeted

nanotherapy none have made a significant impact through clinical translation [154, 173]. The reasons for failure are complex, but a primary concern is a need for new effective biomarkers for disease that allow targeted drug delivery on the correct spatiotemporal scales with minimal off target affects. Previously, nanoparticles have been used that target inflamed endothelium, inflammatory cells, the low-density lipoprotein receptor, thrombi and platelet aggregates [174-181]. While these studies have set a precedent for nanoparticle delivery to atherosclerosis, they depend on molecular determinants of lesions preset after the initiation of the disease. These studies target mature lesions, which implies that these targeting methods cannot be applied prophylactically. In addition, current approaches focus on molecular targets that are known to be up-regulated in atherosclerotic regions. At this point, positive feedback processes are established and reversal of the disease may be impossible. Therefore, new approaches are needed which can target atherosclerosis at its earliest stages and prevent the development of the disease. To accomplish this, novel biomarkers targeting disturbed flow are needed. My thesis work sought to discover novel ligands that target atheroprone flow as the first event that initiates atherosclerosis.

Phage display is a tool to develop targeting strategies for nanomedicine

Phage display is a powerful combinatorial method that can be used to screen and engineer polypeptides, antibodies, and antibody fragments that bind to virtually any target. This technique is particularly useful for nanomedicine, because it allows the discovery of ligands that can be conjugated to the surface of nanoparticles and used for targeting. Peptide phage libraries are ideal for nanomedicine applications because the peptides discovered are generally low molecular weight, are easily synthesized, are

degraded to biocompatible byproducts *in vivo*, and generally elicit less inflammatory response than antibodies [182].

Bacteriophages are viruses that specifically infect bacteria and are one of the simplest "living" organisms. They were first hypothesized to exist by Max Delbrück in the 1930s [183]. Phage display was first described using the *Escherichia coli*- specific bacteriophage M13 in 1985 [184]. Since this discovery, other phage systems including λ-phage T4 phage, and eukaryotic viruses have been employed, however the M13 bacteriophage system is most popular. The M13 phage is a filamentous viral particle approximately 1 µm long and less than 10 nm in diameter consisting of a single stranded DNA core surrounded by five coat proteins (Figure 5) [185]. The major coat protein, protein P-8, covers the majority of each phage particle. The P3, P6, P7 and P9 coat proteins cover the ends of the phage particle, and 5 copies of each are displayed per phage particle. The P3 coat protein is the most complex, and is involved in bacteriophage recognition of the F-pilus of *E. coli* [186].

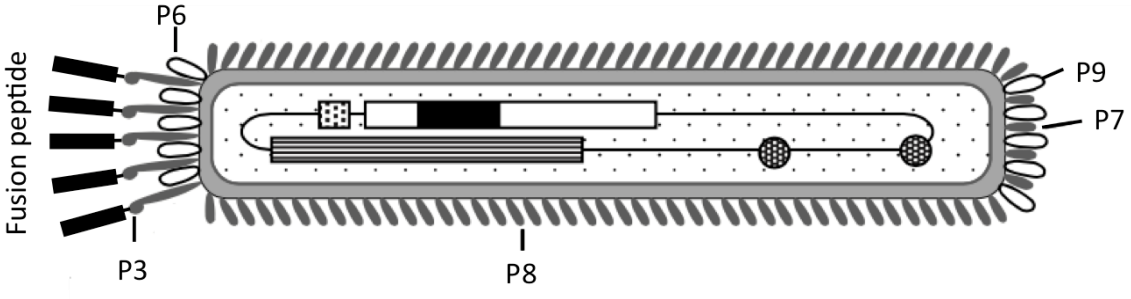

Figure 5. Structure of an M13 bacteriophage phage displayed library. Fusion peptides are attached at the N terminus of all five copies of the P3 coat protein Adapted from [185].

Phage libraries are constructed by inserting random mutations that encode peptide sequences into the coat protein genes of bacteriophages [187]. When the phage is produced in the bacteria, the inserted proteins are displayed in the coat of the bacteriophage. The first generation of random peptide libraries was demonstrated in the late 1980s [188]. Today, the most common phage libraries in use are N-terminal fusions to the P3 coat protein of M13 and phage libraries are readily commercially available. The most important advantage of using phage libraries is that the displayed peptides are directly linked to the DNA sequence of the phage they are displayed on. Practically, this means that peptides selected from phage screening can be readily identified by replication of the viral particle and sequencing of the inserted nucleic acid sequence. The advantages of being able to use standardized biochemical techniques are offset by the possibility for random mutation of the fusion peptide or that the fusion peptide could be fatal to phage replication. This could result in limited diversity of polypeptide display. For example, it is well known that arginine causes a secY-dependent secretion of the PIII, which reduces peptides containing arginine. This is corrected by addition of prlA suppressors during bacterial growth [189]. In spite of these shortcomings, phage libraries are available that represent 10^{12} fusion peptides with unique amino acid sequences [186].

Phage display is used to identify phage clones that bind to a target in a highly specific manner, a process called phage panning. A strength of this technology is that it can identify interactive regions of proteins and other molecules without pre-existing knowledge about the nature of the interaction. The simplest application of this process involves identifying a target and screening phage against the isolated target. In this process the phage library is allowed to interact with the desired target. Nonbinding

phage are washed away and binding phage are amplified and re-used in a serial refinement process (Figure 6).

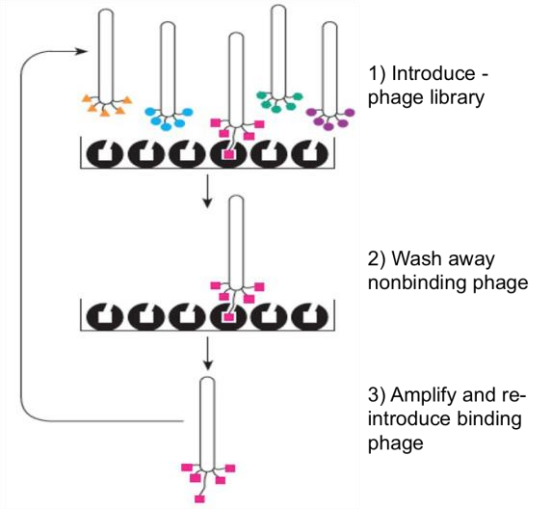

Figure 6. Phage display panning process. Step 1 is introduction of the phage library to a target immobilized on a plate. Step 2 is washing of the plate to remove unbound phage. Step 3 is eluting the bound phage and amplifying the clones recovered for the next round of panning.

More complex phage panning strategies have been employed to determine biomarkers with the ultimate goal of developing targeted drug delivery systems. Pasqualini and Ruoslahti were the first to report using phage display *in vivo* to identify fusion peptides that targeted whole organs such as the brain and kidneys [190]. They later showed that organ-specific targeting can be accomplished by leveraging the heterogeneity of the vascular endothelium [191, 192]. Endothelial heterogeneity is well suited for discovering peptides that mediate targeting to cardiovascular disease, particularly for targeting intravenous nanoparticle delivery.

Three distinct approaches have been used to find ligands for nanoparticle targeting. These include targeted *in vitro* phage display based on previously identified molecular targets such as cell adhesion molecules, screening against cell surfaces and screening against atherosclerosis *in vivo* [192-194]. The first approach is particularly useful when high-value targets have been identified by methods such as gene arrays, but structure-function relationships are unclear and preclude design of targeting ligands. In this context, phage display has been used to identify binding partners for diverse targets including the compliment system, integrins, caspases, metalloproteinases, cell adhesion molecules and glycoproteins [192, 195]. However, the reductionist strategy of isolating specific cell receptors or molecular targets does not necessarily capture their display *in vivo*, or guarantee that they are the most useful for targeting of nanotherapeutics. Therefore, approaches two and three are considered more useful for translational research in nanoparticle targeting.

In the context of atherosclerosis, there have been several efforts to use phage display to identify ligands that target molecular determinates of the disease. Thapa, et al., found peptides that home to activated endothelial cells in atherosclerotic plaques in low density lipoprotein knockout mice using *in vitro* panning against tumor necrosis factor alpha treated bovine aortic endothelial cells [196]. Hong, et al., used phage panning against human atherosclerotic tissue *ex vivo* to identify peptides binging to interleukin 4 receptor [197]. Kelly, et al., used phage screening against cells overexpressing VCAM-1 to identify peptides with homology to very late antigen 4 that target VCAM-1 overexpressing cells [179]. They demonstrated homing of nanoparticles functionalized with these peptides to sites of induced inflammation *in vivo*. Using *in vivo* phage screening in Apolipoprotein (Apo) E deficient mice Kelly, et al., identified several

families of peptides binding to leukemia inhibitory factor receptor, transferrin receptor and VCAM-1 [178]. Using *in vivo* phage display, Liu, et al., identified peptides that that mediate homing to mature atherosclerotic lesions in apolipoprotein E knockout ($ApoE^{-/-}$) mice, and found that the peptides bound to Grp78, as well as identified peptides homologous to TIMP-2 [198]. Hamzah, et al., used *in vivo* phage display to identify peptides binding to fibrin-fibronectin complexes in atherosclerotic lesions of $ApoE^{-/-}$ mice, and showed that a peptide know to target tumor macrophages was also useful for targeting atherosclerotic plaques [180]. These studies demonstrate the utility of phage display in discovering ligands that can be used to target nanomedicines to atherosclerosis. However, a major shortcoming of these studies is that they target mature lesions. An ideal strategy would target atheroprone regions of the vasculature before the development of advanced lesions.

THESIS HYPOTHESIS AND SPECIFIC AIMS

Disturbed flow is a key initiating event in atherosclerotic lesion formation. Atherosclerotic lesions develop when focal endothelial dysfunction caused by disturbed flow is compounded by systemic risk factors such as hypercholesterolemia. Targeted drug delivery to areas of disturbed flow is a promising approach to prevent atherosclerosis before lesions develop. Studies have shown that disturbed flow can develop at many cites, making prediction of these atheroprone areas speculative [199, 200]. Therefore programming nanocarrier functions to navigate to and detect atheroprone areas is an ideal but unmet need. In this thesis, I sought to use phage display to identify biomarkers in endothelial cells exposed to disturbed or atheroprone flow. I hypothesized that peptides targeting atheroprone vascular zip codes could be

identified by phage display, and that these ligands could be leveraged for nanotheraputic targeting to atheroprone vasculature (figure 7).

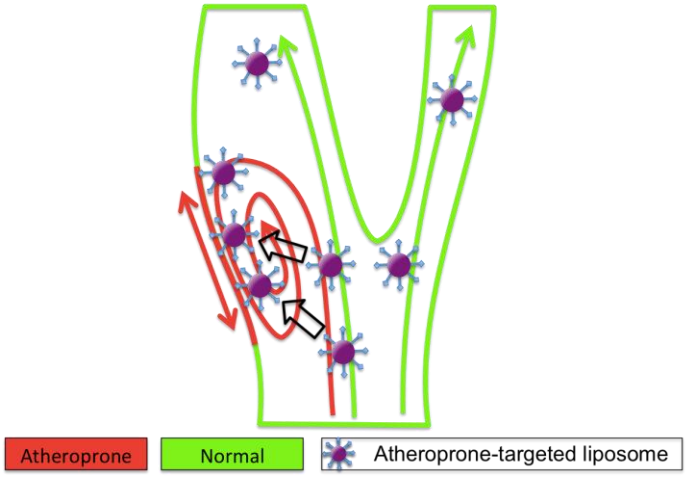

Figure 7. Nanocarrier targeting to atheroprone vasculature (red).

Specific aim 1 – Identification of atheroprone vascular zip codes. In this aim, phage display was utilized to discover novel peptide ligands that selectively target endothelial cells in atheroprone vasculature.

Specific aim 2 – Nanotherapeutic platform development. In this aim we employed phage displayed peptides to create targeted nanoparticles, and evaluated nanoparticle homing to atheroprone vasculature *in vivo*.

Specific aim 3 – Therapeutic delivery. In this aim targeted nanoparticles were used to deliver tetrahydrobiopterin to rescue endothelial dysfunction and prevent atherosclerosis.

CHAPTER II

IDENTIFICATION OF ATHEROPRONE VASCULAR ZIP CODES USING PHAGE DISPLAY

INTRODUCTION

Arterial geometry affects the blood flow profiles in the cardiovascular system. In straight, unbranched vascular segments blood flow is unidirectional and laminar. The time average wall shear stress is high. In contrast, at branch points, sites of curvature and distal to stenosis, blood flow becomes disturbed. Endothelial cells comprise the inner lining of blood vessels and experiencing these changes respond with distinct alterations in phenotype. Disturbed flow predisposes these regions to local lipid deposition, inflammation and focal development of atherosclerosis. Atherosclerotic lesions predominantly occur at these sites: branch points, the proximal coronary arteries and the distal aorta [48, 125, 126]. Current therapies for atherosclerosis do not employ preventative treatments to target vasculature that is prone to develop the disease. Therefore, there is an unmet need to define ligands that can target therapeutics to regions of disturbed flow.

Given the marked differences in gene expression and protein content of endothelial cells exposed to varying flow profiles, we reasoned that there might be differences in peptide binding to the surface of cells exposed to disturbed versus unidirectional laminar shear. This is supported by recent evidence demonstrating that endothelial cells

present a heterogeneous luminal protein milieu specific to their tissue of origin [191, 192, 201, 202]. This diversity of protein expression on the luminal surface of the vasculature is currently being leveraged for the discovery of tissue and disease specific ligands for drug targeting [174, 180, 181, 203]. Phage display employing combinatorial peptide libraries is widely accepted to screen peptide motifs that bind specifically to vascular beds of interest [177, 178, 181, 193, 194, 204-206]. In the context of vascular disease, phage display has facilitated development of affinity agents targeted to mature atherosclerotic lesions [178-180, 207].

APPROACH

In this aim I employed phage display *in vitro* and *in vivo* to identify peptide ligands that bind to endothelial cells exposed to disturbed flow. Consensus peptide sequences targeting atheroprone flow were then validated *in vivo*. To further validate peptide targeting, fluorescently labeled peptides were synthesized and injected in the same murine model system and flow cytometry was performed to identify cell types that preferentially take up peptides in the atheroprone artery.

METHODS

Cone-in-plate culture system

We first attempted to identify targeting ligands to oscillatory shear stress by using phage display *in vitro* in a cone-in-plate culture system. Cone-in-plate cell culture, pioneered by C. Forbes Dewey, has become a well-established method to subject living cells to fluid shear stress [70, 71]. A schematic representation of the cone-in-plate system with calculations for shear stress at the cell surface is shown in Figure 1A. I developed an

improved cone-in-plate culture system based on the Forbes Dewey design (Figure 1B). We employed 9 cm titanium cones, with a one-degree cone angle in this system. The cones were coupled to stepper motors by ½ inch stainless steel shafts using a flexible shaft coupler. The shaft coupler serves to minimize misalignment of the motor with the cone system and reduce wobble caused by a misaligned system. Ten-centimeter culture plates were stabilized in a polymer base with four plate holders. The cones were held in place by type 2 polyvinyl chloride plate covers, which were fastened in place using brass nuts. The plate covers also set the offset height of the cones by holding the shaft in place using a stainless steel shaft collar. The offset height for all cone-in-plate experiments was set to 0.012 inches. Motors were held in place by a ¼ inch G-10 fiberglass platform with motor mounts designed for NEMA 17 stepper motors. Motor drivers adapted from an older cone-in-plate culture system were used to power motors.

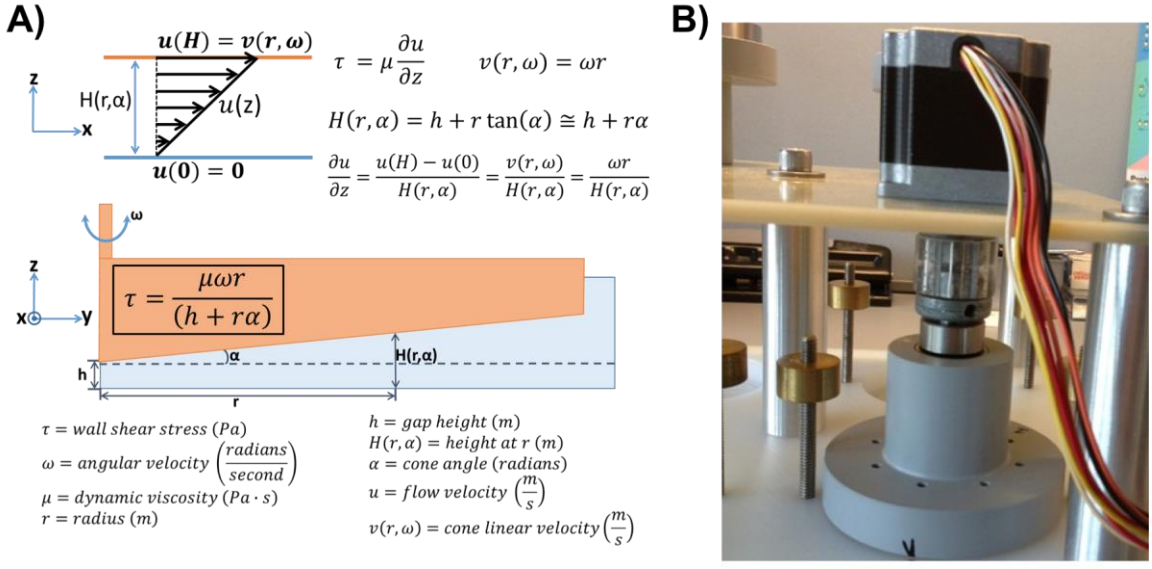

Figure 1. Cone in plate culture system A) Schematic of the cone-in-plate culture system and method for calculating fluid shear stress based on a no-slip condition at the cell surface and Newtonian fluid mechanics using Poiseuille's law B) Cone-in-plate culture

system developed for *in vitro* phage panning. The culture plate is placed underneath the grey type two PVC holder.

Cell culture

Human aortic endothelial cells (hAECs) were purchased from Lonza and cultured according to manufacturers protocols using Endothelial growth medium 2 with a full bullet kit supplement and 3% serum (Lonza, Basel, Switzerland).

In vitro phage display

In vitro panning was performed using subtractive panning against hAECs exposed to laminar (+13 dPa) vs. oscillatory shear (±13 dPa) in a cone-in-plate culture system. Endothelial cells were cultured to confluence and subjected to shear stress for 15 hours 24 hours after confluence was reached. Two M13 bacteriophage peptide libraries, a 7 amino acid cyclic library, and 12 amino acid linear library (New England Biolabs, Ipswich, MA, Cat# E8110S, and E8120S, respectively), were used in screening. Two libraries (i.e., cyclic and linear) were used because structural specificity can impact peptide binding affinity, and the cyclic peptide library displays a common motif in ligand binding. Subtractive panning increases panning stringency and therefore binding specificity of the phage. Subtractive panning involves first incubating the phage library with hAECs exposed to laminar shear and then transferring the supernatant containing un-bound phages to incubate with hAECs exposed to oscillatory shear. A first round of panning was performed against only oscillatory shear exposed hAECs while round 2-4 employed the subtractive panning technique. For all panning rounds hAECs were washed 10 times with tris buffered saline (TBS) containing 0.1% Tween 20 (TBST) after

phage incubation, and then phages were eluted by non-specific elution buffer containing 0.2 M glycine-HCl and 1mg.mL^{-1} BSA with a pH of 2.2.

The eluted phages were then used to transform *Escherichia coli* (*E-coli)* for amplification and to quantify the number of phage binding to the target condition by titration. Visualizing β-galactosidase (β-gal) positive plaques allowed quantification of phage titer. Phage eluted from oscillatory shear hAEC were expanded and then used for the next round of panning (Figure 2).

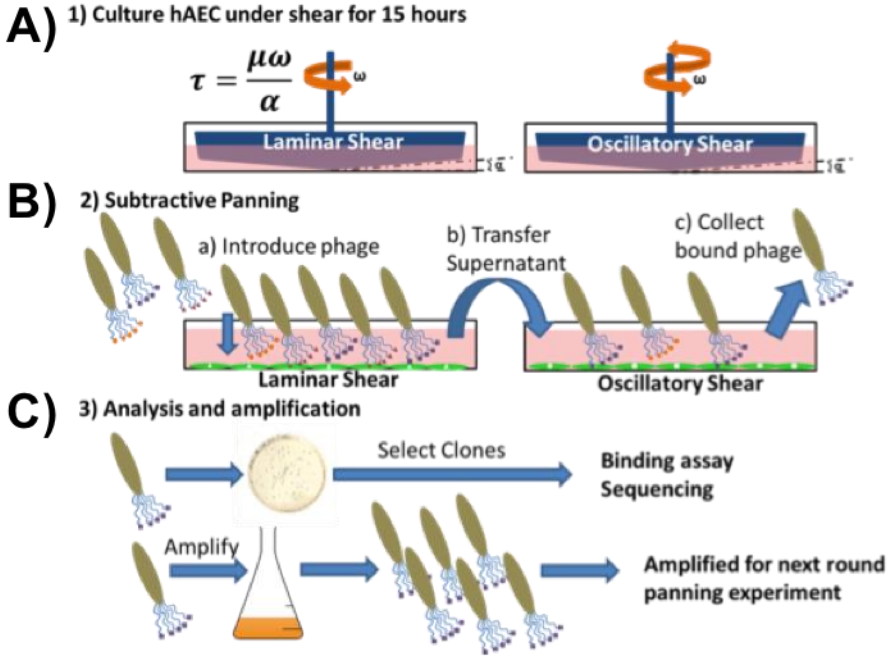

Figure 2. Schematic of *in vitro* phage panning process. A) Schematic of cone-in-plate viscometer cell culture. B) Schematic of subtractive panning, where phage are first introduced to laminar sheared cells then exposed to oscillatory sheared cells. C) Isolation of phage clones after phage panning for titration, sequencing and recycling for the next round of phage display.

Lysogeny broth (LB)-agar plates for titration contained 0.2 mM isopropyl-β-D-thiogalactoside, 0.1 mM 5-Bromo-4-chloro-3-indolyl-β-D-galactoside, 10g.L^{-1} Bacto-Tryptone, 5 g.L^{-1} yeast extract, 10 g.L^{-1} NaCl, and 15 g.L^{-1} agar. Visualizing β-gal positive colonies allowed for quantification of phage titer. After the third and fourth round of phage panning, ten colonies were sequenced from titration plates to identify consensus sequences. For sequencing, colonies were picked using sterile pipet tips and deposited into 30 µL Platinum® PCR Supermix (Invitrogen, Grand Island, NY, Cat# 11306-016) containing 0.5 µM forward and reverse primers (Forward primer 5'-GTCATTGTCGGCGCAACTATCGG-3', Reverse primer 5'-CCC TCA TAG TTA GCG TAA CG-3'). Amplified DNA fragments were purified using QIAquick PCR spin columns (Qiagen, Hilden, Germany, Cat# 28104), and diluted in DNAse free water for sequencing. Sanger sequencing was performed at the Vanderbilt Technologies for Advanced Genomics using the reverse primer from PCR amplification [208].

Animals studied

Wild-type C57BL/6 mice were purchased from Jackson Laboratories (Bar Harbor, ME). The institutional animal care and use committee at Vanderbilt University approved all animal protocols. All *in vivo* experiments were performed in a partial carotid artery ligation model of disturbed flow [74]. Male mice at age of 10 to 14 weeks underwent a surgical procedure in which the left common carotid artery (LCA) was exposed and three of four of its branches: the left external carotid artery (ECA), left internal carotid artery (ICA), and the occipital artery (OA) were ligated with 6-0 silk suture while the superior thyroid artery (STA) was left intact (Figure 3). Care was taken to avoid damaging the superior thyroid artery during ligation. The right common carotid artery (RCA) was surgically exposed, but not ligated, and served as a sham control. Doppler

ultrasound was performed using a VisualSonics Vevo 770 (Fujifilm VisualSonics, Inc., Toronto, Canada) micro imaging system to visualize blood flow in the ligated and un-ligated arteries. Images were acquired using the RMV-704 ultrasound probe transmitting at 100% power at a frequency of 30 MHz with a receiving Doppler gain of 10 dB.

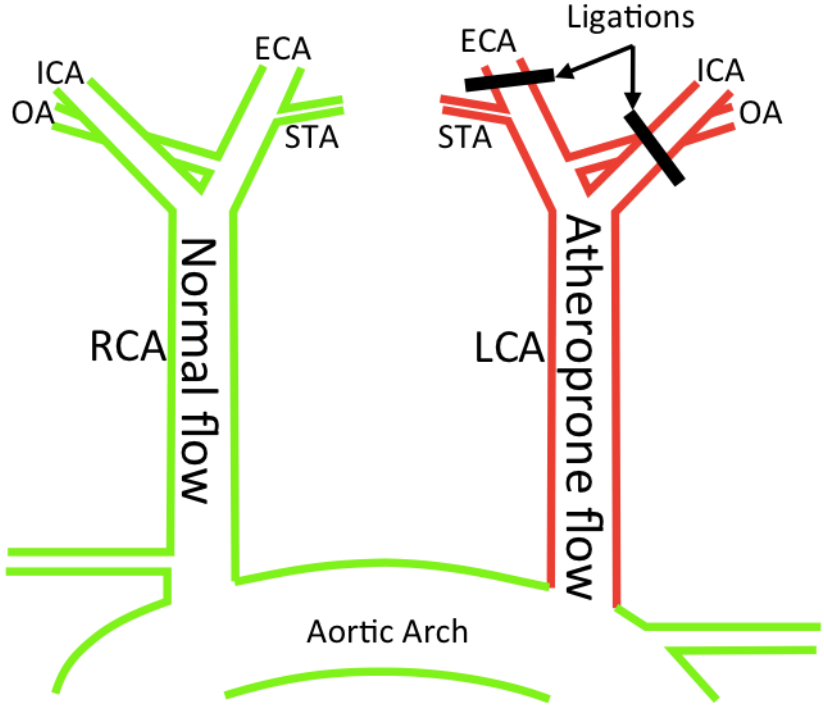

Figure 3. Schematic of the partial carotid artery ligation surgery. Three of the four ascending branches of the left carotid artery are ligated, resulting in partial occlusion of the left carotid artery and disturbed shear in the left common carotid artery.

In vivo *phage display*

In vivo phage display was performed in C57/BL6 mice four days post-ligation. Two peptide libraries were used screened in this study, the Ph.D.-12 and Ph.D.-C7C libraries. Phage peptide libraries were injected into the tail vein of the mice at a

concentration of 2 x 10^{11} plaque forming units to ensure a 100 fold representation of all clones in the phage library containing a theoretical 2 x 10^{9} different clones. After 2.5 hours of circulation time, mice were euthanized by CO_2 asphyxiation, perfused at physiological pressure with normal saline containing 10 $U.mL^{-1}$ heparin, and then both carotid arteries were surgically removed and processed separately. In order to remove un-bound phages, the excised arteries were cannulated with a 30-gauge syringe and washed with 0.5 mL TBST then transferred to fresh TBST. To expose the endothelium, each artery was cut lengthwise with a number 10 scalpel. Arteries were then washed with non-specific elution buffer consisting of 0.1 M glycine-HCl (pH 2.2) with 1 $mg.mL^{-1}$ bovine serum albumin to remove phages bound to the surface of the vessels, and weakly bound phages. Next, phages were eluted with 100 mM triethanolamie in TBS [178]. The eluted phages were then used to transform *E. coli* for amplification, and the number of phages binding to the target condition was quantified by titration according to the manufacturer's protocol. For amplification, *E. coli* were transformed at early-log phase (OD600 = 0.01-0.06) with phages and cultured for 4.5 hours with vigorous shaking. Phages were then purified by ultracentrifugation and overnight precipitation into 20% w/v polyethylene glycol (M.W. = 8000) with 2.5 M NaCl. Amplified phages from the LCA were then used in the subsequent rounds of phage display following the same procedures.

To validate the affinity of consensus sequences, consensus clones were amplified as described previously by inoculating an *E. coli* culture with a consensus clone colony, and injected following the same procedures as *in vivo* phage library panning. Titration of phages binding to the LCA vs. RCA was used to determine the relative affinity for the target condition. The titer of phages recovered was normalized to the protein content of

the corresponding vessel. For measurement of protein concentration carotid artery segments were placed in 50 µL of RIPA lysis buffer (Thermo Scientific, Rockford, IL, Cat# 89900) containing protease and phosphatase inhibitors (Roche, Indianapolis, IN, Cat# 05892970001, and Cat# 04906845001, respectively); and sonicated for one minute on ice to release protein. Protein content was measured by small volume BCA assay (Thermo Scientific, Cat# 23225).

Peptide synthesis

Peptides were synthesized on a PS3 3 channel serial peptide synthesizer (Protein Technologies, Inc. Tucson, AZ) on low substitution glycine loaded Wang or 2-chlorotrityl resin support using standard solid phase Fluorenylmethyloxycarbonyl chloride (Fmoc) chemistry. N-methylpyrrolidone (NMP, Fischer Scientific) was utilized as a solvent in all peptide syntheses. O-(6-Chlorobenzotriazol-1-yl)-N,N,N′,N′-tetramethyluronium hexafluorophosphate was used as an activator (Chempep, Wellington, FL) in the presence of N-methylmorpholine. All amino acids were double coupled in order to maximize yield and purity. Peptides were cleaved and de-protected in trifluoroacetic acid/water/triisopropylsilane (95/2.5/2.5). Successful peptide synthesis was verified through electrospray ionization mass spectrometry (ESI-MS) analysis on a Waters Synapt ESI-MS. The peptide was then further purified by reverse phase high performance liquid chromatography (HPLC) on a Waters 1525 binary HPLC pump outfitted with an extended flow kit, a Waters 2489 UV/Visible detector and a Phenomenex Luna C18(2) AXIA packed column (100A, 250 x 21.2 mm, 5 micron). HPLC grade water with 0.05% formic acid (solvent A) and HPLC grade methanol with 0.05% formic acid (Solvent B) were used as the mobile phases and the peptide was purified utilizing a 90% A to 90% B gradient over 25 minutes at a flow rate of 16 mL.min^{-}

[1]. Methanol was removed from purified fractions with a rotary evaporator and the purified fractions were then frozen and lyophilized. Peptide purity was verified through ESI-MS.

Evaluating peptide uptake in vivo by flow cytometry

To further validate the efficacy of peptide targeting, peptides were injected intravenously, and cellular uptake was determined by flow cytometry. SLSSYNGSALAS (DistL12) and GSPREYTSYMPH (PREY) peptides were fluorescently labeled at the N-terminus by reaction with 5(6)-Carboxyfluorescein (FAM) N-Hydroxysuccinimide ester (NHS). Peptides were dissolved in 0.1 M bicarbonate buffer (pH = 8.3) and reacted overnight on ice with 4 molar eqivalents of NHS-FAM. The resultant FAM-Peptides were purified by gel filtration through Spehadex columns (PD MidiTrap G10, GE Healthcare). Purified FAM-Peptide solutions were frozen and lyophilized to a dry powder.

For flow cytometry experiments, mice underwent partial carotid ligation surgery 4 days before peptide injection. The mice were injected with 4mg.kg^{-1} FAM-peptide 2.5 hours before sacrifice. The mice were then perfused through the left ventricle with ice cold PBS with calcium and magnesium, and arteries were collected and stored on ice. To obtain cell suspensions for single stain and fluorescence minus one (FMO) control experiments the aorta from one FAM-peptide injected mouse and one control mouse were also isolated and cleaned of perivascular fat and lymph nodes prior to processing. For peptide injection samples, two mice were pooled per sample to ensure that enough cells were collected for analysis. To obtain single cell suspension solutions from sample arteries, the arteries were placed into a digestion solution consisting of phenol red free RPMI 1640 medium (Gibco) with glutamine, 10% fetal bovine serum, 1 mg.ml^{-1}

collagenase A, 1 mg.ml^{-1} collagenase B, and 0.1 mg.ml^{-1} DNAse 1 (Roche). The arteries were minced with sharp scissors for two minutes and then placed on a shaker for 30 minutes at 37 ˚C. Next, the arteries were passed through a 70 µm cell strainer to obtain cell suspensions. The cell strainer was washed three times with 10 mL RPMI to recover dissociated cells. Next the cells were spun at 300 xg for 10 minutes and then transferred to fluorescence-assisted cell sorting (FACS) tubes for further processing. All future steps took place in FACS buffer consisting of phosphate buffered saline (PBS) with calcium and magnesium, 1% bovine serum albumin and 0.1% sodium azide. Next, non-specific antibody binding was blocked with anti-CD16/CD32 for 10 min at 4 °C (BDbiosciences, clone 2.4G2, Cat# 553142) (2 µL in 100uL FACS buffer). The cells were then subjected to a low-speed centrifugation at 300 x g for 5 minutes and washed once with 1 mL of FACS buffer. Staining solutions were made by adding 1 µL of each antibody solution to 100 µL FACS buffer. Cells were incubated with staining solutions for 30 minutes at 4 ˚C and then washed twice with FACS buffer. For live/dead staining, the cells were then incubated with 7-aminoactinomycin-D (7-AAD) for 10 minutes at room temperature before running on the flow cytometer. Fluorescein isothiocyanate (FITC) beads were used for single stain and compensation controls to set the detection parameters for the flow cytometer.

Single stain and FMO samples were used to set up gating for positive events. Platelet endothelial cell adhesion molecule (CD31) was used as a marker for endothelial cells, protein tyrosine phosphatase receptor type C (CD45) as a marker for all leukocytes, and epithelial growth factor-like module-containing mucin-like horomone receptor-like 1 (F4/80) as a marker for monocyte/macrophages. Dead cells were eliminated using 7-AAD. Antibody information can be found in Table 1. For analysis, I first gated for live

cells (negative for 7-AAD) and then for single cells based on forward scatter area vs. forward scatter height. Next, I plotted cells positive for CD31 vs. cells positive for CD45 to investigate cell population specific uptake.

Table 1. Flow cytometry antibody information.

Antibody	Fluorophore	Target	Company/cat#	Clone
αCD31	PE	Endothelial cells	BD pharmingen/ 561073	MEC 13.3
αCD45	Brilliant violet 510	Leukocytes	BioLegend/ 103137	30-F11
αF4/80	APC/Cy7	Macrophages	BioLegend/ 123118	BM8
7AAD	PerCP-Cy5.5a	Dead cells	BS Pharmigen 51-68981E	NA

Determining a potential binding partner for the PREY peptide

To determine the binding partner for the PREY peptide, I performed a pull-down followed by proteomics analysis. For proteomics experiments, all peptides were N-acetylated by reaction with acetic anhydride. PREY peptides, and scrambled PREY control peptides were conjugated at the C-terminus with 5-(Biotinamido)pentylamine (pentylamine-biotin) by 1-Ethyl-3-(3-dimethylaminopropyl)carbodiimide (EDC)- *N*-hydroxysulfosuccinimide (sulfoNHS) coupling (EZ-Link Pentylamine-Biotin, Fisher Scientific, Rockford, IL). Conjugates were purified by dialysis overnight to remove excess pentylamine-biotin. Conjugation products were confirmed by esi-MS. Two milligrams of each peptide-biotin conjugate was mixed with 1 milligram streptavidin conjugated paramagnetic particles (Magnesphere, Promega, Madison, WI). To remove excess peptide, beads were washed 5 times prior to use. For pulldown experiments, mice were sacrificed 4 days after partial carotid ligation surgery. Carotid arteries were

removed, immediately frozen in liquid nitrogen and homogenized on dry ice. Artery homogentate was dissolved in 800 µL NP40 buffer (0.5% triton-100 in tris buffered saline pH=7.8 with protease inhibitors), and insoluble proteins were cleared by centrifugation. Four hundred µL of protein was mixed with 100 µg peptide conjugated beads and incubated for 1.5 hours at room temperature. Beads were washed 4 times with NP40 buffer, and proteins were eluted with 30 µL of 1x activated Laemmli buffer by heating to 70 °C for ten minutes.

Shotgun proteomic analysis of eluate was performed by first resolving eluted proteins approximately 1 cm using a 10% Novex precast gel, and then performing in-gel tryptic digestion to recover peptides.

Resulting peptides were analyzed by a 70-minute data dependent LC-MS/MS analysis. Briefly, peptides were autosampled onto a 200 mm by 0.1 mm (Jupiter 3 micron, 300A) self-packed analytical column coupled directly to an LTQ (ThermoFisher) using a nanoelectrospray source and resolved using an aqueous to organic gradient. A series of a full scan mass spectrum followed by 5 data-dependent tandem mass spectra (MS/MS) was collected throughout the run and dynamic exclusion was enabled to minimize acquisition of redundant spectra. MS/MS spectra were searched via SEQUEST against a mouse database that also contained reversed version for each of the entries. (http://www.ncbi.nlm.nih.gov/pubmed/7741214). Identifications were filtered and collated into spectral count numbers at the protein level using Scaffold (Proteome Software).

Immunoblotting

The presence of Fibronectin and Filamin-A in the pulldown was confirmed by western blot. Pulldowns were performed as described previously and eluted protein was used for western blot. Proteins separated by 4-20% sodium dodecyl sulfate polyacrylamide gel electrophoresis (SDS-PAGE), and transferred to polyvinylidene fluoride (PVDF) membranes overnight at 30 V at 4 °C. Membranes were blocked for 1 hour in 5% milk in 0.1% TBST. Anti-Filamin-A antibody (ab51217, Abcam, Cambridge, MA), and anti-fibronectin antibody (ab23750, Abcam) were diluted 1:500 in TBST and incubated with the membranes for 1 hour at room temperature. Filamin-A was visualized as a single band at 281 kDa in western blots. Fibronectin was visualized as a single band at 265 kDa. Because the protein used for western blot was from pulldown, a loading control was not possible. However, the amount of protein loaded onto the peptide-functionalized beads was equivalent, as was the substitution of the peptide on the beads. This indicates that the differences in band intensity from pulldown experiments is due to differences in expression in the vessels, not unequal loading.

Immunostaining

Immunofluorescence staining was performed on fix-perfused mouse carotid arteries embedded in optimum cutting temperature medium (OCT, Tissue-Tek). Five micron sections were sliced in a serial sequence. Samples were permeablized with 0.1% Triton X-100 (Sigma-Aldrich). Antigen blocking was performed with 5% bovine serum albumin (BSA) prior to incubation with anti Filamin-A antibody (ab51217, Abcam). Additional blocking with 10% donkey serum was performed before incubation with secondary antibodies. Donkey polyclonal antibodies conjugated to Alexa Fluor 488, 555 or 647

were used for binding primary antibodies. Where applicable, samples where then subsequently incubated with phallodin-Alexa-488 (Life Technologies) for visualization of F-actin. 4',6-diamidino-2-phenylindole (DAPI, Invitrogen) was added in the last wash following incubation with secondary antibodies or phalloidin. All slides were mounted with Prolong Anti-fade media (Life Technologies).

RESULTS AND DISCUSSION

Cone-in-plate culture

According to calculations performed according to figure 1A, the shear stress experienced by the cells varies from the center of the dish to the outside, but most cells experience physiological shear stress around 13 dPa (Figure 4A). In our system, hAEC were shown to align and elongate under laminar shear, whereas the unaligned, irregular cobblestone morphology was seen when exposed to oscillatory shear stress (Figure 4B**)**. The observed cellular morphology in our culture system is the same as previously observed and validated the physiological response of endothelial cells to differential shear waveforms [209].

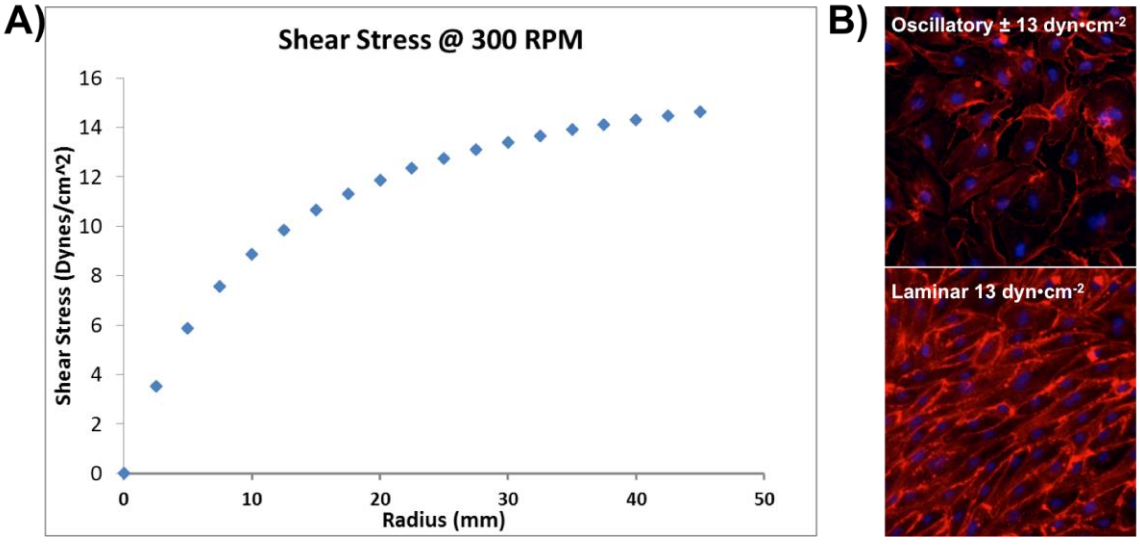

Figure 4. hAEC culture in the cone-in-plate system A) Calculation of shear stress as a function of distance from the center of the plate according to equations from figure 1A. B) Examples of hAEC cultured with oscillatory shear (top) and laminar shear (bottom). Red = F-actin, Blue = nucleus.

In vitro *phage panning*

Eluate titers from the fourth round of *in vitro* panning indicated an increase in specificity for hAEC exposed to oscillatory shear stress of 1.9 fold ($p>0.05$, $n=2$) for linear libraries and 1.37 fold ($p=0.03$, $n=2$) for cyclic libraries. However, no consensus sequence was identified from *in vitro* panning (Figure 5). This result was indicative of successful biopanning, which increased specificity for the target condition but did not result in a consensus. Additionally, the displayed peptides do not contain an abundance of aromatic residues. Aromatic residues have been shown to mediate nonspecific phage binding to polystyrene and other plastics [210]. Therefore, a lack of aromatic residues indicated that the phage bound to cellular targets and not to culture dishes used for these experiments. These results indicated the feasibility of the phage display approach for discovering peptides that preferentially bind to endothelial cells exposed to disturbed flow. It is also notable that the flow pattern achieved in a cone-in-plate culture device are not as complex as observed *in vivo* because it is improbable to create turbulent flow at the length scale of a cone-in-plate culture using more closely Newtonian fluids. While endothelial cells phenotype is similar to the *in vivo* case in terms of gene and protein expression, there is a possibility that the display of proteins on the cell surface in a cone-in-plate culture differs from the display of proteins on the luminal surface of vasculature. This system also lacks the dynamic interaction with circulating blood cells such as platelets, erythrocytes, monocytes and T lymphocytes, which could alter

endothelial phenotype. I decided to pursue *in vivo* phage panning due to these limitations of *in vitro* culture, and the fact that no consensus clones were identified from *in vitro* panning.

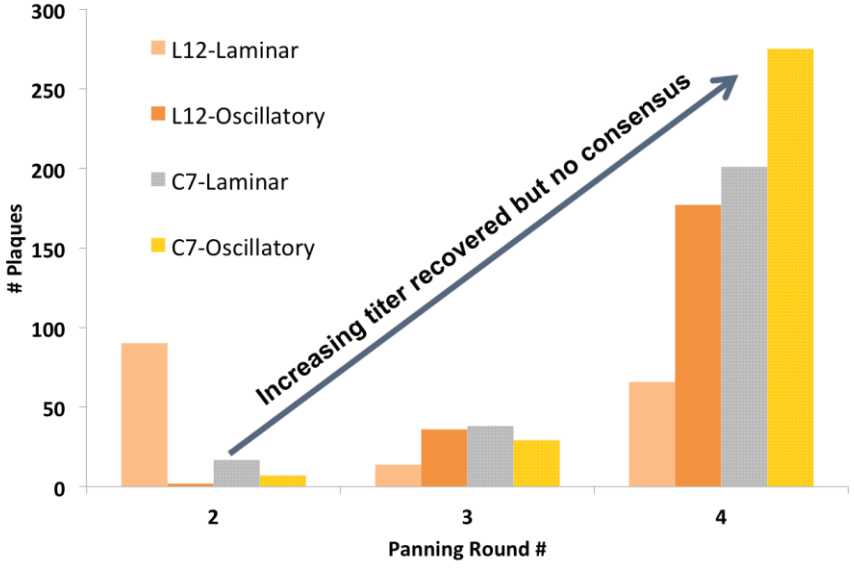

Figure 5. Titration of phage recovered from *in vitro* phage panning. The number of phage recovered from subtractive panning indicated that the *in vitro* phage panning process was selecting phage clones that accumulated in the oscillatory shear condition.

In vivo *phage panning*

In vivo phage panning was performed in the partial carotid artery ligation model of disturbed flow in male C57/BL6J mice [74, 211]. In this surgical model, three of the four major branches of the left common carotid artery (LCA) are ligated. This results in low and oscillatory flow in the LCA,

while flow in the right common carotid artery (RCA) remains normal. Doppler ultrasound imaging confirmed disturbed blood flow in the ligated LCA and normal blood flow in the sham RCA one day after ligation (Figure 6). The ligated left carotid artery is the target for phage display, while the right artery serves as a normal flow control.

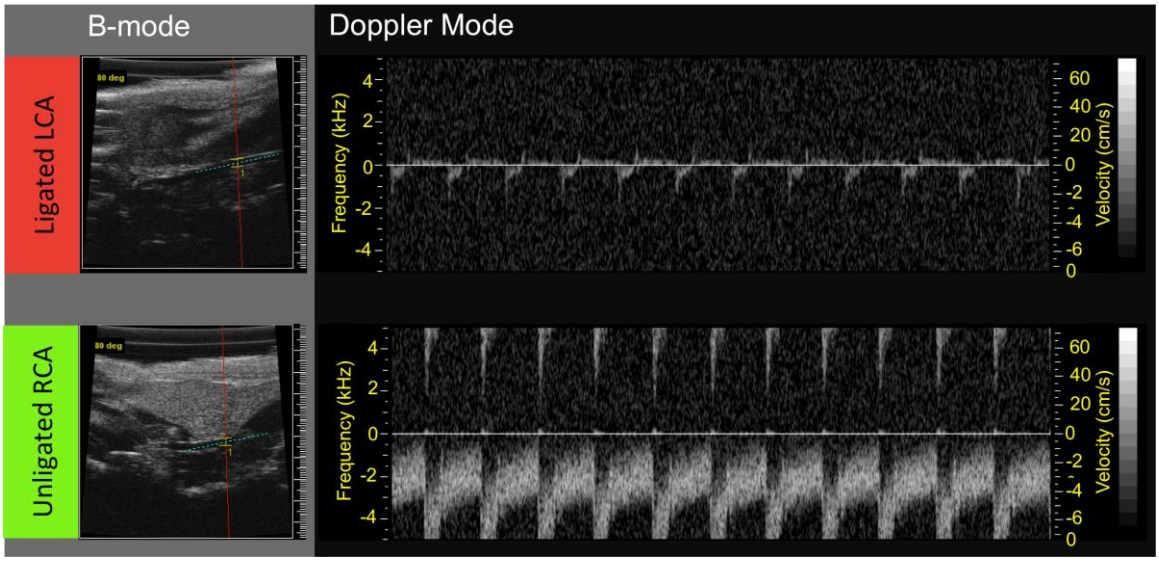

Figure 6. Ultrasound performed 1 day post-ligation demonstrating low velocity atheroprone flow and flow reversal in the ligated LCA (top) and normal pulsatile and unidirectional flow in the unligated RCA (bottom).

Four days post-ligation *in vivo* phage display was performed. Phages were injected into the tail vein of the mice at a concentration of 2 x 10^{11} plaque forming units. After 2.5 hours mice were sacrificed by CO_2 inhalation, and the carotid arteries were surgically isolated, and phages were recovered from the vessels. To increase stringency of the screening process and specificity of the phages for the target condition, arteries were washed with acidic buffer to remove weakly bound phages, and the remaining phages were recovered by cell lysis and amplified in bacteria. These phages were then re-injected in other mice with partial carotid ligation. This strategy of using successive

rounds of injection, isolation by cell lysis and re-amplification has been used previously to isolate phages that are internalized by target cells [178]. Selecting ligands that could mediate nanoparticle internalization into target cells is desired when cytoplasmic delivery of a drug is necessary, and helps to increase signal for imaging applications. After each round of phage display, titration of the phage recovered from the arteries was used to quantify relative uptake in the target LCA and control RCA. After each round, phage isolated from the target LCA were amplified, purified and re-injected for the subsequent round of phage display.

Figure 7 shows examples of phage isolations following each round of injections. From round one to round four there was a progressive increase in the number of phages binding to the target LCA (top) and no increase in binding to the RCA (bottom). The increased binding to the target LCA indicated that clones were being selected that preferentially accumulated in vessels exposed to disturbed flow.

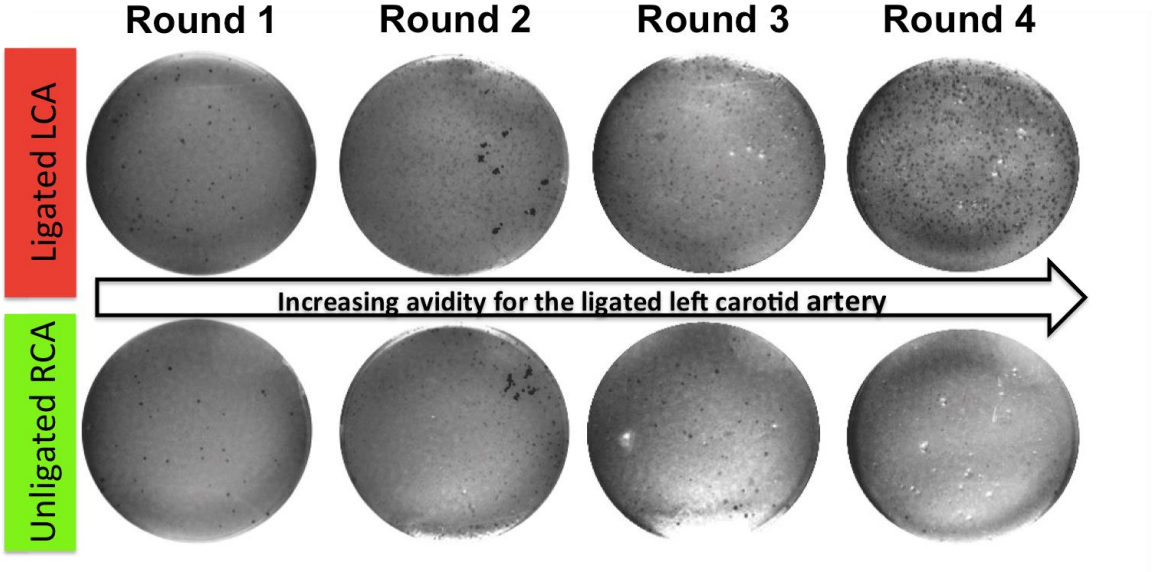

Figure 7. *In vivo* phage display titration results. The top plates are infected with M13 recovered from the ligated LCA and have progressively more plaques (black dots) in each round while the lower plates are infected with M13 from the RCA and do not increase in number with each progressive round of phage display.

After round three and four of phage screening, 10 plaques from titration plates were sequenced. Four peptide sequences were identified as dominating those that selectively accumulated in the regions of disturbed flow. Two of these encoded linear 12 amino acid peptides, SLSSYNGSALAS, and, GSPREYTSYMPH. Two sequences that encoded 7 amino acid cyclic peptides were also identified, ACNTGSPYEC, and, ACTPSFSKIC. Protein BLAST was used to identify potential protein interactions (Table 2).

Table 2. Protein homology of phage displayed consensus peptides.

Sequence	**Name**	**Identity sequence**	**Accession #**
SPREYTSYMPH	Myoferlin	496-SPREYT-501	NP_001093104
SLSSYNGSALAS	Eyes absent homolog 1 isoform 2	27-SLDSFSGSALGS-38	NP_001239121
ACNTGSPYEC	Zinc finger protein	160-CHTGEKPYEC-169	AAA64428
ACTPSFSKIC	Calsyntenin 1, isoform CRA_b	187-CSPQFSQIC-195	EDL14871

Next I sought to verify that the consensus clones selectively target the atheroprone left carotid artery. In additional experiments, I amplified and injected these consensus clones following the same procedures as *in vivo* phage library panning. Titration of phage normalized to the protein content of the corresponding LCA or RCA was used to determine the relative uptake between the target and control arteries. All four consensus clones showed a significantly increased binding to the targeted LCA.

ACTPSFSKIC showed average enrichment of 7.3 fold, SLSSYNGSALAS showed enrichment of 4.9, and ACNTGSPYEC showed enrichment of 6.1, and GSPREYTSYMPH showed enrichment of 4.4 in the target artery (Figure 8). In addition, when these phages were injected into mice that had undergone a sham surgery 4 days previously, they did not accumulate differently between the LCA and RCA, which indicates that the consensus clones do not target the LCA in the absence of disturbed flow. These experiments confirmed that the consensus peptides discovered in the initial screen specifically accumulate in regions of disturbed flow.

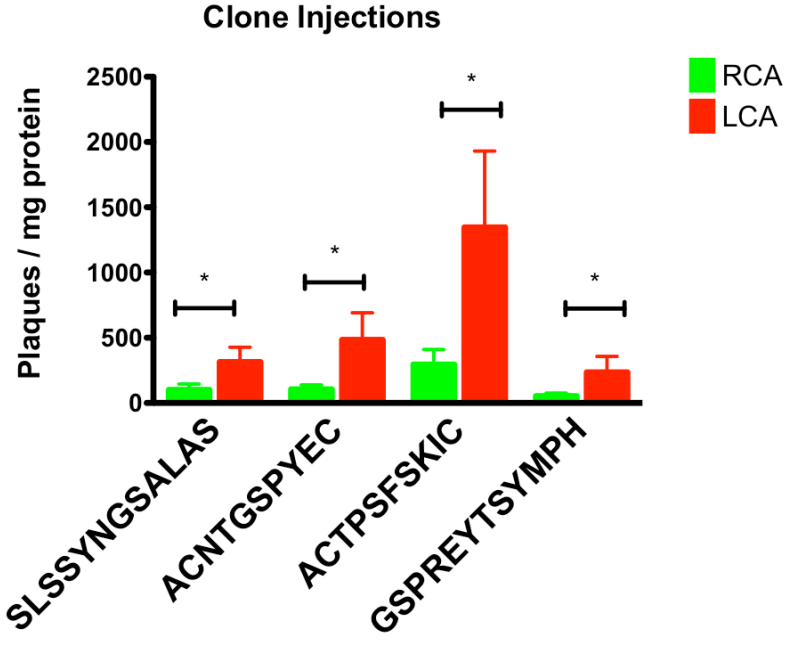

Figure 8. Clone injection titration demonstrates that all phage clones result in significantly greater binding to the ligated LCA. *, $p < 0.05$ between the RCA and LCA.

Next I sought to determine if the consensus peptide sequences targeted atheroprone vasculature in the absence of the phage particle. Two of the phage clones, SLSSYNGSALAS (DistL12) and GSPREYTSYMPH (PREY) were synthesized and

fluorescently labeled in order to measure their uptake in target tissue by flow cytometry. Flow cytometry of ligated arteries demonstrated increased immune cell infiltration into the ligated LCA compared to the unligated RCA, likely due to inflammatory activation of the endothelium as a result of disturbed flow. When individual populations of cells were examined for peptide uptake, the peptide PREY showed significantly greater binding to the atheroprone LCA compared to the un-ligated RCA. In addition, accumulation was seen in both endothelial and leukocytes but not in macrophages or other cells. This indicates that the uptake mechanism is likely due to a specific interaction and not a result of nonspecific uptake by macrophages. When injected intravenously, the fluorescently labeled peptides are cleared from the body very quickly. I hypothesize that rapid renal clearance resulted in minimal uptake in the targeted tissue. I decided to pursue this line of inquiry further with peptide-functionalized nanoparticles, which should have significantly longer circulation time.

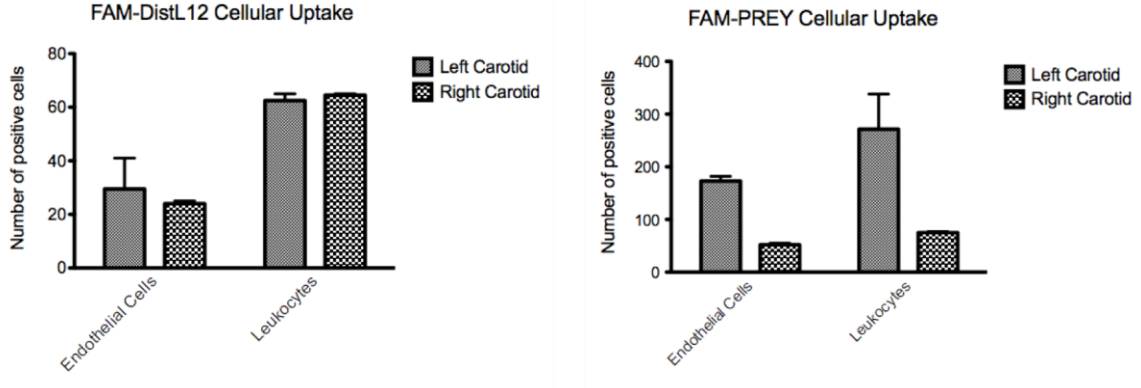

Figure 9. Flow cytometry results after FAM-labeled peptide injections demonstrated increased PREY uptake in the left carotid artery in endothelial cells and leukocytes.

The phage displayed peptide GSPREYTSYMPH (PREY) was chosen for further study due to its homology to murine myoferlin and low level of background binding to right

carotid artery. Myoferlin has regulatory roles in endothelial cells as it is critical for endocytosis, regulates vascular endothelial growth factor receptor-2 (VEGFR2) stability and function, and is implicated in endothelial membrane repair [212-214]. This peptide is an interesting candidate because VEGFR2 is known to play a role in mecahnotransduction, and endothelial membrane damage has been observed in disturbed shear stress. In addition, myoferlin is enriched in caveolae, which are also implicated in endothelial cell response to shear stress [215, 216]. I reasoned that the PREY peptide might bind to Caveolin-1, which is upregulated under oscillatory shear, and performed additional experiments to test this hypothesis.

To determine the binding partner for the PREY peptide, I employed a pull-down followed by proteomics analysis. The phage displayed peptide Acetyl-GSPREYTSYMPHGSGS-COOH (PREY) and the scrambled control peptide Acetyl-THRPMSSYEPGYGSGS-COOH (scrambled PREY) were synthesized by solid phase peptide synthesis. PREY peptides, and scrambled PREY control peptides were conjugated at the C-terminus with pentylamine-biotin by EDC-sulfoNHS coupling Biotinylated peptides were used to functionalize streptavidin conjugated paramagnetic particles. For pull-down experiments, mice were sacrificed 4 days after partial carotid ligation surgery. Carotid arteries were removed, immediately frozen in liquid nitrogen and homogenized on dry ice. Artery homogenate was dissolved in NP40 buffer and insoluble proteins were separated by centrifugation. Artery protein was incubated with peptide-conjugated beads for 1.5 hours. The beads were then washed and bound proteins were eluted in activated Laemmli sample buffer for further analysis.

Proteomic analysis indicated that several proteins from the vessels with disturbed flow bound to PREY but not by scrambled PREY controls (Table 3). The top candidates

identified by proteomic analysis could form a complex and be involved in mechanosensing [217]. I first investigated PREY binding to fibronectin, which is known to play critical roles in endothelial mecahnotransduction and activation. Recent reports have shown that oscillatory shear stress increases fibronectin in the extracellular matrix *in vivo* [218, 219]. I also investigated Filamin-A, an actin binding protein involved in cytoskeletal remodeling, regulation of cell migration and cell shape, and anchoring glycoproteins at the cell surface [220]. Filamin-A interacts with caveolin and myoferlin, and was chosen for further study due to the homology of the PREY peptide to murine myoferlin [221, 222]. In addition, a recent report shows that Filamin-A may be displayed on the cell surface in malignant cells [223]. Microarray studies have shown that Filamin mRNA is increased twofold in murine endothelial cells exposed to oscillatory shear compared to laminar shear [224]. Filamin is also recruited to sites where stress is applied to integrins [225, 226].

Table 3. Proteins identified by proteomics analysis.

Identified Proteins	Accession Number	Molecular Weight	Scrambled Abundance	Targeted Abundance
Myosin-11	tr|E9QPE7|E9QPE7	223 kDa	0	53
Filamin-A	sp|Q8BTM8|FLNA	281 kDa	0	35
Vimentin	sp|P20152|VIME	54 kDa	0	25
Protein Col6a3	tr|E9PWQ3|E9PWQ3	354 kDa	0	24
Fibronectin	sp|P11276|FINC	265 kDa	0	17
Actin, aortic smooth muscle	sp|P62737|ACTA	42 kDa	1	16
Serum albumin	sp|P07724|ALBU	69 kDa	1	15
Basement membrane-specific heparan sulfate proteoglycan core protein	tr|B1B0C7|B1B0C7	469 kDa	0	12
Collagen alpha-1(I) chain	sp|P11087|CO1A1	138 kDa	1	8
Tubulin beta-4B chain	sp|P68372|TBB4B	50 kDa	0	7

Collagen alpha-2(VI) chain	sp|Q02788|CO6A2	110 kDa	0	6
Collagen alpha-2(I) chain	sp|Q01149|CO1A2	130 kDa	1	6
Periostin	sp|Q62009|POSTN	93 kDa	0	6
Fibrinogen beta chain	sp|Q8K0E8|FIBB	55 kDa	0	6
Alpha-actinin-1	sp|Q7TPR4|ACTN1	103 kDa	0	6
Actin, cytoplasmic 1	sp|P60710|ACTB	42 kDa	0	5
Prelamin-A/C	sp|P48678|LMNA	74 kDa	0	5
Biglycan	sp|P28653|PGS1	42 kDa	0	5
Tubulin alpha-1B chain	sp|P05213|TBA1B	50 kDa	0	5
Fibrinogen gamma chain	sp|Q8VCM7|FIBG	49 kDa	0	4
Decorin	sp|P28654|PGS2	40 kDa	0	4
Fibrillin-1	sp|Q61554|FBN1	312 kDa	0	4
Aconitate hydratase, mitochondrial	sp|Q99KI0|ACON	85 kDa	0	4
Protein Fga	tr|E9PV24|E9PV24	87 kDa	0	4
Fatty acid synthase	sp|P19096|FAS	272 kDa	0	4
Collagen alpha-1(VI) chain	sp|Q04857|CO6A1	108 kDa	0	3
Trifunctional enzyme subunit alpha, mitochondrial	sp|Q8BMS1|ECHA	83 kDa	0	3
Heat shock protein HSP 90-beta	sp|P11499|HS90B	83 kDa	0	3
Fibulin-5	sp|Q9WVH9|FBLN5	50 kDa	0	3
Lumican	sp|P51885|LUM	38 kDa	0	2
3-ketoacyl-CoA thiolase, mitochondrial	sp|Q8BWT1|THIM	42 kDa	0	2
Complement C3	sp|P01027|CO3	186 kDa	0	2
Fatty acid-binding protein, adipocyte	sp|P04117|FABP4	15 kDa	0	2
Spectrin alpha chain, non-erythrocytic 1	sp|P16546|SPTN1	285 kDa	0	2
Protein-glutamine gamma-glutamyltransferase 2	sp|P21981|TGM2	77 kDa	0	2
Collagen alpha-1(XVIII) chain	sp|P39061|COIA1	182 kDa	0	2

Myosin-10	sp|Q61879|MYH10	229 kDa	0	2
Asporin	sp|Q99MQ4|ASPN	43 kDa	0	2
Microfibril-associated glycoprotein 4	sp|Q9D1H9|MFAP4	29 kDa	0	2
Beta-globin	tr|A8DUK4|A8DUK4	16 kDa	0	2
Laminin subunit beta-2	sp|Q61292|LAMB2	197 kDa	0	2
Dedicator of cytokinesis protein 11	r-sp|A2AF47|DOC11	238 kDa	0	2

Increased binding of fibronectin and Filamin-A to PREY functionalized beads in vessels with disturbed flow was further confirmed by immunoblotting. Pulldowns were performed as described previously and eluted protein was used for western blot. Fibronectin was visualized as a single band at 265 kDa (Figure 10A) and Filamin-A was visualized as a single band at 281 kDa (Figure 10B). These results showed greatest band intensity in both fibronectin and Filamin-A from ligated LCA with targeted peptide, confirming that the PREY peptide pulls down fibronectin and Filamin-A. These results also demonstrate that fibronectin and Filamin are selectively pulled down in greater quantity from the ligated artery compared to the unligated control. Because the PREY peptide specifically isolated several proteins from artery homogenate, I can hypothesize that the co-precipitation of these proteins is due to binding of the PREY peptide with any one of the proteins identified by proteomics analysis that are connected to one another. These data indicate that the PREY peptide may bind to a protein complex involved in mecahnotransduction of disturbed shear.

In additional experiments, I employed immunofluorescence to visualize Filamin-A in carotid arteries. These confirmed that Filamin-A protein expression is increased in vessels exposed to disturbed flow, and that it appears to localize with the luminal

endothelial cell surface (Figure 10C). Luminal localization of the proteins involved in binding is important considering that intravascular delivery of therapeutics would require a potential target to be displayed on the luminal surface.

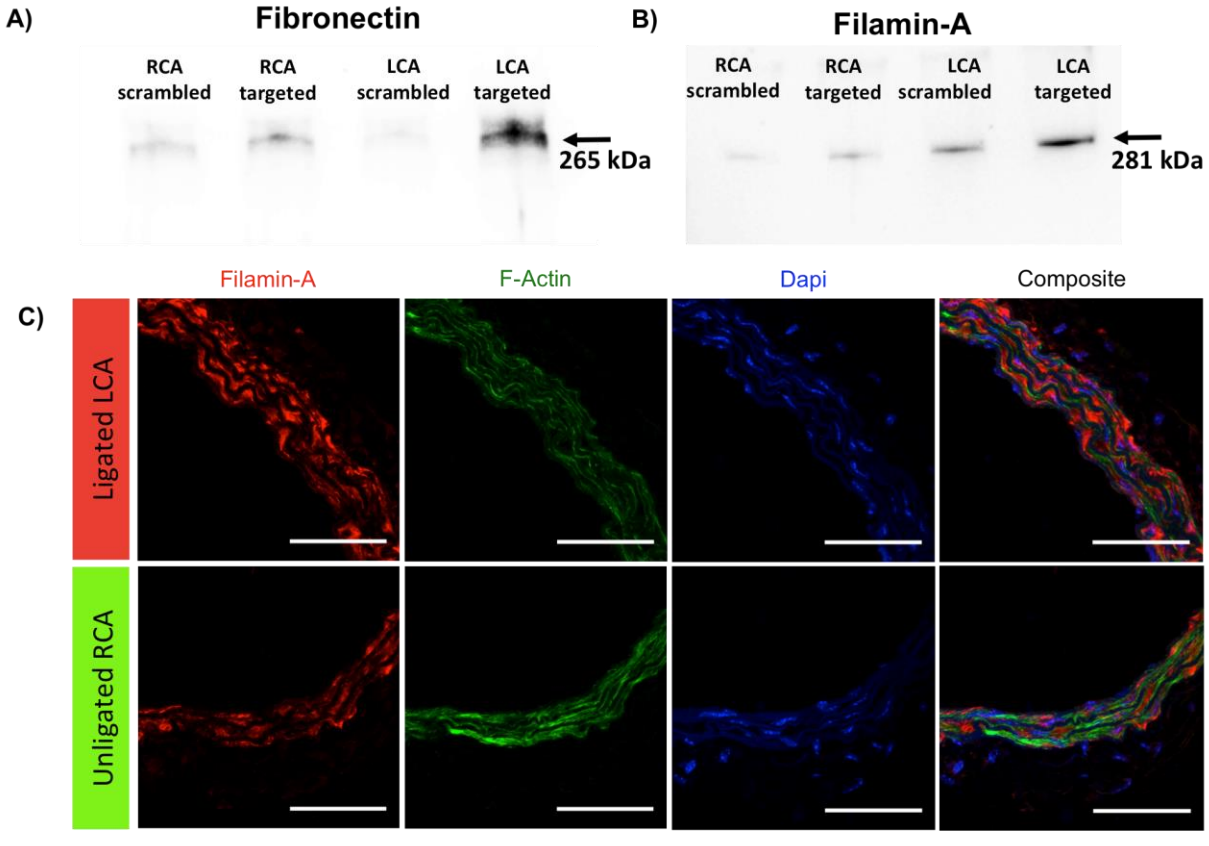

Figure 10. Validation of proteomic analysis A) Immunoblot of fibronectin after pulldown with PREY and scrambled PREY. B) Immunoblot of Filamin-A after pulldown with PREY and scrambled PREY. C) Immunostaining of Filamin-A in mouse carotid artery sections. Red= Filamin-A, Green = F-Actin, Blue = nucleus. Scale bars are 50 µm.

CONCLUSIONS

In this aim, I sought to use phage display biopanning to discover new biomarkers to allow the detection of atheroprone vasculature exposed to oscillatory shear stress. *In vitro* phage display was employed in a cone-in-plate culture system, which was

designed and characterized to show endothelial responses to flow under constant laminar versus oscillatory shear stress. *In vitro* biopanning in this system did not yield consensus peptides that could be used for further experiments. However, *in vitro* panning did demonstrate an increased affinity for the phage library to the cone-in-plate generated condition of disturbed flow. The lack of a consensus sequence from *in vitro* phage panning could indicate that the panning procedure was not stringent enough, or that the presence of too many molecular targets confounded analysis of phage clones recovered. I next performed phage panning *in vivo* in a partial carotid ligation model of disturbed flow. I reasoned that *in vivo* panning would allow me to screen peptides against a more physiologically relevant environment, and would also increase the stringency of the screening process. After four rounds of *in vivo* phage display I identified two linear and two cyclic peptide consensus that dominated the phage displayed libraries. I confirmed that these clones targeted atheroprone vasculature when injected *in vivo*. This indicates that all four of these peptides may be useful for targeting atheroprone vasculature. The two linear peptides were synthesized and fluorescently labeled to determine if the peptides could target atheroprone vasculature in the absence of the phage particle. These experiments demonstrated increased uptake of the PREY peptide in endothelial cells of the ligated artery, and minimal uptake in other cell types. The DistL12 peptide did not show differential uptake between the left and right carotid arteries.

The PREY peptide was chosen for further analysis due to its homology with murine myoferlin, relatively low background biding to the RCA in clone injection experiments, and differential binding in fluorescently labeled peptide injection experiments. I performed a pulldown followed by proteomic analysis to determine a potential binding

partner for the PREY peptide. The top candidates identified in proteomic experiments are all implicated in endothelial response to shear stress. In addition, each of these proteins is potentially involved in integrin mediated signaling, and transferring mechanical tension to the actin cytoskeleton. These experiments demonstrated that the PREY peptide pulls down fibronectin and Filamin-A. From these results I can hypothesize that the PREY peptide is binding to any one of these proteins, which are bound to other top candidates. It is possible that these proteins are involved in mechanosensing of disturbed flow.

CHAPTER III

TARGETED NANOPARTICLE DEVELOPMENT AND IMPLEMENTATION

INTRODUCTION

Given the ability to selectively target atheroprone vasculature, nanomedicine offers a promising set of tools for diagnosing, treating, and preventing atherosclerosis [227]. I therefore sought to use the PREY peptide to deliver nanocarriers to atheroprone vasculature. In this aim, I tested two different nanocarrier formulations Poly(ethylene glycol)-b-poly(propylene sulfide) (PEG-PPS) encapsulated ultrasmall superparamagnetic iron oxide (USPIOs) nanoparticles, and liposomes.

PEG-PPS encapsulated USPIOs were chosen as a well-characterized nanoparticle for imaging applications. Iron oxides are garnering increased acceptance for diagnostic imaging [228]. Biodistribution of iron oxides used as an intravenous contrast agent for magnetic resonance imaging (MRI) is widely studied**.** Site-specific targeting of systemically administered nanoparticles can be achieved through the synergistic effect of molecular targeting and the nanoparticle's physical and chemical properties [229-232]. USPIOs provide several advantages for this application. Iron oxides have been rigorously demonstrated as biocompatible and in clinical use since 1983 [233, 234]. For imaging, they provide T2 and T2* MRI contrast, which enables *in vivo* localization with high sensitivity (roughly 12 times more sensitive than T1 agents) and short image acquisition times [235]. There are many examples of iron oxides encapsulated in PEG-

PPS polymers to provide water dispersiblity and extended circulation time [236-238]. In addition, polymer chemistry can be finely tuned for peptide targeting and therapeutic delivery. Dextran coated USPIOs are clinically approved MRI contrast agents and numerous studies have investigated their biodistribution and clearance from the body [233].

Liposomes have many advantages for vascular nanomedicine due to their well-documented biocompatibility, ability to carry hydrophilic, hydrophobic, or amphiphilic drugs. Liposomes also provide facile chemistry for targeting and extending circulation time [154]. Several liposomal formulations are already clinically approved for the treatment of various diseases, most notably doxorubicin encapsulated in liposomes [173]. In the context of vascular disease various liposomal targeting techniques have been employed for imaging and drug delivery and are reviewed in [227, 239-242].

APPROACH

In this aim I sought to validate nanoparticle targeting to atheroprone vasculature by functionalization of nanoparticles with the novel targeting ligands identified in aim 1. PEG-PPS polymers were synthesized and characterized and then conjugated with the peptides discovered by phage display. These nanocarriers were then evaluated for their ability to target atheroprone vasculature in the mouse partial carotid artery ligation model by MRI imaging. Liposomal nanocarriers were also functionalized with peptides identified by phage display and their ability to target atheroprone vasculature *in vivo* was evaluated by confocal microscopy. In additional experiments, I used flow cytometry to determine the cell types targeted by peptide-functionalized liposomes.

METHODS

USPIO nanoparticle synthesis

Oleic acid stabilized USPIOs with mean diameters of 3, 10, and 22 nm were fabricated by thermal decomposition according to the protocol provided by Prof. Todd D. Giorgio. All magnetic nanoparticles utilized in this project were provided by Dr. Shann Yu from the Giorgio laboratory. To synthesize USPIOS, oleic acid was heated to 100 ˚C in octyl ether in a three-neck flask. $Fe(CO)_5$ was then added and the mixture was refluxed for 4 hours at 280 ˚C. The mixture was cooled to 80 ˚C, aerated overnight, and then refluxed again for 2 hours at 280 ˚C. Varying ratios of $Fe(CO)_5$ to oleic acid were added to achieve different particle diameters. In this synthesis scheme, increasing the molar ratio of oleic acid to decreases USPIO size [236, 243]. The oleic acid USPIOs used in this study having diameters of 3,10, and 22 nm.

Polymer synthesis

Poly(propylene sulfide) (PPS) was synthesized by anionic ring opening polymerization. Under anhydrous conditions, 3 molar equivalents 1,8-Diazabicyclo[5.4.0]undec-7-ene (DBU) was added to 1mole equivalent of ethanethiol initiator and the reaction was brought to 0 ˚C on ice. Propylene sulfide was added by syringe addition with the ratio of propylene sulfide monomer to initiator determining the molecular weight. In this case, 11.2 mL DBU was mixed with 1.85mL ethanethiol, and 19.6mL propylene sulfide and reacted for 90 minutes on ice. Under these conditions, a target molecular weight of 740 g/mol would be achieved at 100% conversion. The product was end capped by reacting with 10 mole equivalents N-(2-bromoethyl)-phthalimide (13.4 g) to yield PPS-phthalamide (PPS-Phth). PPS-Phth was deprotected to yield a free amine by dissolving in ethanol and refluxing overnight at 80 ˚C in the presence of 3 mole equivalents

hydrazine hydrate and under argon atmosphere. The resultant polymer was dissolved in methylene chloride and precipitated into cold hexane 5 times and then dried overnight *in vacuo*. The final polymer product appeared as a viscous pale yellow liquid at this stage.

PS-Phth and PPS-NH_2 were characterized by nuclear magnetic resonance (NMR) and gel permeation chromatography (GPC) for composition, molecular weight and polydispersity. GPC (Agilent) was used to determine molecular weight and polydispersity (Mw/Mn, PDI) of the PPS-Phth and PPS homopolymers using HPLC-grade dimethylformamide (DMF) containing 0.1% LiBr at 60°C as mobile phase. Molecular weight calculations were conducted with ASTRA V software (Wyatt Technology) and were based on calculated dn/dc values for PPS-Phth determined through injection of serial dilutions of the polymer in conjunction with off-line refractive index monitoring.

To create diblock copolymers of NH_2-PEG-PPS, PPS-NH_2 was functionalized by reacting with 1.2 eq of N-Succinimidyl iodoacetate in DMF overnight at room temperature in the dark. The resulting PPS-N-Hydroxysuccinimide was then precipitated in cold diethylether and dried *in vacuo* and appeared as a dark red viscous liquid. Care was taken to avoid excess exposure to light. This product was then reacted by mixing with 1eq NH_2-PEG-SH (3400M.W. from Laysan Bio; Arab, AL) under an inert atmosphere for 24 hours at room temperature (Scheme 1). PEG-PPS was confirmed by NMR in anhydrous D_6MSO and GPC.

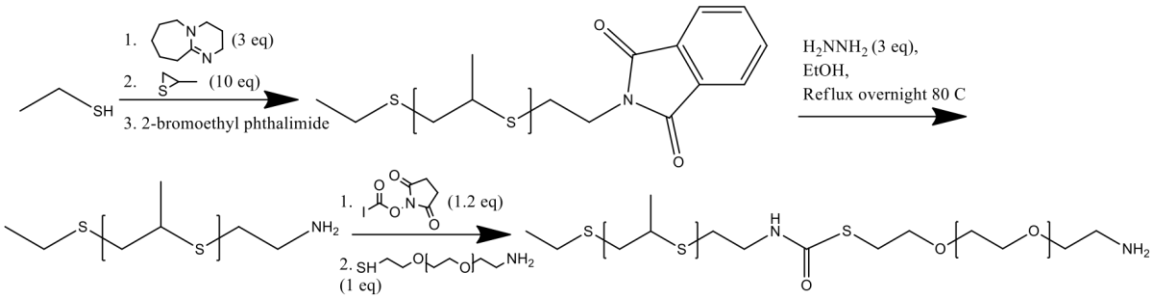

Scheme 1. PEG-PPS synthesis scheme. Step 1 is polymerization of Phth terminated PPS, step 2 is deprotection of the PPS-Phth to yield PPS-NH_2, step 3 is conjugation of PPS-NH_2 with the thiol terminus of SH-PEG-NH_2.

PEG-PPS micelle formation

Micelles were formed by a direct hydration method. PEG-PPS polymers and USPIOs were dissolved at a 1.5 polymer:USPIO ratio into a small amount of anhydrous dimethylsulfoxide (DMSO) and added to PBS without calcium and magnesium drop-wise at a rate of 8 $mL.hour^{-1}$ to a final polymer concentration of 2 $mg.mL^{-1}$. Next, excess USPIOs were removed by pelleting on a strong magnet and centrifuging at 3500 xg for 5 min and filtered through a 0.45 µm PTFE syringe filter. Micelles were characterized by dynamic light scattering (DLS), zeta potential, transmission electron microscopy (TEM), and MRI. For TEM, non USPIO containing samples were prepared by negative staining with uranyl acetate. DLS and zeta potential measurements were performed using a Malvern Zetasizer Range at a concentration of 100 $ug.mL^{-1}$. For MRI analysis, USPIO polymer samples were prepared by serial dilution from 2 $mg.mL_{-1}$ stocks, loaded into 5 mm NMR tubes, and imaged using a 4.7 T Varian small animal MRI with a 31 cm bore. Molar relaxivity (r2) values were calculated based on a linear regression of R2 values dependent on the polymer concentration in the samples.

Peptide functionalized micelle synthesis

Peptide conjugation to H_2N-PEG-PPS was performed by activation of the carboxyl terminus with 4eq of N-Hydroxysuccinimide in the presence of 4 molar equivalents dicyclohexylcarbodiimide (DCC) in DMSO. The reactants were dissolved separately in a small amount of DMSO and degassed for 30 minutes under constant nitrogen flow. Following degassing, the reagents were mixed together by syringe addition. The reaction was brought to 0 ˚C on ice for 4 hours and allowed to proceed overnight at room temperature. The resulting Peptide-NHS was precipitated into cold dietheylether five times and dried under vacuum. To perform conjugation the NHS-Peptide and H_2N-PEG-PPS were mixed in anhydrous DMSO and allowed to react for 48 hours. This product was precipitated five times into cold diethyl ether and then dried *in vacuo*. Next, the Fmoc protecting group was removed from the N-terminus of the peptide by reaction with 20% piperidine in N-Methyl-2-pyrrolidone (NMP) for 20 minutes, and then precipitated again into cold diethyl ether and dried *in vacuo*. The resultant peptide-polymer conjugates were purified by dialysis against DMSO for 24 hours and subsequently water for 48 hours. The dialyzed product was then lyophilized.

Mixed micelle characterization

Mixed micelles of Peptide-PEG-PPS were then tested for size and stability. Micelles were formed as previously described with varying ratios of Peptide-PEG-PPS to H_2N-PEG-PPS (75, 50, and 25%). The sizes of mixed micelles were then measured by DLS following the same method to characterize H_2N-PEG-PPS micelles.

MRI imaging of atheroprone vasculature

For MRI experiments, mice were injected with nanoparticles at four days post ligation at a dose of 10mg.kg^{-1} polymer. Injections were performed immediately before imaging. MRI was performed at 7.0 Tesla using a 35mm bird cage coil and mouse cradle. Mice were anesthetized with a 4% isoflurane in air mixture before being maintained under anesthesia with 1.5-2% isoflurane in air mixture. Isoflurane concentration was adjusted to maintain a respiration rate of 40-60 breaths per minute. Two MRI pulse sequences were utilized for T2 and T2* weighted contrast, and pulse acquisition was respiration gated to minimize movement artifacts.

Targeted liposome synthesis and characterization

The phage displayed peptide Acetyl-GSPREYTSYMPHGSGS-COOH (PREY) and the scrambled control peptide Acetyl-THRPMSSYEPGYGSGS-COOH (Scrambled PREY) were conjugated to 1,2-Dipalmitoyl-sn-Glycero-3-Phosphoethanolamine-N-(hexanoylamine) (DPHE, Avanti Polar Lipids, Alabaster, AL, Cat# 870125C) to form targeted liposomes by anhydrous NHS-DCC reaction (Scheme 2). Two molar equivalents of the acetylated peptide was added to 4 eq. DCC and NHS and mixed with 1 eq. DPHE dissolved in a 1:1 mixture of anhydrous DMF and anhydrous methanol under nitrogen at room temperature. Two molar equivalents triethylamine in DMF was added to the reaction to act as a catalyst. The reaction was allowed to proceed overnight, however, robust precipitation of dicyclohexylurea was observed after 30 minutes. Dicyclohexulurea is a reaction product of DCC coupling and indicates progression of the reaction. The reaction product was filtered through a 0.45 µm PTFE filter to remove insoluble products, precipitated twice into cold diethylether and dried *in*

vacuo. Reaction products were then dissolved in a 65/35/8 mixture of chloroform/methanol/water, diluted into water, and purified by flash chromatography over disposable octadecyl C_{18} columns (Bakerbond spe, Avantor Performance Materials, Center Valley, PA, Cat# 720-06). Purified peptide-DPHE products were eluted with 100% methanol, precipitated into cold diethylether, and dried *in vacuo*. Reaction products were confirmed by ESI-MS.

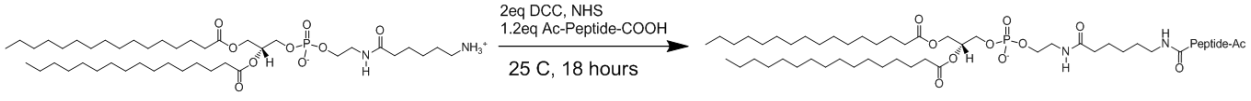

Scheme 2. DHPE conjugation to peptides. The NH2 terminus of the DPHE is conjugated to the COOH terminus of acetylated peptides by DCC/NHS coupling.

Liposomes were formed using a 97.6:2.4 molar ratio of 1,2-dipalmitoyl-sn-glycero-3-phosphocholine (DPPC, Avanti Polar Lipids, Cat# 850355C) and AcPEPTIDE-DPHE conjugates. 1,1'-Dioctadecyl-3,3,3',3'-Tetramethylindodicarbocyanine Perchlorate (DiD) or 1,1'-Dioctadecyl-3,3,3',3'-Tetramethylindotricarbocyanine Iodide (DiR) were added to the liposome mixture as a fluorescent tracer. To form liposomes, 2.08 µmol DPPC (25 $mg.mL^{-1}$ in chloroform), and 0.052 µmol AcPEPTIDE-DPHE (12.5 $mg.mL^{-1}$ in methanol), and either 0.15 µmol DiD (25 $mg.mL^{-1}$ in methanol) or 0.14 µmol DiR (25 $mg.mL^{-1}$ in methanol) were combined mixed well in a 13 x 100 mm glass test tube, dried under nitrogen and subsequently *in vacuo* for at least two hours. The mixture was re-suspended in 1.3 mL hanks buffered saline (HBS) solution containing 100 mM NaCl, 20 mM Hepes/NaOH pH 7.5 and 0.02% w/v sodium azide and sonicated for 1.5 hours to yield a 1.6 mM liposome solution containing 0.12 mM DiD or DiR. DiD containing

liposomes were used for confocal imaging, and DiR containing liposomes were used for flow cytometry, IVIS imaging, and liposome characterization experiments.

The hydrodynamic diameter was characterized on a Malvern Zetasizer Nano-ZS (Malvern Instruments Ltd., Worcestershire, U.K.).

Whole blood compatibility

Whole blood compatibility of the liposomes was determined by performing a whole blood aggregation assay as previously described [244]. Targeted liposomes were formed as previously described at 1.6 mM concentration in HBS. Serial dilutions of the liposomes were then added to human whole blood at a final liposome concentration of 1, 0.1, and 0.01 mM. As a control, the micelles were also added to HBS at the same concentration. Blood-liposome mixtures were placed on a shaker for 5 minutes and incubated at 37°C for an hour. The plates were then centrifuged at 500 ×g for 5 minutes. One hundred µL of supernatant from each well was transferred to a black, clear bottom 96-well plate and DiR fluorescence was measured with excitation λ= 750 nm and emission wavelength λ= 780 nm on a TECAN Infinite M1000 Pro plate reader (Tecan Group Ltd, Mannedorf, Switzerland).

Liposome injections

For liposome localization and targeting experiments, liposome solutions were administered to mice by intravenous injection through the tail vein four days after partial carotid ligation at a concentration of 0.9 mg fluorophore per kg body weight. Fifteen hours post injection mice were euthanized by CO_2 inhalation, and perfused with heparinized saline as described previously. Arteries were then analyzed for liposome

uptake by flow cytometry, IVIS imaging, and confocal microscopy. Liposome uptake was compared between LCA and RCA using scrambled peptide-targeted liposomes as a control.

Flow cytometry

To obtain single cell suspension solutions from sample arteries, carotid arteries were surgically removed and placed into a digestion solution consisting of phenol red free RPMI 1640 medium (Life Technologies, Grand Island, NY) with L-glutamine, 10% fetal bovine serum, 1 $mg.ml^{-1}$ collagenase A, 1 $mg.ml^{-1}$ collagenase B, and 0.1 $mg.ml^{-1}$ DNAse 1 (Roche Diagnostics, Indianapolis, IN Cat# 10103578001, 11088807001 and 10104159001, respectively). The arteries were minced with sharp scissors for two minutes and then placed on a shaker for 30 minutes at 37 ˚C. Next, the arteries were filtered using a 70 µm cell strainer to obtain cell suspensions. The cell strainer was washed three times with 10 mL RPMI 1640 to recover dissociated cells. Next, the cells were centrifuged at 300 xg for 10 minutes and then transferred to FACS tubes for the rest of processing. All subsequent steps took place in FACS buffer consisting of 1x PBS with Ca^{2+} and Mg^{2+}, 1% bovine serum albumin and 0.1% sodium azide. The cell samples were first processed by blocking Fc receptors with CD16/CD32 for 10 min at 4°C (BDbiosciences, clone 2.4G2, Cat# 553142) for 10 minutes on ice. The cells were centrifuged at 300 xg for 5 minutes and washed once with 1 mL of FACS buffer. Cell populations were characterized by Brilliant Violet 510 (BV510)-conjugated anti-CD45 antibody (BioLegend, clone 30-F11, Cat# 103137), phycoerythrin-conjugated anti-CD31 antibody (BD pharmingen, clone MEC13.3, Cat# 561073), and fluorescein isothiocyanate-conjugated anti-Ly-6A/E (Sca1) antibody (BD Pharmingen, clone E13-161.7, Cat# 553335). CD31 was considered a marker for endothelial cells, CD45 as a

marker for all leukocytes, and Sca1 as a marker for stem cells [245]. Cells were incubated with staining solutions for 30 minutes at 4 ˚C and then washed twice with FACS buffer. For dead cell staining, 7-aminoactinomycin-D (7-AAD) (eBioscience, Cat# 00-6993-50) was added to cells 10 minutes prior to sorting. Acquisition of minimum of 500,000 events was on BD FACS Canto II™ system (8-color, blue, red, violet, Cat# 338962), and analysis was performed on BD FACSDiva software version 6.1.3 (BD Biosciences).

Gating was applied based on the single stain and flow minus one controls. Dead cells and cell clumps were excluded by gating on 7-AAD and then for single cells based on forward scatter area vs. forward scatter height.

Confocal microscopy

For confocal microscopy experiments, liposomes were formulated with DiD. For all imaging experiments, mice were euthanized by CO_2 asphyxiation 15 hours post injection, and perfused with heparinized saline as described previously. For aortic arch samples mice were subsequently perfused at physiological pressure with 10% neutral buffered formalin for 5 minutes and then dissected to isolate a tissue block containing the heart, lungs, and whole aorta. Tissue blocks were further fixed in 10% buffered formalin for 24 hours, and subsequently paraffin-embedded and sectioned at 5 µm. The Vanderbilt Translational Pathology Shared Resource performed all embedding and sectioning. For carotid artery samples, the carotid arteries were surgically isolated, cannulated with 30-gauge syringe, and washed with TBST. Next, arteries were cut longitudinally to expose the endothelium, and mounted on microscope slides with 4% paraformaldehyde in PBS without Ca^{2+} and Mg^{2+}. Carotid artery samples were

counterstained with Hoechst to visualize nuclei. Fluorescence images were acquired using a Zeiss 710 confocal laser microscope.

RESULTS AND DISCUSSION

Studies with peptide targeted micelles

PPS-Phth was successfully synthesized as described previously. GPC analysis demonstrated a dn/dc = 0.1244 +/- 0.0018 mL/g. PPS-NH_2 was successfully synthesized having a molecular weight of 846 Da as determined by NMR and a polydispersity of 1.32 +/- 0.096 as determined by GPC. PEG-b-PPS synthesis was confirmed by NMR.

PEG-PPS micelles were found to have a diameter of 149.27 ± 57 nm by dynamic light scattering and 169.53± 55 nm by TEM (Figure 1A). USPIO loading in micelles was confirmed by TEM and zeta potential measurements. TEM showed a drastic increase in the electron density of the micelles after USPIO loading (Figure 1B). Loading USPIOs into polymeric micelles caused a shift in the zeta potential from negative to nearly neutral, demonstrating a shielding of the negative charge of the oleic acid stabilizing layer by the polymeric micelles (Figure 1C). The nearly neutral zeta potential is also a requirement for intravascular delivery [246].

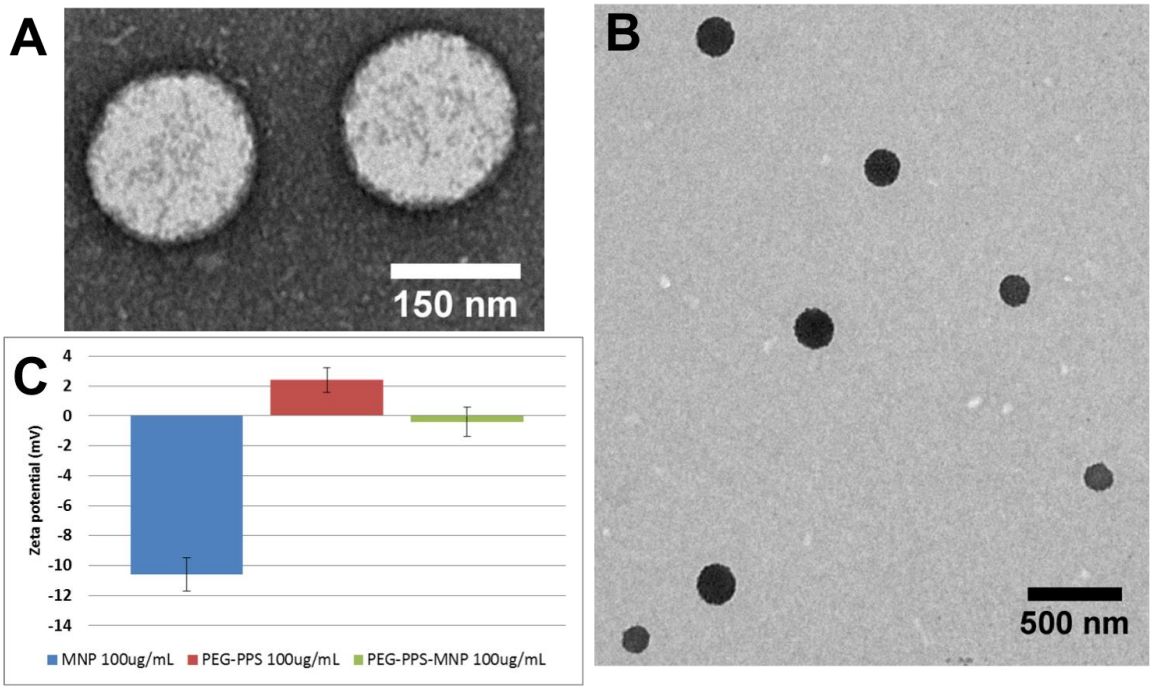

Figure 1. Characterization of PEG-PPS-USPIO micelles. A) TEM of PEG-PPS micelles demonstrated a diameter of around 170 nm. B) Encapsulation of USPIOs in PEG-PPS micelles causes an increased electron density in the core of the micelle structure, which indicates successful encapsulation. C) Charge shielding of negatively charged USPIOS was demonstrated by zeta potential measurements, which further confirmed USPIO encapsulation in PEG-PPS polymer micelles.

MRI demonstrated that loaded polymeric micelles have a molar relaxivity of 6.76 $mM^{-1}.s^{-1}$ relative to the concentration of polymer in the sample (Figure 2). This relaxivity can give a reasonable signal to noise ratio for *in vivo* targeting of these nanoparticles [235].

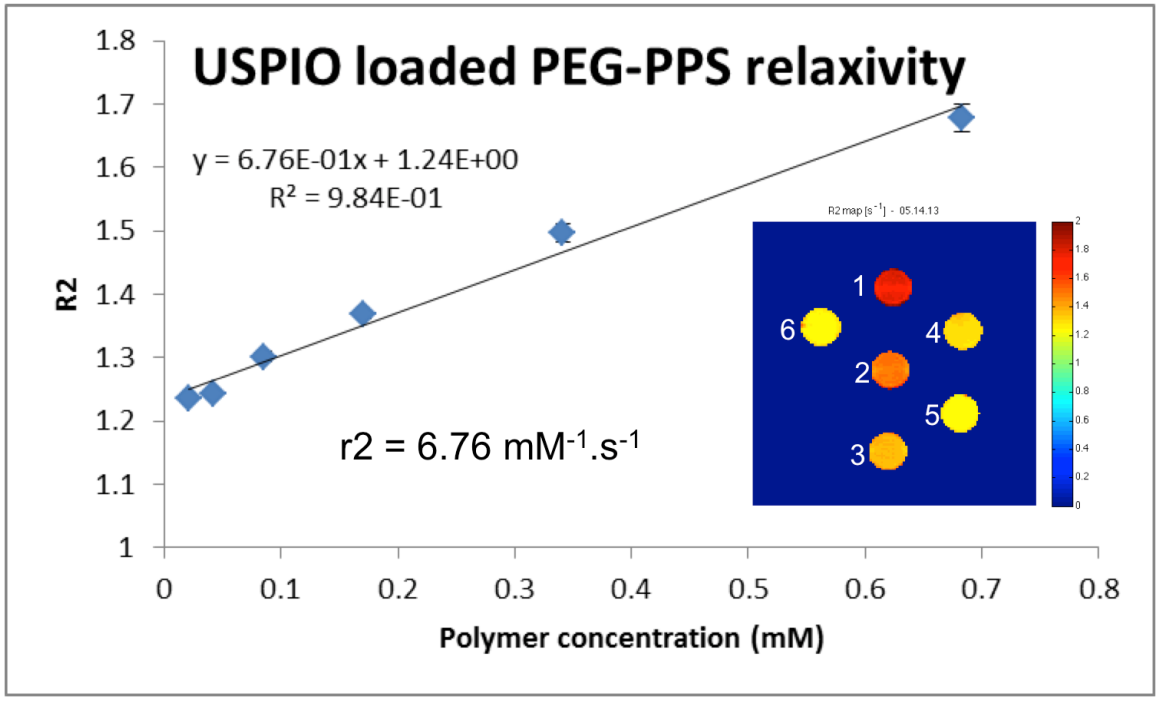

Figure 2. USPIO loaded PEG-PPS micelle molar relaxivity. The slope of the concentration versus transverse relaxation gives the molar relaxivity of the PEG-PPS-USPIO nanoparticles. The inset shows heatmap of transverse relaxivity taken as a cross section of nanoparticle samples in the MRI.

Mixed micelles of 25 and 50% DistL12-PEG-PPS, and FAM-PREY-PEG-PPS content were found to be stable in PBS at a concentration of 100 mg.mL^{-1}. Micelles of 75% DistL12-PEG-PPS, 25% PEG-PPS and 75% FAM-PREY-PEG-PPS, 25% PEG-PPS content were found to destabilize at the same concentration (mg.mL^{-1}) as evidenced by the formation of large aggregates during DLS measurements (Figure 3). Due to the destabilizing effect of the DistL12 peptide, 20% DistL12-PEG-PPS and FAM-PREY-PEG-PPS containing micelles were used for MRI imaging experiments.

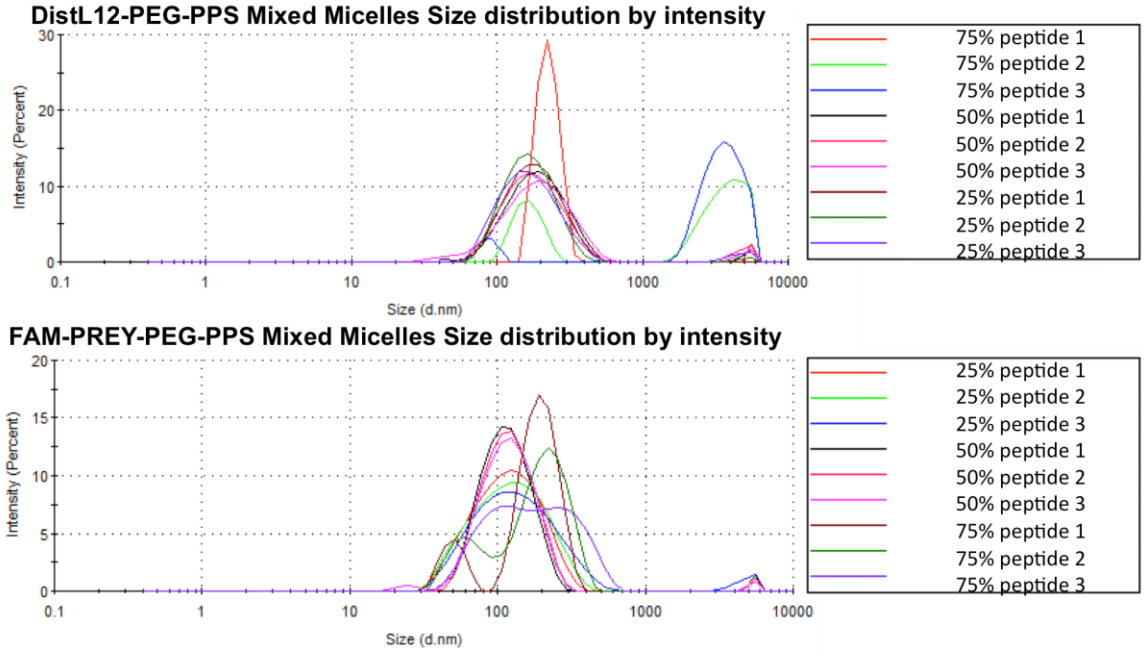

Figure 3. Mixed micelle stability. Increasing Peptide-PEG-PPS concentration resulted in a destabilization of the mixed micelles with both DistL12 and PREY peptides as evidenced by the formation of large aggregates and changes in micelle hydrodynamic diameter.

The results of this experiment using the DistL12 and FAM-PREY targeted nanoparticles are shown in figure 4. The T2* image using a bright blood Fast Low Angle Shot (FLASH) sequence shows the left carotid arteries and jugular veins clearly. I was not able to identify any signal decay as a result of iron oxide nanoparticle accumulation in the carotid arteries. Potential issues include renal clearance, low concentrations of iron oxides, and instability of PEG-PPS-USPIO nanoparticles. Published values for similar studies indicate dosages of around 5-30 $mg.kg^{-1}$ of iron injected and the concentration that was used for this study was 10 $mg.kg^{-1}$ [179, 247]. Another potential issue with these nanoparticles is instability in blood. The core block polymer synthesized was around 850 Da while the PEG block was 3500 Da. Generally, amphiphilic polymers

synthesized for micelle applications should have a hydrophobic core block around 2 times the molecular weight of the hydrophilic block. Based on these results, PEG-PPS-USPIO nanoparticles were not pursued as a delivery platform.

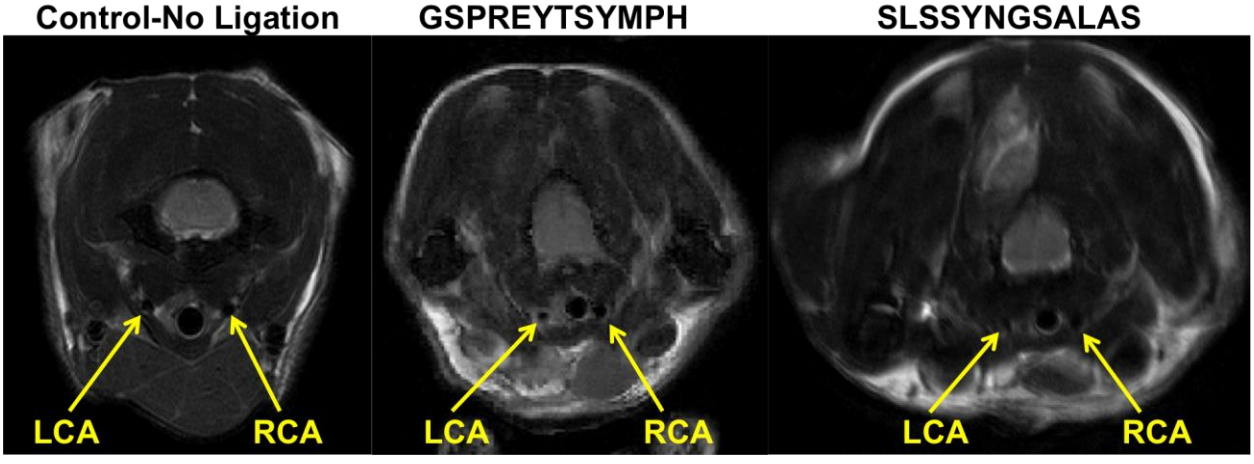

Figure 4. MRI images after targeted micelle injection. Accumulation of USPIOs should result in a signal drop (dark region). No noticeable signal drop was observed for either peptide candidate investigated.

Studies with peptide targeted liposomes

Peptide-targeted liposomes were found to have an average hydrodynamic diameter of 64 nm with a polydispersity of 0.295 by dynamic light scattering (Figure 5A). This size of liposome is inside the acceptable size range for vascular delivery of nanoparticles [248]. When incubated with whole blood or in buffer, I observed no difference in liposome stability (Figure 5B). These results indicate that targeted liposomes are compatible with blood and suitable for vascular delivery.

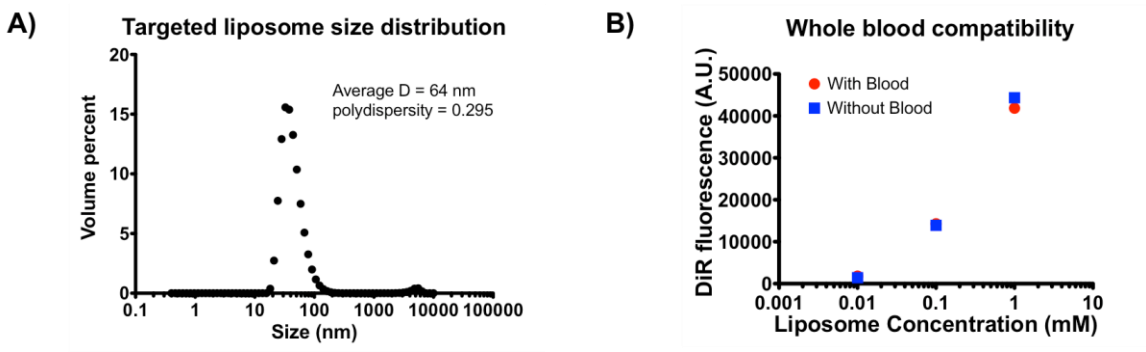

Figure 5. Liposome characterization. A) DLS measurements of targeted liposomes showed a hydrodynamic diameter of 64 nm and a polydispersity of 0.295. B) Whole blood compatibility of liposomes showed no difference between liposomes incubated in whole blood versus buffer, indicating that liposomes are stable in blood.

When injected into mice, liposomes accumulated in the spleen and liver, with negligible accumulation in the heart, lungs, kidneys, and other tissues (Figure 6). This biodistribution is characteristic for clearance of liposomes with similar composition, and also indicates a low risk for cardiac or pulmonary toxicity [249].

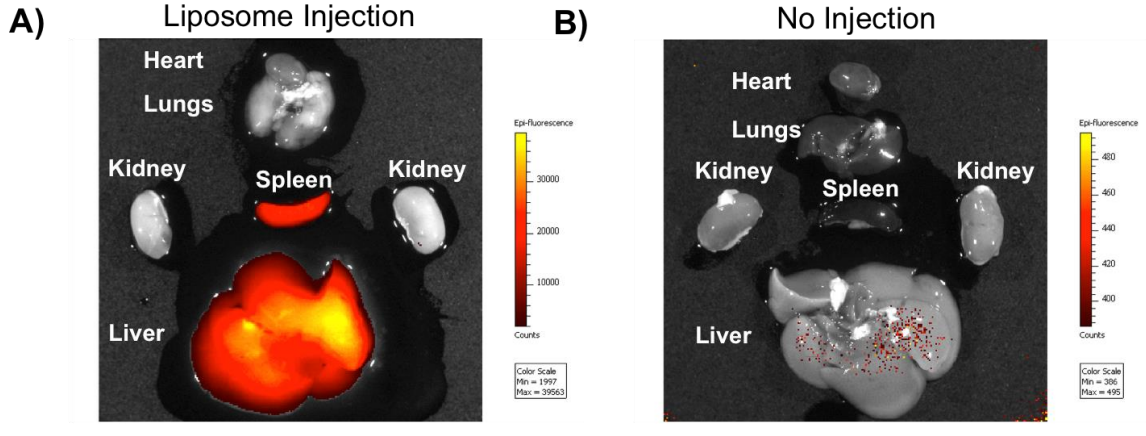

Figure 6. Liposome biodistrubution measured by IVIS. A) Liposome injection B) No liposome injection. These results demonstrated clearance routes similar to other liposomes of comparable physical characteristics.

To visualize nanoparticle targeting to atheroprone vasculature, liposome solutions (0.9 mg fluorophore per kg body weight, 1.6 mM lipids in HBS) were administered to mice by intravenous injection through the tail vein four days after the partial ligation procedure. Fifteen hours post injection, mice were euthanized and arteries were analyzed for liposome targeting. Liposome uptake was compared between LCA and RCA using scrambled PREY-conjugated liposomes as a control.

Figure 7A shows *en face* preparations of ligated left carotid arteries after liposome injection. I found that PREY-targeted liposomes accumulate in the partially ligated LCA (Figure 7A, bottom) while scrambled PREY-conjugated liposomes showed minimal uptake in the ligated vessel (Figure 7A, top). I also investigated uptake of targeted nanoparticles in the lesser curvature of the aortic arch, another vascular location known to have disturbed flow [67]. Figure 7C shows a cross section of the aortic arch of a mouse after liposome injection. I observed accumulation of PREY targeted liposomes in the lumen at the inner curvature of the aortic arch in mice without partial carotid ligation surgery. These results demonstrate that PREY-targeted liposomes home to natural regions of disturbed flow *in vivo.*

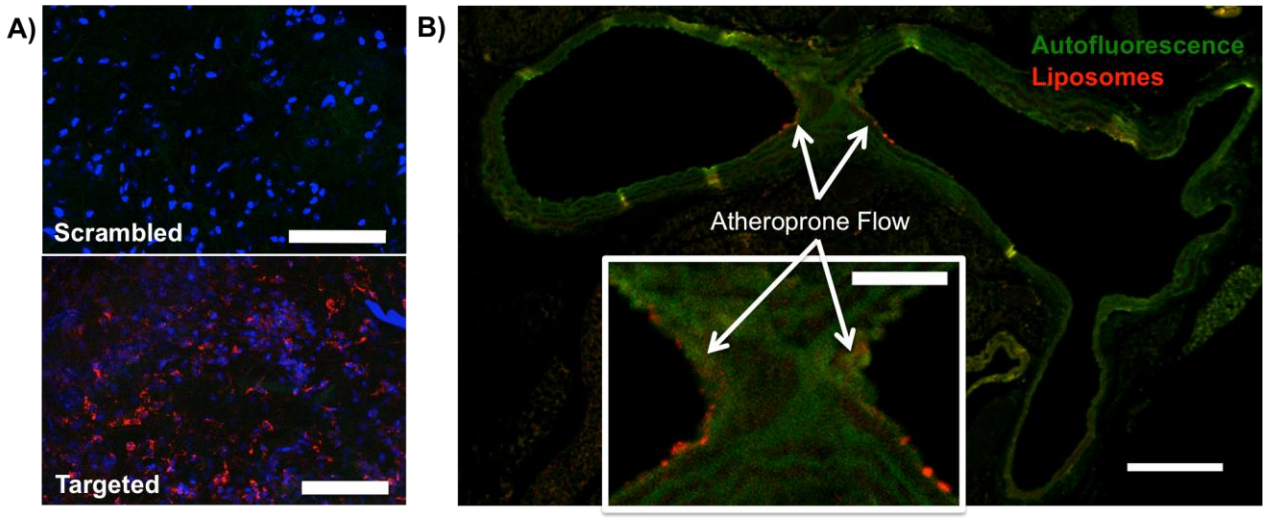

Figure 7. *En face* preparations of ligated left carotid arteries with scrambled and targeted liposome injections. Red = liposome fluorescence, blue = nuclei, Green = Elastin autofluorescence, scale bars = 100 µm. D) Cross section of a mouse aortic arch showing targeted liposome accumulation in the lesser curvature of the aortic arch (inset). Green = elastin autofluorescence, Red = Liposome fluorescence, scale bar = 250 µm, inset scale bar = 100 µm.

Next I sought to determine the vascular cell type targeted by PREY liposomes. To do this, I performed flow cytometry on arteries after liposome injection. Single cell suspensions from the LCA and RCA were co-stained with platelet endothelial cell adhesion molecule (CD31) as a marker for endothelial cells, protein tyrosine phosphatase receptor type C (CD45) as a marker for all leukocytes, and stem cell antigen-1 (Sca1) as a marker for stem cells which are known to reside in the vascular adventitia [245]. Dead cells and cell clusters were excluded from analysis. This analysis showed that PREY-targeted liposomes accumulate in $CD31^+$ endothelial cells significantly more than scrambled PREY-conjugated liposomes (Figure 8A). Increased uptake of liposomes in the left carotid artery was also observed in $CD45^+$ and $Sca1^+$ cells; however, no significant difference was observed between PREY and scrambled

PREY liposomes (Figure 8B, C). This is likely due to nonspecific uptake of liposomes by these cell types, which are known to accumulate in vasculature with activated endothelium.

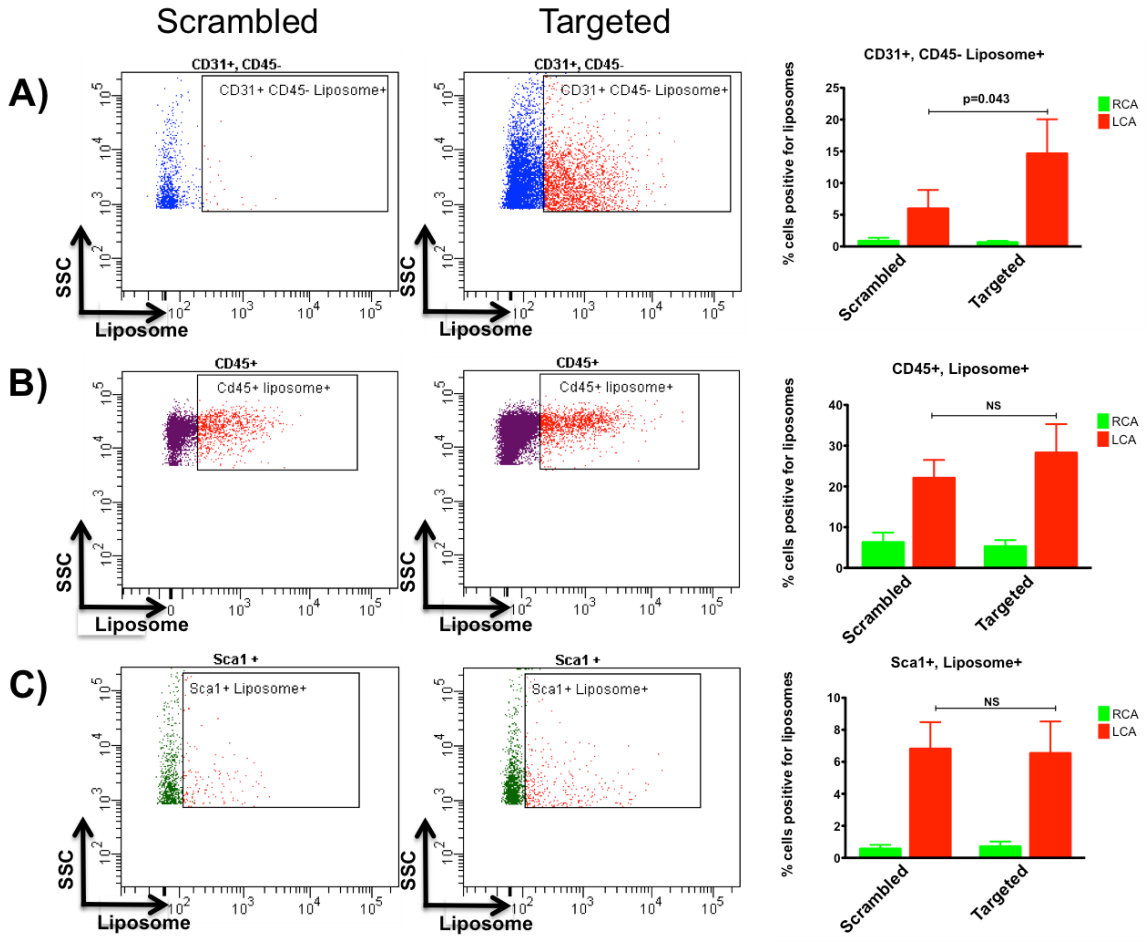

Figure 8. Flow cytometry analysis of cellular targeting. A) $CD31^+$, $CD45^-$ cell population B) $CD45^+$ cell population C) $Sca1^+$ cell population. These results demonstrate significantly greater uptake of PREY targeted liposomes compared to scrambled PREY liposomes in endothelial cells but not leukocytes of stem cells.

CONCLUSIONS

Atherosclerotic lesions develop when focal endothelial dysfunction caused by

disturbed shear stress is compounded by systemic risk factors such as hypercholesterolemia. Targeted drug delivery to areas of disturbed flow is a promising approach to prevent atherosclerosis before lesions develop. Because prediction of these atheroprone areas is speculative, programming nanocarrier functions to navigate to and detect atheroprone areas is an ideal but unmet need. I accomplished this with peptides discovered by *in vivo* phage display and functionalized two nanoparticle candidates; PEG-PPS-USPIO nanoparticles for MRI imaging, and liposomes for drug delivery.

PEG-PPS polymers were successfully synthesized and were found to encapsulate USPIOs in 160 nm micelles. These USPIO loaded PEG-PPS nanoparticles were functionalized with two peptide candidates from *in vivo* phage display to form targeted nanoparticles for MRI imaging of atheroprone vasculature. *In vivo* injections of the nanoparticles were performed and did not result in discernable signal drop in the targeted LCA. Additionally, the drug candidate used in aim 3 is hydrophilic and PEG-PPS-USPIO nanoparticles are not able to encapsulate hydrophilic drugs. Based on the results of studies with PEG-PPS-USPIO nanoparticles, they were abandoned as theranostic delivery platforms for the remainder of my work.

PREY-functionalized liposomes were synthesized with a diameter of around 65 nm and were shown to be stable in whole blood. I also demonstrated that PREY-targeted liposomes accumulate in areas of disturbed shear *in vivo*. Using flow cytometry, I showed that PREY-targeted liposomes home to endothelial cells in atheroprone vasculature, making this nanocarrier a promising candidate for drug delivery to treat endothelial dysfunction. In the next experiments, I demonstrated drug delivery to areas of disturbed flow *in vivo* using the PREY-targeted liposomes

developed in this aim.

CHAPTER IV

TARGETED DELIVERY OF THERAPEUTIC LIPOSOMES

INTRODUCTION

Oxidative stress is a major cause of endothelial dysfunction in diseases such as atherosclerosis, hypertension and diabetes [9, 10]. Previous studies have shown that a major source of reactive oxygen species in endothelial cells exposed to disturbed flow is uncoupled nitric oxide synthase [28]. Tetrahydrobiopterin (BH_4) is a critical co-factor for the NO synthases. BH_4 permits transfer of electrons from the prosthetic heme group to the guanidino-nitrogens of L-arginine, allowing formation of NO. In the absence of BH_4, electrons from the NOS heme group reduce oxygen to produce superoxide. Disturbed shear on endothelial cells results in an uncoupling of the eNOS enzyme while laminar shear causes a 2 fold increase GTPCH-1 phosphorylation and increases its activity 30 fold. This increases the synthesis of BH_4, while it is deficient in endothelial cells exposed to oscillatory shear stress [33, 127]. BH_4 oxidation to inactive BH_2 also occurs in endothelial cells exposed to disturbed flow and further depletes intracellular BH_4. In the partial carotid ligation model, studies have confirmed that BH_4 levels are reduced, and that oral supplementation of BH_4 can recouple NOS and abrogate the accelerated atherosclerosis that occurs in the ligated artery [28, 57, 153]. Challenges associated with delivery of exogenous BH_4 include oxidation and poor cellular uptake in endothelial and parenchymal cells [62]. BH_4 is also a cofactor for the synthesis of catecholamines, which could lead to unexpected effects on neurological and vascular function if administered systemically [33]. I therefore sought to use the PREY-targeted

liposomal nanocarriers to protect BH_4 from oxidation in circulation and deliver BH_4 to endothelial cells in atheroprone regions.

APPROACH

Previous experiments demonstrated that PREY-targeted liposomes home to endothelial cells in regions of disturbed flow, making them an ideal candidate to deliver therapeutics to dysfunctional endothelium. Studies have also shown that delivery of BH_4 can rescue endothelial dysfunction in response to disturbed shear stress. In this aim, I sought to deliver BH_4 using PREY-targeted liposomes. We examined the delivery of BH_4 to target tissue, and measured superoxide as a functional readout of endothelial dysfunction. In additional experiments, I investigated the effect of PREY-liposome BH_4 delivery on endothelium dependent relaxation and plaque formation in $ApoE^{-/-}$ mice.

METHODS

Tetrahydrobiopterin (BH_4) encapsulation and protection from oxidation

BH_4 was encapsulated in liposomes by a thin film rehydration technique [250]. First, lipids in organic solvent were dried as previously described. Immediately before formation of liposomes, BH_4 was dissolved in HBS at 17 mM. Lipids were then reconstituted in 17 mM BH_4 in HBS, and sonicated for 1.5 hours to form liposomes. We tested the encapsulation efficiency by dialyzing liposome solutions overnight against HBS buffer using 3500 molecular weight cutoff cellulose acetate dialysis tubing and measuring BH_4 concentrations post-dialysis (Spectrum labs, Grand Rapids, MI). BH_4 is commonly administered with L-ascorbic acid as an antioxidant, therefore, I also tested co-encapsulation of BH_4 with L-ascorbic acid, by adding 0.04% L-ascorbic acid to HBS

buffer before addition of BH_4 [57]. Because BH_4 rapidly oxidizes in physiological conditions, the ability of the liposomes to protect BH_4 from oxidation was examined. Liposomes formed with BH_4 were incubated at 1.7 mM in 50% FBS in HBS. Samples were collected at 30 minutes and 24 hours to determine the amount of BH_4 remaining in solution.

Nanoparticle delivery of BH_4

Liposomes containing BH_4 were administered one-day post ligation by tail vein injection at 0.9 mg fluorophore per kg body weight. Animals studied included apolipoprotein E knockout ($ApoE^{-/-}$) and C57/BL6J mice. Seven days post ligation, animals were sacrificed and endpoint analysis performed.

Quantification of BH_4

BH_4 concentrations were measured by HPLC as previously described [28, 251]. To analyze arterial levels of BH_4, seven days post ligation mice were sacrificed by CO_2 inhalation and perfused with ice cold heparinized PBS. Carotid arteries were surgically isolated, and care was taken not to stretch or damage the arteries. Carotid arteries were then snap frozen in liquid nitrogen. To obtain artery homogenate, carotid arteries were ground using a mortar and pestle pre-cooled on dry ice. Artery homogenate was then dissolved in 110 µL lysis buffer (50mM Tris-HCl, pH 7.4, 1 mM dithiothreitol, and 1 mM ethylenediaminetetraacetic acid) and 12.5 µL of a 1:1 mixture of 1.5 M $HClO_4$ with 2 M H_3PO_4 was added to precipitate proteins. Samples were then centrifuged at 13,500 g for 2 minutes at 4 °C. Next, differential oxidation was performed in acid and alkaline preparations. BH_4 was detected by fluorescence (Ex. 350 nm Em. 450 nm) at a retention time of 9.5 minutes using a 5 x 250 mm x 5 um C_{18} column was used with an

isocratic solvent system consisting of 95% water with 5% methanol at a flow rate of 1 $mL.min^{-1}$. Concentrations were normalized to protein content as measured by BCA assay according to manufacturer's protocol.

Measurement of superoxide

To evaluate the effect of nanoparticle treatment on vascular ROS production, 2-hydroxyethidium formation from dihydroethidium (DHE) was measured by HPLC as previously described [252]. To measure arterial superoxide, 7 days post ligation mice were sacrificed by CO_2 inhalation and perfused with ice-cold Krebs-HEPES buffer containing 99 mM NaCl, 4.69 mM KCl, 25 mM $NaHCO_3$, 1.03 mM KH_2PO_4, 5.6 mM D(+) Glucose, 20 mM Na-HEPES, 2.5 mM $CaCl_2$ x $2H_2O$, and 1.2mM $MgSO_4$ x $7H_2O$. Carotid arteries were surgically isolated and care was taken not to stretch or damage the arteries. Each carotid artery was placed on 1 mL ice-cold krebs-HEPES buffer and carefully trimmed to remove adventitial fat. Each artery was then cut into 5 equally sized rings. A 5 µM stock solution of DHE in anhydrous DMSO was created by degassing DMSO under nitrogen for 30 minutes and adding to fresh DHE. 5 µL of this stock solution was added to each artery, and the samples were incubated in the dark at 37 °C for 30 minutes. Next, the artery rings were placed in 300 µL ice-cold methanol and homogenized using a dounce homogenizer. Samples were then filtered through 0.2 µm PTFE filters and stored at -80 °C in the dark until running. 2-hydroxyethidium was detected by fluorescence (Ex. 480 nm, Em. 580 nm) at a retention time of 13.5 minutes using a 4.5 x 250 mm reverse phase C_{18} column (Nucleosil, Sigma-Aldrich, St. Louis, MO) and a mobile phase of 60% acetonitrile with 0.1% trifluoroacetic acid with a linear increase in acetonitrile concentration from 37% to 47% over 23 minutes at a flow rate of 0.5 $mL.min^{-1}$.

Endothelium dependent relaxation

To quantify endothelium dependent relaxation, 7 days post ligation carotid rings from the ligated LCA of ApoE$^{-/-}$ animals were subjected to isometric tension studies using a multi-wire myograph system. Artery rings were equilibrated for 30 minutes with in myography buffer, pre-constricted using phenylephrine, and then exposed to increasing concentrations of acetylcholine to assess endothelium dependent vasodilation. Endothelium independent relaxation in response to NO donor sodium nitroprusside was also examined [153].

Quantification of plaque burden in ApoE$^{-/-}$ mice

ApoE$^{-/-}$ mice received the partial carotid artery ligation surgery and were immediately fed a western diet (Teklad #88137, 42% from fat, Harlan Laboratories, Indianapolis, IN) [253]. Seven days post ligation mice were sacrificed by CO_2 inhalation. Mice were then perfused with ice-cold heparinized saline and then perfused at physiological pressure with 10% neutral buffered formalin. Next, carotid arteries were surgically removed, cleaned of excess adventitial fat, and mounted in optimal cutting temperature (OCT) mounting medium (TissueTek, VWR, Radnor, PA). Cryosections were obtained at 5 µm thickness. Sections were stained with Hematoxylin and Eosin. To quantify plaque burden, lumen area was traced and plaque area expressed as a percentage of the total lumen area. Average lumen area covered was calculated for N=4 animals per group.

Serum lipid analyses

Blood was collected into a heparinized syringe by cardiac puncture after sacrifice. The serum total cholesterol and triglyceride levels were determined in serum samples using enzymatic assays (Roche). Fast performance liquid chromatography was performed on an HPLC system model 600 (Waters, Milford, MA) using a Superose 6 column (Pharmacia, Piscataway, NJ) in both groups of samples (n=4 and n=4).

RESULTS AND DISCUSSION

I sought to determine if PREY-targeted nanoparticles could be used for drug delivery to improve endothelial function in atheroprone areas under disturbed flow. BH_4 was encapsulated in liposomes by a thin film rehydration technique [250]. BH_4-containing liposomes were found to have the same hydrodynamic diameter of 65 nm as liposomes prepared without BH_4. I measured the encapsulation efficiency of BH_4 by dialyzing liposomes formed with BH_4 for 18 hours and measuring BH_4 concentration remaining by HPLC. These experiments demonstrated a loading efficiency of around 6%. This loading efficiency is expected for the encapsulation technique used [250, 254, 255]. In addition, it is possible that some BH_4 is oxidized during dialysis, and therefore the resulting BH_4 measured after dialysis could result in artificially lower encapsulation efficiency. In addition, incorporation of L-ascorbic acid as an antioxidant buffer destabilized the liposomes and resulted in zero encapsulation. Based on these results, for all the following experiments I used liposome encapsulated BH_4 as formed, without addition of L-ascorbic acid and without overnight dialysis. In this setting, I found that liposome encapsulated BH_4 was significantly more stable than free BH_4 over 24 hour incubation in 50% serum (Figure 1). This result demonstrated that liposome stability

was not compromised by encapsulation of BH_4 and that liposomes could be used to deliver BH_4 to target tissues.

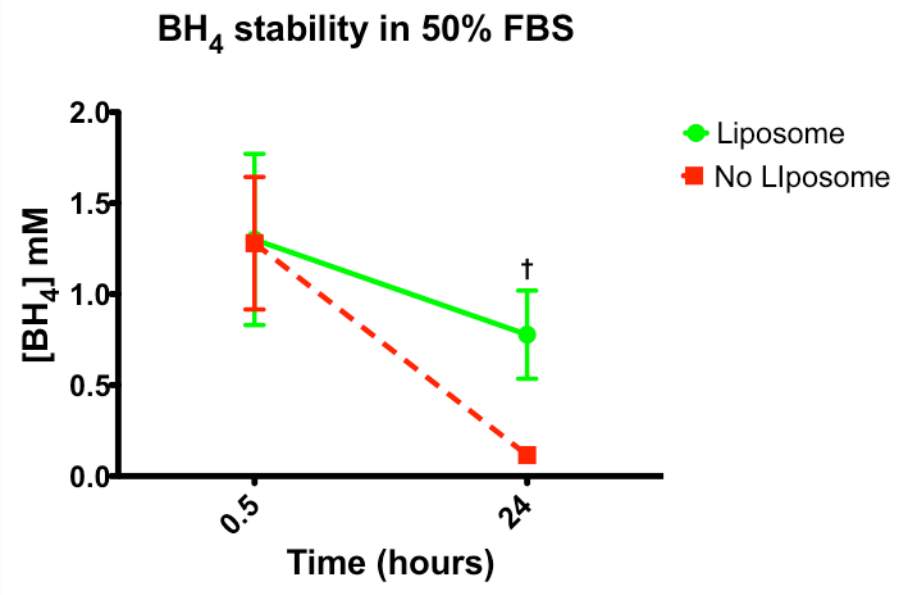

Figure 1. Liposomes maintained the stability of BH_4 in serum significantly more than un-encapsulated BH_4 after 24 hours, indicating the ability of liposomes to encapsulate and protect BH_4 from oxidation. †, $p = 0.017$.

To determine if targeted nanoparticles could increase BH_4 concentration in target tissue, targeted nanoparticles containing BH_4 were injected by tail vein one-day post ligation in wild-type mice and the carotids were removed for measurement of pterins seven days later. PREY targeted nanoparticles were found to significantly increase BH_4 concentration in target tissue compared to scrambled PREY controls (Figure 2). In mice without liposome treatment, BH_4 levels in the ligated artery are around 50% of the unligated artery. In these experiments scrambled PREY liposomes resulted in a modest increase in BH_4 in the ligated artery. This is likely due to uptake of scrambled PREY liposomes by monocytes in the ligated artery, as observed in flow cytometry

experiments from aim 2. Earlier experiments showed that PREY-targeted liposomes selectively target endothelial cells in the ligated LCA. Because eNOS is the dominant NOS isoform in vasculature, I reasoned that increases in BH_4 in the PREY targeted group were largely delivered to endothelial cells. BH_4 delivery to endothelial cells would reduce total vascular superoxide resulting from recoupling of eNOS, therefore I next measured vascular superoxide after nanoparticle delivery.

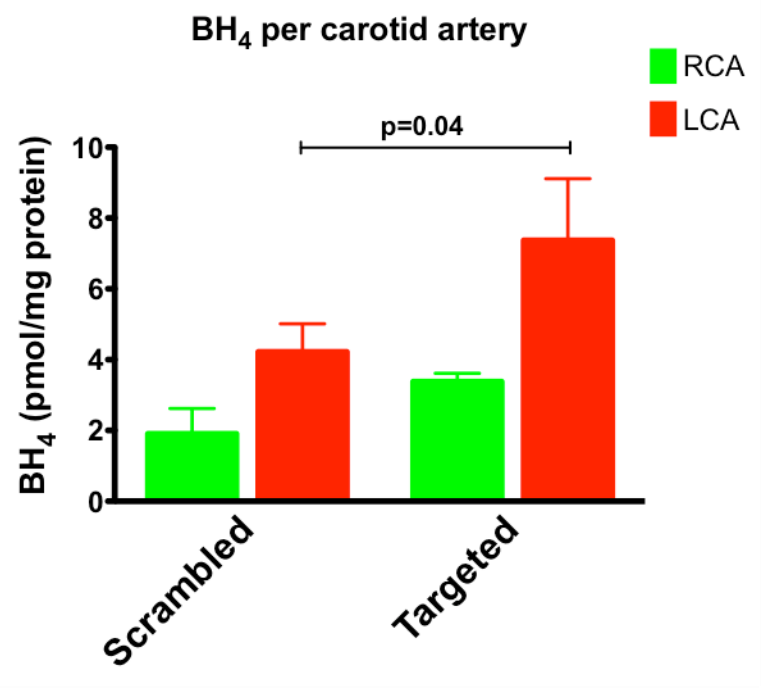

Figure 2. Liposome delivery significantly increased BH_4 concentration in the ligated artery with targeted liposomes but not with scrambled controls. This result indicates the efficacy of PREY-targeting in delivering BH_4 to atheroprone arteries.

I measured superoxide levels in carotid arteries by monitoring the conversion of DHE to its superoxide adduct, 2-hydroxyethidium. PREY-targeted liposome delivery of BH_4 significantly decreased superoxide in the ligated artery compared to scrambled peptide controls (Figure 3). In animals without liposome treatment, superoxide levels are around

2 times greater in the ligated artery. This trend is mirrored by scrambled PREY liposomes in this experiment. Combined with a modest increase in BH_4 levels in the ligated artery in scrambled PREY treated animals, this result further confirms that increased BH_4 observed from scrambled PREY liposomes were due to uptake by immune cells in the ligated artery. These results indicate that targeted delivery of BH_4 can successfully increase the availability of this critical cofactor in endothelial cells and reduce oxidative stress in ligated arteries resulting from uncoupled nitric oxide synthase.

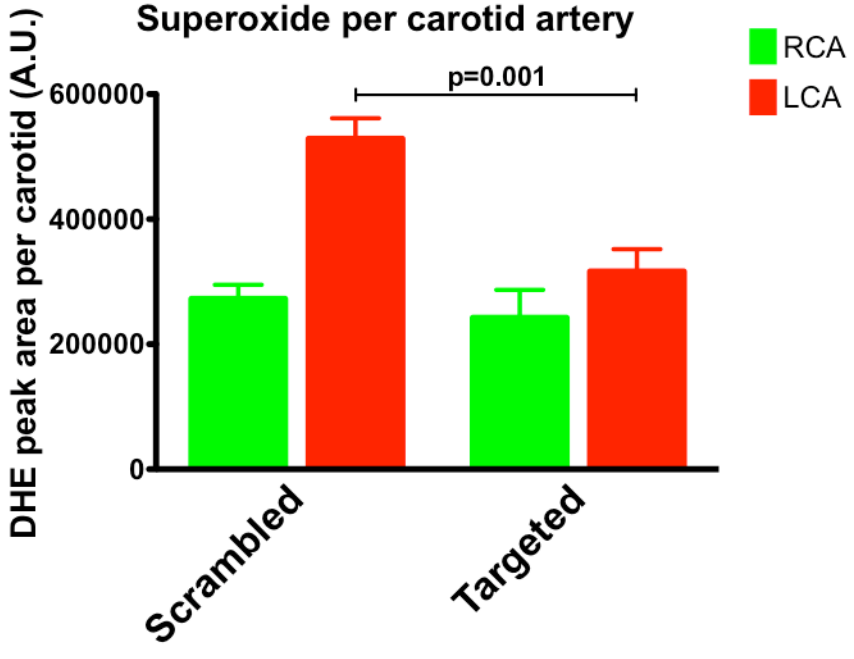

Figure 3. Liposomal delivery of superoxide significantly decreased superoxide concentration in the ligated artery with targeted liposomes but not with scrambled controls. This result indicates the ability of PREY-targeted delivery of BH_4 to reduce oxidative stress caused by eNOS uncoupling.

To determine if targeted BH_4 delivery can prevent vascular dysfunction in response to disturbed flow and hypercholesterolemia, $ApoE^{-/-}$ mice underwent partial carotid artery

ligation surgery and were fat fed to induce atherosclerosis [253, 256]. This model leads to accelerated atherosclerotic lesions after one week of high fat diet [74]. Mice received nanoparticle injections at one-day post ligation and endpoint experiments were conducted at seven days post ligation.

I first measured endothelium dependent relaxation as a measure of endothelial dysfunction. In these animals, carotid ligation results in uncoupled eNOS in the ligated artery, which should impair endothelium dependent relaxation in response to acetylcholine. In animals treated with PREY-targeted liposomes I observed improved endothelium dependent relaxation compared to scrambled controls (Figure 4). This result further confirmed that liposomal delivery of BH_4 rescues eNOS uncoupling and improves endothelial function, even in the case of severe hypercholesterolemia.

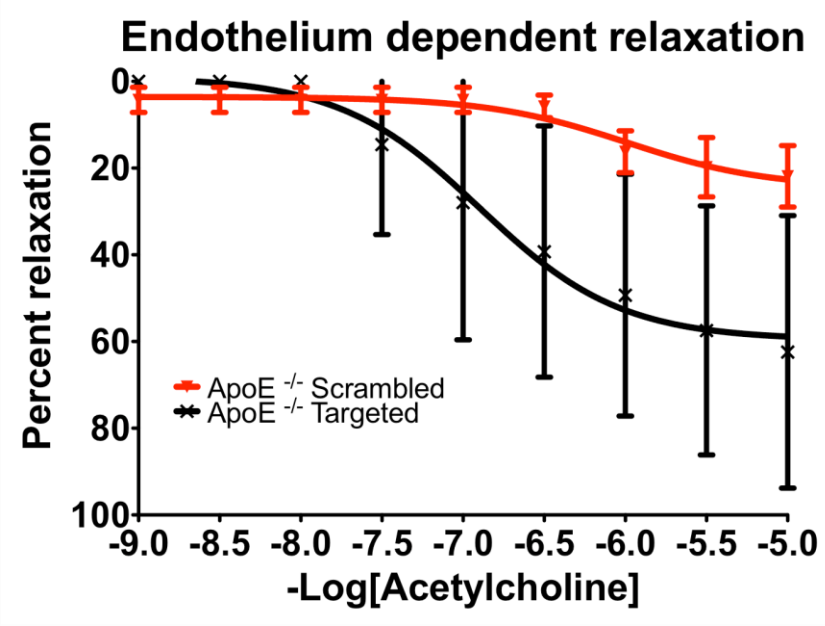

Figure 4. Endothelium dependent relaxation in ApoE$^{-/-}$ mice 7 days post ligation. This result indicates that PREY-targeted delivery of BH_4 improves endothelial function in the ligated artery. Scrambled EC_{50} = -6.813 to -5.169 Targeted EC_{50} = -7.514 to -6.277.

As another functional readout of effective targeted liposome treatment, I measured lumen area in the same ApoE$^{-/-}$ model. I found a significant decrease in plaque burden in the ligated left carotid artery of mice that received PREY-targeted liposome injections compared to scrambled controls (Figure 5).

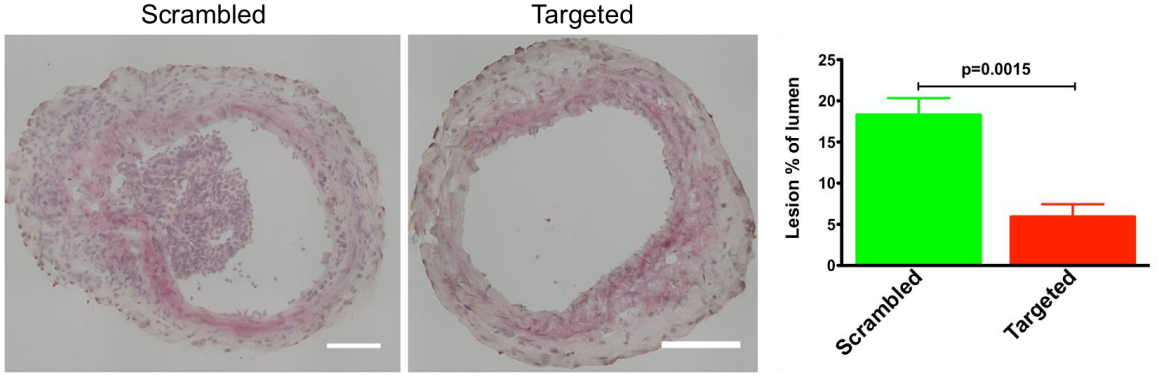

Figure 5. Liposomal delivery of BH_4 significantly reduced plaque burden in the ligated left carotid artery of ApoE$^{-/-}$ mice fed a high fat diet for 7 days. Plaque area quantification shows that PREY-targeted delivery of BH_4 prevents formation of lesions in the ligated artery of ApoE$^{-/-}$ mice fed a high fat diet for 7 days.

In order to determine if reduction in plaque area was due to altered lipid metabolism, I measured plasma lipids in mice receiving PREY and scrambled PREY liposomes containing BH_4. BH_4 containing PREY-targeted liposomes did not significantly alter total cholesterol or triglycerides in these animals compared to scrambled PREY controls (Figure 6). This indicates that nanocarrier delivery of BH_4 prevents atherosclerosis caused by endothelial dysfunction in areas of disturbed flow, even in the case of hypercholesterolemia.

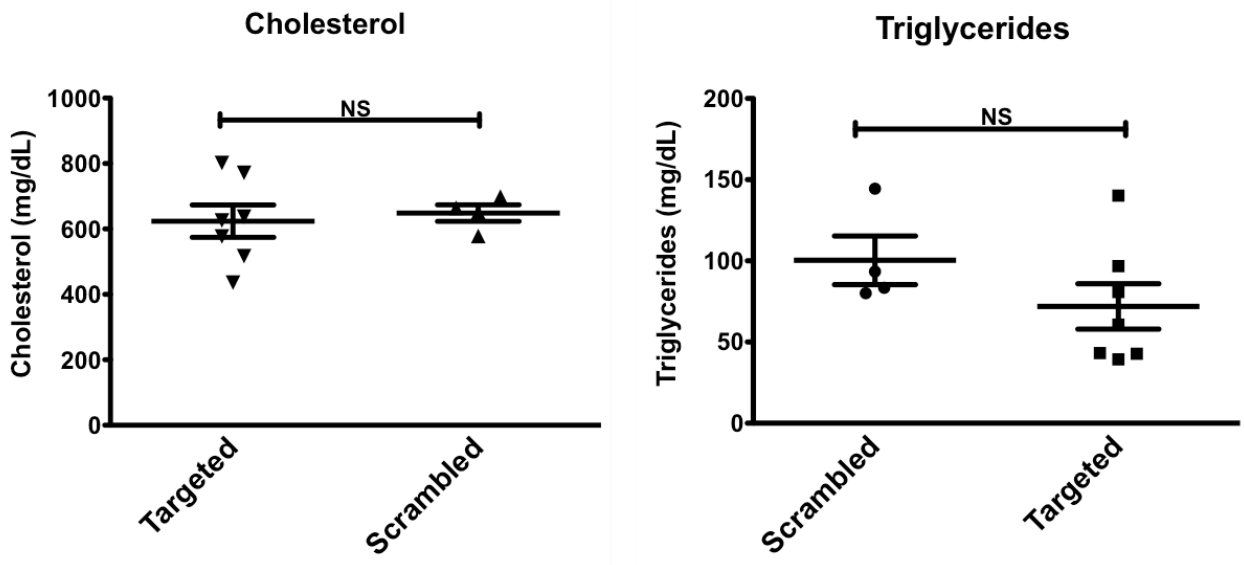

Figure 6. Liposome delivery did not change lipid metabolism as measured by total serum cholesterol and triglycerides. This result supports the conclusion that PREY-targeted delivery of BH_4 to atheroprone arteries reduces atherosclerosis by rescuing endothelial dysfunction and is not an effect of altered lipid metabolism.

CONCLUSIONS

To improve endothelial function caused by disturbed flow I targeted uncoupled nitric oxide synthase by delivering BH_4 as a candidate drug. PREY-targeted liposomes were shown to overcome known delivery barriers for BH_4 by stabilizing BH_4 in serum, and delivering BH_4 to target tissue. BH_4 delivery was shown to reduce vascular superoxide in the ligated artery of C57/BL6J mice, and improve endothelium dependent relaxation and reduce plaque formation in the ligated artery of $ApoE^{-/-}$ mice. Our results indicate that PREY-targeted nanocarrier delivery of BH_4 could be used as a prophylactic treatment for atherosclerosis.

CHAPTER V

THESIS CONCLUSIONS AND FUTURE PERSPECTIVES

INTRODUCTION

Arterial geometry affects the blood flow profiles in the cardiovascular system. In straight, unbranched vascular segments blood flow is unidirectional and laminar and time average wall shear stress due to viscous drag is high. In contrast, at branch points, sites of curvature and distal to stenoses blood flow becomes disturbed. Such regions can display flow separation, vortical shedding and low and oscillatory shear stresses [67]. The vascular endothelium is in direct contact with flowing blood and displays remarkable plasticity in response to varying shear stresses [75]. In the setting of unidirectional laminar shear stress, endothelial cells elongate and align in the direction of flow and develop an anti-inflammatory and anti-thrombotic phenotype [65]. These effects are associated with acute changes in endothelial cell signaling and marked changes in gene expression over the long term [75, 124]. As examples, in response to laminar unidirectional shear endothelial cells increase nitric oxide (NO), and endothelial nitric oxide synthase (eNOS), and exhibit decreases in inflammatory mediators [10]. In contrast, endothelial cells exposed to disturbed flow do not align and elongate, and become pro-inflammatory and pro-thrombotic. This phenotype is associated with sustained activation of pro-inflammatory signals with increased expression of inflammatory mediators including vascular cell adhesion molecule-1, intracellular adhesion molecule-1 and chemokines such as the monocyte chemoattractant peptide-1

[65, 74, 125-127]. The changes in endothelial cell phenotype caused by disturbed flow predispose these regions to local lipid deposition, inflammation and the focal development of atherosclerosis. Thus, atherosclerotic lesions predominantly occur at sites known to have disturbed flow such as branch points, the proximal coronary arteries and the distal aorta [48, 125, 126].

Most current treatments for atherosclerosis focus on correcting systemic risk factors such as hyperlipidemia, hypertension and diabetes. None of these therapies completely prevent cardiovascular events resulting from atherosclerosis. As an example, HMG Co-A reductase inhibitors reduce cardiovascular events by approximately 40 to 50% indicating that there are residual risks that persist after lipid lowering [146, 147]. One explanation of this residual risk is that current treatments do not target vasculature that is atheroprone. Such regions might require a local dose of drug not achieved by systemic administration.

Nanocarriers are an attractive platform for targeting therapy to regions of the circulation at risk for atherosclerosis. Nanoparticles can be functionalized to home to specific vascular regions affected by inflammation, lipid accumulation or oxidative injury, and can be used to deliver either therapeutic or imaging agents. Previously, nanoparticles have been used that target inflamed endothelium, inflammatory cells, the low-density lipoprotein receptor, thrombi and platelet aggregates [174-181]. While these studies have set a precedent for nanoparticle delivery to atherosclerosis, they depend on the presence of lesions formed after the initiation of the disease.

In the present study, I sought to develop a novel nanotherapy to target atheroprone regions of the circulation prior to atherosclerotic lesion development. Given the marked

differences in gene expression and protein content of endothelial cells exposed to varying flow profiles, I reasoned that there might be differences in peptide binding to the surface of cells exposed to disturbed versus unidirectional laminar shear. Using combinatorial phage display, I identified peptides that preferentially accumulate in an area of disturbed flow created by partial carotid occlusion in mice. A candidate peptide identified in this screen was used to functionalize liposomal nanocarriers. Subsequent studies proved that these nanocarriers also targeted regions of disturbed flow and could be used to deliver effective anti-atherosclerotic therapy to these regions.

CONCLUSIONS

Atherosclerotic lesions develop when focal endothelial dysfunction caused by disturbed flow is compounded by systemic risk factors such as hypercholesterolemia. Targeted drug delivery to areas of disturbed flow is a promising approach to prevent atherosclerosis before lesions develop. Because prediction of these atheroprone areas is speculative, programming nanocarrier functions to navigate to and detect atheroprone areas is but unmet need. To accomplish this, I first developed a method to target atheroprone vasculature by *in vivo* phage display. I discovered four peptides that selectively target atheroprone vasculature. A candidate peptide, PREY was used to form targeted liposomal nanocarriers, which were observed to accumulate in areas of disturbed flow *in vivo*. I also showed that the PREY-targeted liposomes home to endothelial cells in atheroprone vasculature, making this nanocarrier a promising candidate to treat endothelial dysfunction. To improve endothelial function caused by disturbed flow I targeted uncoupled nitric oxide synthase by delivering BH_4 as a candidate drug. PREY-targeted liposomes were shown to overcome known delivery barriers for BH_4 by stabilizing BH_4 in serum, and delivering BH_4 to target tissue. BH_4

delivery was shown to reduce vascular superoxide in the ligated artery of C57/BL6J mice and improve endothelial function and reduce plaque formation in the ligated artery of ApoE$^{-/-}$ mice.

FUTURE PERSPECTIVES

There are numerous druggable targets available for the treatment of cardiovascular disease, and almost all can benefit from targeted delivery [257, 258]. Therefore, additional studies could also test the delivery of alternative therapies, such as antioxidants. Clinical trials with nonspecific antioxidants have not shown benefit, and in some cases harm [259, 260]. A key oversight in a nonspecific antioxidant approach is that ROS play important physiological roles in cell signaling, innate immunity, hormone biosynthesis, and inflammation. To effectively oxidative stress with broad-spectrum antioxidants, a targeted approach that eliminates disease-causing ROS without disturbing physiological ROS signaling is essential [261]. Therefore, PREY-targeted nanocarriers could be utilized to deliver antioxidants, or inhibitors of ROS sources such as small molecule NOX inhibitors in a site-specific manner. Targeted approaches would also benefit inhibition of pathologic lipid metabolism and anti-inflammatory drugs such as dexamethasone. Delivery of therapeutic macromolecules such as peptides and RNA interference molecules such as siRNA and microRNAs are garnering increased acceptance as therapeutics due to advances in RNA delivery using synthetic nanoparticles [237, 262, 263]. Recent reports also demonstrate that high density lipoprotein (HDL) is able to carry microRNAs, and could be a useful therapeutic for cardiovascular disease [264]. Targeting these types of nanoparticles using peptides like PREY could be a useful strategy to prevent development of atherosclerosis.

In addition to allowing nanoparticle drug delivery, peptides like PREY may be useful for diagnostic imaging to define new risk factors for cardiovascular disease such as the number and location of areas of atheroprone vasculature. As a first step to investigate the use of PREY-targeted nanoparticles as a diagnostic platform, I would create targeted MRI contrast agents by incorporation of Gadolinium (III) chelates in the lipid membrane of PREY-targeted liposomes. MRI is an attractive platform because it is widely used in the clinic for diagnosis of cardiovascular pathologies by techniques such as angiography. Gadolinium chelates are commonly used in MRI imaging, and since its approval for clinical use in 1988, around 30% of MRI procedures use gadolinium chelates as contrast agents [265]. “Theranositc,” liposomes have been utilized for dual delivery of therapeutics and gadolinium chelates [266]. Other nanoparticle systems, such as USPIOs could also be used for MRI imaging of atheroprone vasculature by utilizing PREY-targeting. An alternative to MRI imaging would be positron emission tomography (PET). This approach offers increased sensitivity over MRI approaches, however, is much more expensive, the radioactive probes required have limited shelf lives and require specialized equipment to produce, and PET is much less common in clinical application. Ultrasound is a more attractive methodology because its use in cardiology is widespread, and PREY peptides could be used to target ultrasound contrast agents such as microbubbles [267]. Another attractive theranositc platform is HDL, or recombinant HDL. Studies have shown that HDL is a versatile naturally occurring nanoparticle, and can be loaded with imaging agents, therapeutics, and has naturally beneficial effects in the context of atherosclerosis [268-271].

Finally, this thesis demonstrates an exciting new possibility for drug targeting to pathological stimuli rather than symptoms of disease and sets a precedent for expanding the availability of biomarkers for preventative treatments.

REFERENCES

1. Murray, C.D., *The Physiological Principle of Minimum Work: II. Oxygen Exchange in Capillaries.* Proc Natl Acad Sci U S A, 1926. **12**(5): p. 299-304.
2. Murray, C.D., *The Physiological Principle of Minimum Work: I. The Vascular System and the Cost of Blood Volume.* Proc Natl Acad Sci U S A, 1926. **12**(3): p. 207-214.
3. Cines, D.B., E.S. Pollak, C.A. Buck, J. Loscalzo, G.A. Zimmerman, R.P. McEver, . . . D.M. Stern, *Endothelial cells in physiology and in the pathophysiology of vascular disorders.* Blood, 1998. **91**(10): p. 3527-3561.
4. Aird, W.C., *Phenotypic heterogeneity of the endothelium I. Structure, function, and mechanisms.* Circulation Research, 2007. **100**(2): p. 158-173.
5. Mc, D.D., *The relation of pulsatile pressure to flow in arteries.* J Physiol, 1955. **127**(3): p. 533-552.
6. Mozaffarian, D., E.J. Benjamin, A.S. Go, D.K. Arnett, M.J. Blaha, M. Cushman, . . . S. Stroke Statistics, *Heart disease and stroke statistics-2015 update: a report from the american heart association.* Circulation, 2015. **131**(4): p. e29-e322.
7. Stary, H.C., A.B. Chandler, S. Glagov, J.R. Guyton, W. Insull, M.E. Rosenfeld, . . . R.W. Wissler, *A Definition of Initial, Fatty Streak, and Intermediate Lesions of Atherosclerosis - a Report from the Committee on Vascular-Lesions of the Council on Arteriosclerosis, American-Heart-Association.* Arteriosclerosis and Thrombosis, 1994. **14**(5): p. 840-856.
8. Ross, R., *Atherosclerosis is an inflammatory disease.* American Heart Journal, 1999. **138**(5): p. S419-S420.
9. McNally, J.S., M.E. Davis, D.P. Giddens, A. Saha, J. Hwang, S. Dikalov, . . . D.G. Harrison, *Role of xanthine oxidoreductase and NAD(P)H oxidase in endothelial superoxide production in response to oscillatory shear stress.* American journal of physiology. Heart and circulatory physiology, 2003. **285**(6): p. H2290-2297.
10. Harrison, D.G., J. Widder, I. Grumbach, W. Chen, M. Weber, and C. Searles, *Endothelial mechanotransduction, nitric oxide and vascular inflammation.* J Intern Med, 2006. **259**(4): p. 351-363.
11. Paravicini, T.M. and R.M. Touyz, *NADPH oxidases, reactive oxygen species, and hypertension: clinical implications and therapeutic possibilities.* Diabetes Care, 2008. **31 Suppl 2**: p. S170-180.
12. O'Driscoll, J.G., D.J. Green, J.M. Rankin, and R.R. Taylor, *Nitric oxide-dependent endothelial function is unaffected by allopurinol in hypercholesterolaemic subjects.* Clinical and Experimental Pharmacology and Physiology, 1999. **26**(10): p. 779-783.
13. Forstermann, U., E.I. Closs, J.S. Pollock, M. Nakane, P. Schwarz, I. Gath, and H. Kleinert, *Nitric oxide synthase isozymes. Characterization, purification, molecular cloning, and functions.* Hypertension, 1994. **23**(6 Pt 2): p. 1121-1131.
14. Raman, C.S., H. Li, P. Martasek, V. Kral, B.S. Masters, and T.L. Poulos, *Crystal structure of constitutive endothelial nitric oxide synthase: a paradigm for pterin function involving a novel metal center.* Cell, 1998. **95**(7): p. 939-950.
15. Chen, P.F., A.L. Tsai, V. Berka, and K.K. Wu, *Mutation of Glu-361 in human endothelial nitric-oxide synthase selectively abolishes L-arginine binding without perturbing the behavior of heme and other redox centers.* J Biol Chem, 1997. **272**(10): p. 6114-6118.
16. Sessa, W.C., J.K. Harrison, C.M. Barber, D. Zeng, M.E. Durieux, D.D. D'Angelo, . . . M.J. Peach, *Molecular cloning and expression of a cDNA encoding endothelial cell nitric oxide synthase.* J Biol Chem, 1992. **267**(22): p. 15274-15276.

17. Ghosh, D.K., M.B. Rashid, B. Crane, V. Taskar, M. Mast, M.A. Misukonis, . . . N.T. Eissa, *Characterization of key residues in the subdomain encoded by exons 8 and 9 of human inducible nitric oxide synthase: a critical role for Asp-280 in substrate binding and subunit interactions.* Proc Natl Acad Sci U S A, 2001. **98**(18): p. 10392-10397.
18. Crane, B.R., A.S. Arvai, D.K. Ghosh, C. Wu, E.D. Getzoff, D.J. Stuehr, and J.A. Tainer, *Structure of nitric oxide synthase oxygenase dimer with pterin and substrate.* Science, 1998. **279**(5359): p. 2121-2126.
19. Presta, A., J. Liu, W.C. Sessa, and D.J. Stuehr, *Substrate binding and calmodulin binding to endothelial nitric oxide synthase coregulate its enzymatic activity.* Nitric Oxide, 1997. **1**(1): p. 74-87.
20. Stuehr, D., S. Pou, and G.M. Rosen, *Oxygen reduction by nitric-oxide synthases.* J Biol Chem, 2001. **276**(18): p. 14533-14536.
21. Palmer, R.M., A.G. Ferrige, and S. Moncada, *Nitric oxide release accounts for the biological activity of endothelium-derived relaxing factor.* Nature, 1987. **327**(6122): p. 524-526.
22. Furchgott, R.F. and J.V. Zawadzki, *The obligatory role of endothelial cells in the relaxation of arterial smooth muscle by acetylcholine.* Nature, 1980. **288**(5789): p. 373-376.
23. Gruetter, C.A., P.J. Kadowitz, and L.J. Ignarro, *Methylene blue inhibits coronary arterial relaxation and guanylate cyclase activation by nitroglycerin, sodium nitrite, and amyl nitrite.* Can J Physiol Pharmacol, 1981. **59**(2): p. 150-156.
24. Katsuki, S., W. Arnold, C. Mittal, and F. Murad, *Stimulation of guanylate cyclase by sodium nitroprusside, nitroglycerin and nitric oxide in various tissue preparations and comparison to the effects of sodium azide and hydroxylamine.* J Cyclic Nucleotide Res, 1977. **3**(1): p. 23-35.
25. Hahn, C. and M.A. Schwartz, *Mechanotransduction in vascular physiology and atherogenesis.* Nature reviews. Molecular cell biology, 2009. **10**(1): p. 53-62.
26. Harrison, D.G., J. Widder, I. Grumbach, W. Chen, M. Weber, and C. Searles, *Endothelial mechanotransduction, nitric oxide and vascular inflammation.* Journal of internal medicine, 2006. **259**(4): p. 351-363.
27. Forstermann, U. and T. Munzel, *Endothelial nitric oxide synthase in vascular disease: from marvel to menace.* Circulation, 2006. **113**(13): p. 1708-1714.
28. Landmesser, U., S. Dikalov, S.R. Price, L. McCann, T. Fukai, S.M. Holland, . . . D.G. Harrison, *Oxidation of tetrahydrobiopterin leads to uncoupling of endothelial cell nitric oxide synthase in hypertension.* J Clin Invest, 2003. **111**(8): p. 1201-1209.
29. Cai, H. and D.G. Harrison, *Endothelial dysfunction in cardiovascular diseases: the role of oxidant stress.* Circ Res, 2000. **87**(10): p. 840-844.
30. Beckman, J.S., T.W. Beckman, J. Chen, P.A. Marshall, and B.A. Freeman, *Apparent hydroxyl radical production by peroxynitrite: implications for endothelial injury from nitric oxide and superoxide.* Proc Natl Acad Sci U S A, 1990. **87**(4): p. 1620-1624.
31. Huie, R.E. and S. Padmaja, *The Reaction of No with Superoxide.* Free Radical Research Communications, 1993. **18**(4): p. 195-199.
32. Thomson, L., M. Trujillo, R. Telleri, and R. Radi, *Kinetics of cytochrome c2+ oxidation by peroxynitrite: implications for superoxide measurements in nitric oxide-producing biological systems.* Arch Biochem Biophys, 1995. **319**(2): p. 491-497.
33. Shi, W., C.J. Meininger, T.E. Haynes, K. Hatakeyama, and G. Wu, *Regulation of tetrahydrobiopterin synthesis and bioavailability in endothelial cells.* Cell biochemistry and biophysics, 2004. **41**(3): p. 415-434.
34. Knorr, M., M. Hausding, S. Kroller-Schuhmacher, S. Steven, M. Oelze, T. Heeren, . . . T. Munzel, *Nitroglycerin-induced endothelial dysfunction and tolerance involve adverse phosphorylation and S-Glutathionylation of endothelial nitric oxide synthase: beneficial effects of therapy with the AT1 receptor blocker telmisartan.* Arterioscler Thromb Vasc Biol, 2011. **31**(10): p. 2223-2231.

35. Harrison, D.G. and J.N. Bates, *The nitrovasodilators. New ideas about old drugs.* Circulation, 1993. **87**(5): p. 1461-1467.
36. Marks, G.S., K. Nakatsu, B. McLaughlin, J. Kawamoto, C. Slack, and J.F. Brien, *The role of nitric oxide formation in organic nitrate-induced vasodilation and organic nitrate tolerance.* Z Kardiol, 1989. **78 Suppl 2**: p. 18-21; discussion 64-17.
37. Nakamura, Y., A.J. Moss, M.W. Brown, M. Kinoshita, and C. Kawai, *Long-term nitrate use may be deleterious in ischemic heart disease: A study using the databases from two large-scale postinfarction studies. Multicenter Myocardial Ischemia Research Group.* Am Heart J, 1999. **138**(3 Pt 1): p. 577-585.
38. Munzel, T., H. Sayegh, B.A. Freeman, M.M. Tarpey, and D.G. Harrison, *Evidence for enhanced vascular superoxide anion production in nitrate tolerance. A novel mechanism underlying tolerance and cross-tolerance.* J Clin Invest, 1995. **95**(1): p. 187-194.
39. Munzel, T., *Does nitroglycerin therapy hit the endothelium?* J Am Coll Cardiol, 2001. **38**(4): p. 1102-1105.
40. Pollock, J.S., U. Forstermann, J.A. Mitchell, T.D. Warner, H.H. Schmidt, M. Nakane, and F. Murad, *Purification and characterization of particulate endothelium-derived relaxing factor synthase from cultured and native bovine aortic endothelial cells.* Proc Natl Acad Sci U S A, 1991. **88**(23): p. 10480-10484.
41. Landmesser, U., S. Dikalov, S.R. Price, L. McCann, T. Fukai, S.M. Holland, . . . D.G. Harrison, *Oxidation of tetrahydrobiopterin leads to uncoupling of endothelial cell nitric oxide synthase in hypertension.* Journal of Clinical Investigation, 2003. **111**(8): p. 1201-1209.
42. Cosentino, F. and Z.S. Katusic, *Tetrahydrobiopterin and dysfunction of endothelial nitric oxide synthase in coronary arteries.* Circulation, 1995. **91**(1): p. 139-144.
43. Chen, C.A., L.J. Druhan, S. Varadharaj, Y.R. Chen, and J.L. Zweier, *Phosphorylation of endothelial nitric-oxide synthase regulates superoxide generation from the enzyme.* J Biol Chem, 2008. **283**(40): p. 27038-27047.
44. Xia, Y., A.L. Tsai, V. Berka, and J.L. Zweier, *Superoxide generation from endothelial nitric-oxide synthase. A Ca2+/calmodulin-dependent and tetrahydrobiopterin regulatory process.* J Biol Chem, 1998. **273**(40): p. 25804-25808.
45. Ohara, Y., T.E. Peterson, and D.G. Harrison, *Hypercholesterolemia increases endothelial superoxide anion production.* J Clin Invest, 1993. **91**(6): p. 2546-2551.
46. Pritchard, K.A., Jr., L. Groszek, D.M. Smalley, W.C. Sessa, M. Wu, P. Villalon, . . . M.B. Stemerman, *Native low-density lipoprotein increases endothelial cell nitric oxide synthase generation of superoxide anion.* Circ Res, 1995. **77**(3): p. 510-518.
47. Kossmann, S., H. Hu, S. Steven, T. Schonfelder, D. Fraccarollo, Y. Mikhed, . . . P. Wenzel, *Inflammatory monocytes determine endothelial nitric-oxide synthase uncoupling and nitro-oxidative stress induced by angiotensin II.* J Biol Chem, 2014. **289**(40): p. 27540-27550.
48. Channon, K.M., *Tetrahydrobiopterin: a vascular redox target to improve endothelial function.* Current vascular pharmacology, 2012. **10**(6): p. 705-708.
49. Stroes, E., J. Kastelein, F. Cosentino, W. Erkelens, R. Wever, H. Koomans, . . . T. Rabelink, *Tetrahydrobiopterin restores endothelial function in hypercholesterolemia.* J Clin Invest, 1997. **99**(1): p. 41-46.
50. Heitzer, T., K. Krohn, S. Albers, and T. Meinertz, *Tetrahydrobiopterin improves endothelium-dependent vasodilation by increasing nitric oxide activity in patients with Type II diabetes mellitus.* Diabetologia, 2000. **43**(11): p. 1435-1438.
51. Heitzer, T., C. Brockhoff, B. Mayer, A. Warnholtz, H. Mollnau, S. Henne, . . . T. Munzel, *Tetrahydrobiopterin improves endothelium-dependent vasodilation in chronic smokers : evidence for a dysfunctional nitric oxide synthase.* Circ Res, 2000. **86**(2): p. E36-41.

52. Higashi, Y., S. Sasaki, K. Nakagawa, Y. Fukuda, H. Matsuura, T. Oshima, and K. Chayama, *Tetrahydrobiopterin enhances forearm vascular response to acetylcholine in both normotensive and hypertensive individuals.* Am J Hypertens, 2002. **15**(4 Pt 1): p. 326-332.
53. Bevers, L.M., B. Braam, J.A. Post, A.J. van Zonneveld, T.J. Rabelink, H.A. Koomans, . . . J.A. Joles, *Tetrahydrobiopterin, but not L-arginine, decreases NO synthase uncoupling in cells expressing high levels of endothelial NO synthase.* Hypertension, 2006. **47**(1): p. 87-94.
54. Li, H., K. Witte, M. August, I. Brausch, U. Godtel-Armbrust, A. Habermeier, . . . U. Forstermann, *Reversal of endothelial nitric oxide synthase uncoupling and up-regulation of endothelial nitric oxide synthase expression lowers blood pressure in hypertensive rats.* J Am Coll Cardiol, 2006. **47**(12): p. 2536-2544.
55. Abd El Dayem, S.M., A.A. Battah, A. El-Shehaby, and M. El Bohy Ael, *Asymmetric dimethyl L-arginine, nitric oxide and cardiovascular disease in adolescent type 1 diabetics.* J Pediatr Endocrinol Metab, 2014. **27**(5-6): p. 437-444.
56. McMillan, K., M. Adler, D.S. Auld, J.J. Baldwin, E. Blasko, L.J. Browne, . . . J.J. Devlin, *Allosteric inhibitors of inducible nitric oxide synthase dimerization discovered via combinatorial chemistry.* Proc Natl Acad Sci U S A, 2000. **97**(4): p. 1506-1511.
57. Li, L., W. Chen, A. Rezvan, H. Jo, and D.G. Harrison, *Tetrahydrobiopterin Deficiency and Nitric Oxide Synthase Uncoupling Contribute to Atherosclerosis Induced by Disturbed Flow.* Arteriosclerosis Thrombosis and Vascular Biology, 2011. **31**(7): p. 1547-1554.
58. Channon, K.M., *Tetrahydrobiopterin: regulator of endothelial nitric oxide synthase in vascular disease.* Trends Cardiovasc Med, 2004. **14**(8): p. 323-327.
59. Thony, B., G. Auerbach, and N. Blau, *Tetrahydrobiopterin biosynthesis, regeneration and functions.* Biochem J, 2000. **347 Pt 1**: p. 1-16.
60. Hoang, H.H., S.V. Padgham, and C.J. Meininger, *L-arginine, tetrahydrobiopterin, nitric oxide and diabetes.* Curr Opin Clin Nutr Metab Care, 2013. **16**(1): p. 76-82.
61. Franco Mdo, C., Z.B. Fortes, E.H. Akamine, E.M. Kawamoto, C. Scavone, L.R. de Britto, . . . D. Nigro, *Tetrahydrobiopterin improves endothelial dysfunction and vascular oxidative stress in microvessels of intrauterine undernourished rats.* J Physiol, 2004. **558**(Pt 1): p. 239-248.
62. Hasegawa, H., K. Sawabe, N. Nakanishi, and O.K. Wakasugi, *Delivery of exogenous tetrahydrobiopterin (BH4) to cells of target organs: role of salvage pathway and uptake of its precursor in effective elevation of tissue BH4.* Molecular genetics and metabolism, 2005. **86 Suppl 1**: p. S2-10.
63. McNally, J.S., M.E. Davis, D.P. Giddens, A. Saha, J. Hwang, S. Dikalov, . . . D.G. Harrison, *Role of xanthine oxidoreductase and NAD(P)H oxidase in endothelial superoxide production in response to oscillatory shear stress.* Am J Physiol Heart Circ Physiol, 2003. **285**(6): p. H2290-2297.
64. Godber, B.L., J.J. Doel, J. Durgan, R. Eisenthal, and R. Harrison, *A new route to peroxynitrite: a role for xanthine oxidoreductase.* FEBS Lett, 2000. **475**(2): p. 93-96.
65. Hahn, C. and M.A. Schwartz, *Mechanotransduction in vascular physiology and atherogenesis.* Nature Reviews Molecular Cell Biology, 2009. **10**(1): p. 53-62.
66. Avila, K., D. Moxey, A. de Lozar, M. Avila, D. Barkley, and B. Hof, *The Onset of Turbulence in Pipe Flow.* Science, 2011. **333**(6039): p. 192-196.
67. Ku, D.N., D.P. Giddens, C.K. Zarins, and S. Glagov, *Pulsatile flow and atherosclerosis in the human carotid bifurcation. Positive correlation between plaque location and low oscillating shear stress.* Arteriosclerosis, 1985. **5**(3): p. 293-302.
68. Zarins, C.K., D.P. Giddens, B.K. Bharadvaj, V.S. Sottiurai, R.F. Mabon, and S. Glagov, *Carotid bifurcation atherosclerosis. Quantitative correlation of plaque localization with flow velocity profiles and wall shear stress.* Circ Res, 1983. **53**(4): p. 502-514.
69. Brown, T.D., *Techniques for mechanical stimulation of cells in vitro: a review.* J Biomech, 2000. **33**(1): p. 3-14.

70. Bussolari, S.R., C.F. Dewey, Jr., and M.A. Gimbrone, Jr., *Apparatus for subjecting living cells to fluid shear stress.* The Review of scientific instruments, 1982. **53**(12): p. 1851-1854.
71. Uematsu, M., Y. Ohara, J.P. Navas, K. Nishida, T.J. Murphy, R.W. Alexander, . . . D.G. Harrison, *Regulation of endothelial cell nitric oxide synthase mRNA expression by shear stress.* The American journal of physiology, 1995. **269**(6 Pt 1): p. C1371-1378.
72. Booth, R.F., J.F. Martin, A.C. Honey, D.G. Hassall, J.E. Beesley, and S. Moncada, *Rapid development of atherosclerotic lesions in the rabbit carotid artery induced by perivascular manipulation.* Atherosclerosis, 1989. **76**(2-3): p. 257-268.
73. von der Thusen, J.H., T.J. van Berkel, and E.A. Biessen, *Induction of rapid atherogenesis by perivascular carotid collar placement in apolipoprotein E-deficient and low-density lipoprotein receptor-deficient mice.* Circulation, 2001. **103**(8): p. 1164-1170.
74. Nam, D., C.-W. Ni, A. Rezvan, J. Suo, K. Budzyn, A. Llanos, . . . H. Jo, *Partial carotid ligation is a model of acutely induced disturbed flow, leading to rapid endothelial dysfunction and atherosclerosis.* American Journal of Physiology - Heart and Circulatory Physiology, 2009. **297**(4): p. H1535-H1543.
75. Davies, P.F., *Flow-mediated endothelial mechanotransduction.* Physiol Rev, 1995. **75**(3): p. 519-560.
76. Ni, C.W., H.W. Qiu, A. Rezvan, K. Kwon, D. Nam, D.J. Son, . . . H. Jo, *Discovery of novel mechanosensitive genes in vivo using mouse carotid artery endothelium exposed to disturbed flow.* Blood, 2010. **116**(15): p. E66-E73.
77. Rowell, L.B., *Human cardiovascular adjustments to exercise and thermal stress.* Physiol Rev, 1974. **54**(1): p. 75-159.
78. Rubanyi, G.M., J.C. Romero, and P.M. Vanhoutte, *Flow-induced release of endothelium-derived relaxing factor.* Am J Physiol, 1986. **250**(6 Pt 2): p. H1145-1149.
79. Kamiya, A. and T. Togawa, *Adaptive regulation of wall shear stress to flow change in the canine carotid artery.* Am J Physiol, 1980. **239**(1): p. H14-21.
80. Zarins, C.K., M.A. Zatina, D.P. Giddens, D.N. Ku, and S. Glagov, *Shear stress regulation of artery lumen diameter in experimental atherogenesis.* J Vasc Surg, 1987. **5**(3): p. 413-420.
81. Langille, B.L. and F. O'Donnell, *Reductions in arterial diameter produced by chronic decreases in blood flow are endothelium-dependent.* Science, 1986. **231**(4736): p. 405-407.
82. Ando, J. and K. Yamamoto, *Vascular mechanobiology: endothelial cell responses to fluid shear stress.* Circulation journal : official journal of the Japanese Circulation Society, 2009. **73**(11): p. 1983-1992.
83. Ingber, D.E., *Cellular tensegrity: defining new rules of biological design that govern the cytoskeleton.* J Cell Sci, 1993. **104 (Pt 3)**: p. 613-627.
84. Ingber, D.E., L. Dike, L. Hansen, S. Karp, H. Liley, A. Maniotis, . . . et al., *Cellular tensegrity: exploring how mechanical changes in the cytoskeleton regulate cell growth, migration, and tissue pattern during morphogenesis.* Int Rev Cytol, 1994. **150**: p. 173-224.
85. Stamenovic, D., J.J. Fredberg, N. Wang, J.P. Butler, and D.E. Ingber, *A microstructural approach to cytoskeletal mechanics based on tensegrity.* J Theor Biol, 1996. **181**(2): p. 125-136.
86. Ingber, D.E., *Integrins, tensegrity, and mechanotransduction.* Gravit Space Biol Bull, 1997. **10**(2): p. 49-55.
87. Hutcheson, I.R. and T.M. Griffith, *Mechanotransduction through the endothelial cytoskeleton: mediation of flow- but not agonist-induced EDRF release.* Br J Pharmacol, 1996. **118**(3): p. 720-726.
88. Schiffers, P.M., D. Henrion, C.M. Boulanger, E. Colucci-Guyon, F. Langa-Vuves, H. van Essen, . . . J.G. De Mey, *Altered flow-induced arterial remodeling in vimentin-deficient mice.* Arterioscler Thromb Vasc Biol, 2000. **20**(3): p. 611-616.
89. Knudsen, H.L. and J.A. Frangos, *Role of cytoskeleton in shear stress-induced endothelial nitric oxide production.* Am J Physiol, 1997. **273**(1 Pt 2): p. H347-355.

90. Butler, P.J., G. Norwich, S. Weinbaum, and S. Chien, *Shear stress induces a time- and position-dependent increase in endothelial cell membrane fluidity.* Am J Physiol Cell Physiol, 2001. **280**(4): p. C962-969.
91. White, C.R. and J.A. Frangos, *The shear stress of it all: the cell membrane and mechanochemical transduction.* Philos Trans R Soc Lond B Biol Sci, 2007. **362**(1484): p. 1459-1467.
92. Yu, J., S. Bergaya, T. Murata, I.F. Alp, M.P. Bauer, M.I. Lin, . . . W.C. Sessa, *Direct evidence for the role of caveolin-1 and caveolae in mechanotransduction and remodeling of blood vessels.* J Clin Invest, 2006. **116**(5): p. 1284-1291.
93. Anderson, R.G., *Caveolae: where incoming and outgoing messengers meet.* Proc Natl Acad Sci U S A, 1993. **90**(23): p. 10909-10913.
94. Rizzo, V., D.P. McIntosh, P. Oh, and J.E. Schnitzer, *In situ flow activates endothelial nitric oxide synthase in luminal caveolae of endothelium with rapid caveolin dissociation and calmodulin association.* J Biol Chem, 1998. **273**(52): p. 34724-34729.
95. Gudi, S., J.P. Nolan, and J.A. Frangos, *Modulation of GTPase activity of G proteins by fluid shear stress and phospholipid composition.* Proc Natl Acad Sci U S A, 1998. **95**(5): p. 2515-2519.
96. Gudi, S.R., C.B. Clark, and J.A. Frangos, *Fluid flow rapidly activates G proteins in human endothelial cells. Involvement of G proteins in mechanochemical signal transduction.* Circ Res, 1996. **79**(4): p. 834-839.
97. Jo, H., K. Sipos, Y.M. Go, R. Law, J. Rong, and J.M. McDonald, *Differential effect of shear stress on extracellular signal-regulated kinase and N-terminal Jun kinase in endothelial cells. Gi2- and Gbeta/gamma-dependent signaling pathways.* J Biol Chem, 1997. **272**(2): p. 1395-1401.
98. Chachisvilis, M., Y.L. Zhang, and J.A. Frangos, *G protein-coupled receptors sense fluid shear stress in endothelial cells.* Proc Natl Acad Sci U S A, 2006. **103**(42): p. 15463-15468.
99. Olesen, S.P., D.E. Clapham, and P.F. Davies, *Haemodynamic shear stress activates a K+ current in vascular endothelial cells.* Nature, 1988. **331**(6152): p. 168-170.
100. Nakache, M. and H.E. Gaub, *Hydrodynamic hyperpolarization of endothelial cells.* Proc Natl Acad Sci U S A, 1988. **85**(6): p. 1841-1843.
101. Barakat, A.I., E.V. Leaver, P.A. Pappone, and P.F. Davies, *A flow-activated chloride-selective membrane current in vascular endothelial cells.* Circ Res, 1999. **85**(9): p. 820-828.
102. Hoger, J.H., V.I. Ilyin, S. Forsyth, and A. Hoger, *Shear stress regulates the endothelial Kir2.1 ion channel.* Proc Natl Acad Sci U S A, 2002. **99**(11): p. 7780-7785.
103. Ando, J., T. Komatsuda, and A. Kamiya, *Cytoplasmic calcium response to fluid shear stress in cultured vascular endothelial cells.* In Vitro Cell Dev Biol, 1988. **24**(9): p. 871-877.
104. Bodin, P. and G. Burnstock, *Evidence that release of adenosine triphosphate from endothelial cells during increased shear stress is vesicular.* J Cardiovasc Pharmacol, 2001. **38**(6): p. 900-908.
105. Milner, P., P. Bodin, A. Loesch, and G. Burnstock, *Increased shear stress leads to differential release of endothelin and ATP from isolated endothelial cells from 4- and 12-month-old male rabbit aorta.* J Vasc Res, 1992. **29**(6): p. 420-425.
106. Yamamoto, K., N. Shimizu, S. Obi, S. Kumagaya, Y. Taketani, A. Kamiya, and J. Ando, *Involvement of cell surface ATP synthase in flow-induced ATP release by vascular endothelial cells.* Am J Physiol Heart Circ Physiol, 2007. **293**(3): p. H1646-1653.
107. Bodin, P., D. Bailey, and G. Burnstock, *Increased flow-induced ATP release from isolated vascular endothelial cells but not smooth muscle cells.* Br J Pharmacol, 1991. **103**(1): p. 1203-1205.
108. Milner, P., P. Bodin, A. Loesch, and G. Burnstock, *Rapid release of endothelin and ATP from isolated aortic endothelial cells exposed to increased flow.* Biochem Biophys Res Commun, 1990. **170**(2): p. 649-656.
109. Vink, H. and B.R. Duling, *Capillary endothelial surface layer selectively reduces plasma solute distribution volume.* Am J Physiol Heart Circ Physiol, 2000. **278**(1): p. H285-289.
110. Smith, M.L., D.S. Long, E.R. Damiano, and K. Ley, *Near-wall micro-PIV reveals a hydrodynamically relevant endothelial surface layer in venules in vivo.* Biophys J, 2003. **85**(1): p. 637-645.

111. Weinbaum, S., J.M. Tarbell, and E.R. Damiano, *The structure and function of the endothelial glycocalyx layer.* Annu Rev Biomed Eng, 2007. **9**: p. 121-167.
112. Mochizuki, S., H. Vink, O. Hiramatsu, T. Kajita, F. Shigeto, J.A. Spaan, and F. Kajiya, *Role of hyaluronic acid glycosaminoglycans in shear-induced endothelium-derived nitric oxide release.* Am J Physiol Heart Circ Physiol, 2003. **285**(2): p. H722-726.
113. Florian, J.A., J.R. Kosky, K. Ainslie, Z. Pang, R.O. Dull, and J.M. Tarbell, *Heparan sulfate proteoglycan is a mechanosensor on endothelial cells.* Circ Res, 2003. **93**(10): p. e136-142.
114. Siegel, G., A. Walter, A. Kauschmann, M. Malmsten, and E. Buddecke, *Anionic biopolymers as blood flow sensors.* Biosens Bioelectron, 1996. **11**(3): p. 281-294.
115. Schwartz, M.A. and R.K. Assoian, *Integrins and cell proliferation: regulation of cyclin-dependent kinases via cytoplasmic signaling pathways.* J Cell Sci, 2001. **114**(Pt 14): p. 2553-2560.
116. Katsumi, A., A.W. Orr, E. Tzima, and M.A. Schwartz, *Integrins in mechanotransduction.* J Biol Chem, 2004. **279**(13): p. 12001-12004.
117. Kim, K., I. Drummond, O. Ibraghimov-Beskrovnaya, K. Klinger, and M.A. Arnaout, *Polycystin 1 is required for the structural integrity of blood vessels.* Proc Natl Acad Sci U S A, 2000. **97**(4): p. 1731-1736.
118. Iomini, C., K. Tejada, W. Mo, H. Vaananen, and G. Piperno, *Primary cilia of human endothelial cells disassemble under laminar shear stress.* J Cell Biol, 2004. **164**(6): p. 811-817.
119. Van der Heiden, K., B.P. Hierck, R. Krams, R. de Crom, C. Cheng, M. Baiker, . . . R.E. Poelmann, *Endothelial primary cilia in areas of disturbed flow are at the base of atherosclerosis.* Atherosclerosis, 2008. **196**(2): p. 542-550.
120. Hierck, B.P., K. Van der Heiden, F.E. Alkemade, S. Van de Pas, J.V. Van Thienen, B.C. Groenendijk, . . . R.E. Poelmann, *Primary cilia sensitize endothelial cells for fluid shear stress.* Dev Dyn, 2008. **237**(3): p. 725-735.
121. Nauli, S.M., Y. Kawanabe, J.J. Kaminski, W.J. Pearce, D.E. Ingber, and J. Zhou, *Endothelial cilia are fluid shear sensors that regulate calcium signaling and nitric oxide production through polycystin-1.* Circulation, 2008. **117**(9): p. 1161-1171.
122. AbouAlaiwi, W.A., M. Takahashi, B.R. Mell, T.J. Jones, S. Ratnam, R.J. Kolb, and S.M. Nauli, *Ciliary polycystin-2 is a mechanosensitive calcium channel involved in nitric oxide signaling cascades.* Circ Res, 2009. **104**(7): p. 860-869.
123. Tzima, E., M. Irani-Tehrani, W.B. Kiosses, E. Dejana, D.A. Schultz, B. Engelhardt, . . . M.A. Schwartz, *A mechanosensory complex that mediates the endothelial cell response to fluid shear stress.* Nature, 2005. **437**(7057): p. 426-431.
124. Dewey, C.F., S.R. Bussolari, M.A. Gimbrone, and P.F. Davies, *The Dynamic-Response of Vascular Endothelial-Cells to Fluid Shear-Stress.* Journal of Biomechanical Engineering-Transactions of the Asme, 1981. **103**(3): p. 177-185.
125. Hwang, J., A. Saha, Y.C. Boo, G.P. Sorescu, J.S. McNally, S.M. Holland, . . . H. Jo, *Oscillatory shear stress stimulates endothelial production of O2- from p47phox-dependent NAD(P)H oxidases, leading to monocyte adhesion.* The Journal of biological chemistry, 2003. **278**(47): p. 47291-47298.
126. Davis, M.E., I.M. Grumbach, T. Fukai, A. Cutchins, and D.G. Harrison, *Shear stress regulates endothelial nitric-oxide synthase promoter activity through nuclear factor kappaB binding.* The Journal of biological chemistry, 2004. **279**(1): p. 163-168.
127. Widder, J.D., W. Chen, L. Li, S. Dikalov, B. Thony, K. Hatakeyama, and D.G. Harrison, *Regulation of tetrahydrobiopterin biosynthesis by shear stress.* Circulation Research, 2007. **101**(8): p. 830-838.
128. Dai, G.H., M.R. Kaazempur-Mofrad, S. Natarajan, Y.Z. Zhang, S. Vaughn, B.R. Blackman, . . . M.A. Gimbrone, *Distinct endothelial phenotypes evoked by arterial waveforms derived from atherosclerosis-susceptible and -resistant regions of human vasculature.* Proceedings of the National Academy of Sciences of the United States of America, 2004. **101**(41): p. 14871-14876.

129. Kuchan, M.J. and J.A. Frangos, *Role of calcium and calmodulin in flow-induced nitric oxide production in endothelial cells.* Am J Physiol, 1994. **266**(3 Pt 1): p. C628-636.
130. Boo, Y.C. and H. Jo, *Flow-dependent regulation of endothelial nitric oxide synthase: role of protein kinases.* Am J Physiol Cell Physiol, 2003. **285**(3): p. C499-508.
131. Fisslthaler, B., S. Dimmeler, C. Hermann, R. Busse, and I. Fleming, *Phosphorylation and activation of the endothelial nitric oxide synthase by fluid shear stress.* Acta Physiol Scand, 2000. **168**(1): p. 81-88.
132. Dimmeler, S., I. Fleming, B. Fisslthaler, C. Hermann, R. Busse, and A.M. Zeiher, *Activation of nitric oxide synthase in endothelial cells by Akt-dependent phosphorylation.* Nature, 1999. **399**(6736): p. 601-605.
133. Corson, M.A., N.L. James, S.E. Latta, R.M. Nerem, B.C. Berk, and D.G. Harrison, *Phosphorylation of endothelial nitric oxide synthase in response to fluid shear stress.* Circ Res, 1996. **79**(5): p. 984-991.
134. Davis, M.E., I.M. Grumbach, T. Fukai, A. Cutchins, and D.G. Harrison, *Shear stress regulates endothelial nitric-oxide synthase promoter activity through nuclear factor kappaB binding.* J Biol Chem, 2004. **279**(1): p. 163-168.
135. Matthews, J.R., C.H. Botting, M. Panico, H.R. Morris, and R.T. Hay, *Inhibition of NF-kappaB DNA binding by nitric oxide.* Nucleic Acids Res, 1996. **24**(12): p. 2236-2242.
136. Grumbach, I.M., W. Chen, S.A. Mertens, and D.G. Harrison, *A negative feedback mechanism involving nitric oxide and nuclear factor kappa-B modulates endothelial nitric oxide synthase transcription.* J Mol Cell Cardiol, 2005. **39**(4): p. 595-603.
137. De Keulenaer, G.W., D.C. Chappell, N. Ishizaka, R.M. Nerem, R.W. Alexander, and K.K. Griendling, *Oscillatory and steady laminar shear stress differentially affect human endothelial redox state: role of a superoxide-producing NADH oxidase.* Circ Res, 1998. **82**(10): p. 1094-1101.
138. Fukai, T., M.R. Siegfried, M. Ushio-Fukai, Y. Cheng, G. Kojda, and D.G. Harrison, *Regulation of the vascular extracellular superoxide dismutase by nitric oxide and exercise training.* J Clin Invest, 2000. **105**(11): p. 1631-1639.
139. Inoue, N., S. Ramasamy, T. Fukai, R.M. Nerem, and D.G. Harrison, *Shear stress modulates expression of Cu/Zn superoxide dismutase in human aortic endothelial cells.* Circ Res, 1996. **79**(1): p. 32-37.
140. Laurindo, F.R., A. Pedro Mde, H.V. Barbeiro, F. Pileggi, M.H. Carvalho, O. Augusto, and P.L. da Luz, *Vascular free radical release. Ex vivo and in vivo evidence for a flow-dependent endothelial mechanism.* Circ Res, 1994. **74**(4): p. 700-709.
141. Stralin, P., K. Karlsson, B.O. Johansson, and S.L. Marklund, *The interstitium of the human arterial wall contains very large amounts of extracellular superoxide dismutase.* Arterioscler Thromb Vasc Biol, 1995. **15**(11): p. 2032-2036.
142. Takeshita, S., N. Inoue, T. Ueyama, S. Kawashima, and M. Yokoyama, *Shear stress enhances glutathione peroxidase expression in endothelial cells.* Biochem Biophys Res Commun, 2000. **273**(1): p. 66-71.
143. Huang, A.N., Y.Y. Zhang, K. Chen, K. Hatakeyama, and J.F. Keaney, *Cytokine-stimulated GTP cyclohydrolase I expression in endothelial cells requires coordinated activation of nuclear factor-kappa B and Stat1/Stat3.* Circulation Research, 2005. **96**(2): p. 164-171.
144. Shimizu, S., K. Shiota, S. Yamamoto, Y. Miyasaka, M. Ishii, T. Watabe, . . . Y. Kiuchi, *Hydrogen peroxide stimulates tetrahydrobiopterin synthesis through the induction of GTP-cyclohydrolase I and increases nitric oxide synthase activity in vascular endothelial cells.* Free Radic Biol Med, 2003. **34**(10): p. 1343-1352.
145. Hattori, Y., N. Nakanishi, K. Kasai, and S.I. Shimoda, *GTP cyclohydrolase I mRNA induction and tetrahydrobiopterin synthesis in human endothelial cells.* Biochim Biophys Acta, 1997. **1358**(1): p. 61-66.

146. Collaborators, C.T.T., *Efficacy and safety of cholesterol-lowering treatment: prospective meta-analysis of data from 90,056 participants in 14 randomised trials of statins.* The Lancet, 2005. **366**(9493): p. 1267-1278.
147. Cannon, C.P., E. Braunwald, C.H. McCabe, D.J. Rader, J.L. Rouleau, R. Belder, . . . I. Infection Therapy-Thrombolysis in Myocardial Infarction, *Intensive versus moderate lipid lowering with statins after acute coronary syndromes.* N Engl J Med, 2004. **350**(15): p. 1495-1504.
148. Ingall, T.J., W.M. O'Fallon, K. Asplund, L.R. Goldfrank, V.S. Hertzberg, T.A. Louis, and T.J. Christianson, *Findings from the reanalysis of the NINDS tissue plasminogen activator for acute ischemic stroke treatment trial.* Stroke, 2004. **35**(10): p. 2418-2424.
149. Kwiatkowski, T.G., R.B. Libman, M. Frankel, B.C. Tilley, L.B. Morgenstern, M. Lu, . . . T. Brott, *Effects of tissue plasminogen activator for acute ischemic stroke at one year. National Institute of Neurological Disorders and Stroke Recombinant Tissue Plasminogen Activator Stroke Study Group.* N Engl J Med, 1999. **340**(23): p. 1781-1787.
150. Wechsler, L.R., *Intravenous thrombolytic therapy for acute ischemic stroke.* N Engl J Med, 2011. **364**(22): p. 2138-2146.
151. Swarnkar, A.S., C.A. Jungreis, L.R. Wechsler, and J.J. Wehner, *Combined intravenous and intraarterial thrombolytic therapy for treatment of an acute ischemic stroke: a case report.* J Stroke Cerebrovasc Dis, 1999. **8**(4): p. 264-267.
152. Korin, N., M. Kanapathipillai, B.D. Matthews, M. Crescente, A. Brill, T. Mammoto, . . . D.E. Ingber, *Shear-activated nanotherapeutics for drug targeting to obstructed blood vessels.* Science, 2012. **337**(6095): p. 738-742.
153. Li, L., W. Chen, A. Rezvan, H. Jo, and D.G. Harrison, *Tetrahydrobiopterin deficiency and nitric oxide synthase uncoupling contribute to atherosclerosis induced by disturbed flow.* Arteriosclerosis, thrombosis, and vascular biology, 2011. **31**(7): p. 1547-1554.
154. Farokhzad, O.C. and R. Langer, *Impact of nanotechnology on drug delivery.* ACS Nano, 2009. **3**(1): p. 16-20.
155. Simone, E., B.S. Ding, and V. Muzykantov, *Targeted delivery of therapeutics to endothelium.* Cell Tissue Res, 2009. **335**(1): p. 283-300.
156. Bangham, A.D., M.M. Standish, and J.C. Watkins, *Diffusion of univalent ions across the lamellae of swollen phospholipids.* J Mol Biol, 1965. **13**(1): p. 238-252.
157. Chang, H.I. and M.K. Yeh, *Clinical development of liposome-based drugs: formulation, characterization, and therapeutic efficacy.* Int J Nanomedicine, 2012. **7**: p. 49-60.
158. Leserman, L.D., J. Barbet, F. Kourilsky, and J.N. Weinstein, *Targeting to cells of fluorescent liposomes covalently coupled with monoclonal antibody or protein A.* Nature, 1980. **288**(5791): p. 602-604.
159. Heath, T.D., R.T. Fraley, and D. Papahdjopoulos, *Antibody targeting of liposomes: cell specificity obtained by conjugation of F(ab')2 to vesicle surface.* Science, 1980. **210**(4469): p. 539-541.
160. Maeda, H., J. Wu, T. Sawa, Y. Matsumura, and K. Hori, *Tumor vascular permeability and the EPR effect in macromolecular therapeutics: a review.* J Control Release, 2000. **65**(1-2): p. 271-284.
161. Knop, K., R. Hoogenboom, D. Fischer, and U.S. Schubert, *Poly(ethylene glycol) in drug delivery: pros and cons as well as potential alternatives.* Angew Chem Int Ed Engl, 2010. **49**(36): p. 6288-6308.
162. Campbell, R.B., B. Ying, G.M. Kuesters, and R. Hemphill, *Fighting cancer: from the bench to bedside using second generation cationic liposomal therapeutics.* J Pharm Sci, 2009. **98**(2): p. 411-429.
163. Homem de Bittencourt, P.I., Jr., D.J. Lagranha, A. Maslinkiewicz, S.M. Senna, A.M. Tavares, L.P. Baldissera, . . . R. Curi, *LipoCardium: endothelium-directed cyclopentenone prostaglandin-based liposome formulation that completely reverses atherosclerotic lesions.* Atherosclerosis, 2007. **193**(2): p. 245-258.

164. Demos, S.M., H. Alkan-Onyuksel, B.J. Kane, K. Ramani, A. Nagaraj, R. Greene, . . . D.D. McPherson, *In vivo targeting of acoustically reflective liposomes for intravascular and transvascular ultrasonic enhancement.* J Am Coll Cardiol, 1999. **33**(3): p. 867-875.
165. Gupta, A.S., G. Huang, B.J. Lestini, S. Sagnella, K. Kottke-Marchant, and R.E. Marchant, *RGD-modified liposomes targeted to activated platelets as a potential vascular drug delivery system.* Thromb Haemost, 2005. **93**(1): p. 106-114.
166. Srinivasan, R., R.E. Marchant, and A.S. Gupta, *In vitro and in vivo platelet targeting by cyclic RGD-modified liposomes.* J Biomed Mater Res A, 2010. **93**(3): p. 1004-1015.
167. Nguyen, P.D., E.A. O'Rear, A.E. Johnson, E. Patterson, T.L. Whitsett, and R. Bhakta, *Accelerated thrombolysis and reperfusion in a canine model of myocardial infarction by liposomal encapsulation of streptokinase.* Circ Res, 1990. **66**(3): p. 875-878.
168. Heeremans, J.L., R. Prevost, M.E. Bekkers, P. Los, J.J. Emeis, C. Kluft, and D.J. Crommelin, *Thrombolytic treatment with tissue-type plasminogen activator (t-PA) containing liposomes in rabbits: a comparison with free t-PA.* Thromb Haemost, 1995. **73**(3): p. 488-494.
169. Zheng, J., J. Liu, M. Dunne, D.A. Jaffray, and C. Allen, *In vivo performance of a liposomal vascular contrast agent for CT and MR-based image guidance applications.* Pharm Res, 2007. **24**(6): p. 1193-1201.
170. Maiseyeu, A., G. Mihai, T. Kampfrath, O.P. Simonetti, C.K. Sen, S. Roy, . . . S. Parthasarathy, *Gadolinium-containing phosphatidylserine liposomes for molecular imaging of atherosclerosis.* J Lipid Res, 2009. **50**(11): p. 2157-2163.
171. Rensen, P.C., M.C. van Dijk, E.C. Havenaar, M.K. Bijsterbosch, J.K. Kruijt, and T.J. van Berkel, *Selective liver targeting of antivirals by recombinant chylomicrons--a new therapeutic approach to hepatitis B.* Nat Med, 1995. **1**(3): p. 221-225.
172. Mulder, W.J., K. Douma, G.A. Koning, M.A. van Zandvoort, E. Lutgens, M.J. Daemen, . . . G.J. Strijkers, *Liposome-enhanced MRI of neointimal lesions in the ApoE-KO mouse.* Magn Reson Med, 2006. **55**(5): p. 1170-1174.
173. Barenholz, Y., *Doxil(R)--the first FDA-approved nano-drug: lessons learned.* Journal of controlled release : official journal of the Controlled Release Society, 2012. **160**(2): p. 117-134.
174. Peters, D., M. Kastantin, V.R. Kotamraju, P.P. Karmali, K. Gujraty, M. Tirrell, and E. Ruoslahti, *Targeting atherosclerosis by using modular, multifunctional micelles.* Proceedings of the National Academy of Sciences of the United States of America, 2009. **106**(24): p. 9815-9819.
175. Srinivasan, R., R.E. Marchant, and A.S. Gupta, *In vitro and in vivo platelet targeting by cyclic RGD-modified liposomes.* Journal of biomedical materials research. Part A, 2010. **93**(3): p. 1004-1015.
176. Maiseyeu, A., G. Mihai, T. Kampfrath, O.P. Simonetti, C.K. Sen, S. Roy, . . . S. Parthasarathy, *Gadolinium-containing phosphatidylserine liposomes for molecular imaging of atherosclerosis.* Journal of lipid research, 2009. **50**(11): p. 2157-2163.
177. Cai, J.O., Z.F. Liu, F. Wang, and F. Li, *Phage Display Applications for Molecular Imaging.* Current Pharmaceutical Biotechnology, 2010. **11**(6): p. 603-609.
178. Kelly, K.A., M. Nahrendorf, A.M. Yu, F. Reynolds, and R. Weissleder, *In vivo phage display selection yields atherosclerotic plaque targeted peptides for imaging.* Molecular Imaging and Biology, 2006. **8**(4): p. 201-207.
179. Kelly, K.A., J.R. Allport, A. Tsourkas, V.R. Shinde-Patil, L. Josephson, and R. Weissleder, *Detection of vascular adhesion molecule-1 expression using a novel multimodal nanoparticle.* Circulation Research, 2005. **96**(3): p. 327-336.
180. Hamzah, J., V.R. Kotamraju, J.W. Seo, L. Agemy, V. Fogal, L.M. Mahakian, . . . E. Ruoslahti, *Specific penetration and accumulation of a homing peptide within atherosclerotic plaques of apolipoprotein E-deficient mice.* Proceedings of the National Academy of Sciences of the United States of America, 2011. **108**(17): p. 7154-7159.

181. Hallahan, D., L. Geng, S.M. Qu, C. Scarfone, T. Giorgio, E. Donnelly, . . . J. Clanton, *Integrin-mediated targeting of drug delivery to irradiated tumor blood vessels.* Cancer Cell, 2003. **3**(1): p. 63-74.
182. Ladner, R.C., A.K. Sato, J. Gorzelany, and M. de Souza, *Phage display-derived peptides as therapeutic alternatives to antibodies.* Drug Discov Today, 2004. **9**(12): p. 525-529.
183. Ellis, E.L. and M. Delbruck, *The Growth of Bacteriophage.* J Gen Physiol, 1939. **22**(3): p. 365-384.
184. Smith, G.P., *Filamentous fusion phage: novel expression vectors that display cloned antigens on the virion surface.* Science, 1985. **228**(4705): p. 1315-1317.
185. Sidhu, S.S., *Engineering M13 for phage display.* Biomol Eng, 2001. **18**(2): p. 57-63.
186. Sidhu, S.S., *Phage display in pharmaceutical biotechnology.* Curr Opin Biotechnol, 2000. **11**(6): p. 610-616.
187. Rodi, D.J. and L. Makowski, *Phage-display technology--finding a needle in a vast molecular haystack.* Curr Opin Biotechnol, 1999. **10**(1): p. 87-93.
188. Parmley, S.F. and G.P. Smith, *Antibody-selectable filamentous fd phage vectors: affinity purification of target genes.* Gene, 1988. **73**(2): p. 305-318.
189. Peters, E.A., P.J. Schatz, S.S. Johnson, and W.J. Dower, *Membrane insertion defects caused by positive charges in the early mature region of protein pIII of filamentous phage fd can be corrected by prlA suppressors.* J Bacteriol, 1994. **176**(14): p. 4296-4305.
190. Pasqualini, R. and E. Ruoslahti, *Organ targeting in vivo using phage display peptide libraries.* Nature, 1996. **380**(6572): p. 364-366.
191. Rajotte, D., W. Arap, M. Hagedorn, E. Koivunen, R. Pasqualini, and E. Ruoslahti, *Molecular heterogeneity of the vascular endothelium revealed by in vivo phage display.* Journal of Clinical Investigation, 1998. **102**(2): p. 430-437.
192. Pasqualini, R., B.J. Moeller, and W. Arap, *Leveraging Molecular Heterogeneity of the Vascular Endothelium for Targeted Drug Delivery and Imaging.* Seminars in Thrombosis and Hemostasis, 2010. **36**(3): p. 343-351.
193. Brown, K.C., *New approaches for cell-specific targeting: identification of cell-selective peptides from combinatorial libraries.* Current Opinion in Chemical Biology, 2000. **4**(1): p. 16-21.
194. Sergeeva, A., M.G. Kolonin, J.J. Molldrem, R. Pasqualini, and W. Arap, *Display technologies: Application for the discovery of drug and gene delivery agents.* Advanced Drug Delivery Reviews, 2006. **58**(15): p. 1622-1654.
195. Lee, G.Y., J.H. Kim, G.T. Oh, B.H. Lee, I.C. Kwon, and I.S. Kim, *Molecular targeting of atherosclerotic plaques by a stabilin-2-specific peptide ligand.* J Control Release, 2011. **155**(2): p. 211-217.
196. Thapa, N., H.Y. Hong, P. Sangeetha, I.S. Kim, J. Yoo, K. Rhee, . . . B.H. Lee, *Identification of a peptide ligand recognizing dysfunctional endothelial cells for targeting atherosclerosis.* J Control Release, 2008. **131**(1): p. 27-33.
197. Hong, H.Y., H.Y. Lee, W. Kwak, J. Yoo, M.H. Na, I.S. So, . . . B.H. Lee, *Phage display selection of peptides that home to atherosclerotic plaques: IL-4 receptor as a candidate target in atherosclerosis.* J Cell Mol Med, 2008. **12**(5B): p. 2003-2014.
198. Liu, C., G. Bhattacharjee, W. Boisvert, R. Dilley, and T. Edgington, *In vivo interrogation of the molecular display of atherosclerotic lesion surfaces.* Am J Pathol, 2003. **163**(5): p. 1859-1871.
199. Eshtehardi, P., M.C. McDaniel, J. Suo, S.S. Dhawan, L.H. Timmins, J.N. Binongo, . . . H. Samady, *Association of coronary wall shear stress with atherosclerotic plaque burden, composition, and distribution in patients with coronary artery disease.* J Am Heart Assoc, 2012. **1**(4): p. e002543.
200. Samady, H., P. Eshtehardi, M.C. McDaniel, J. Suo, S.S. Dhawan, C. Maynard, . . . D.P. Giddens, *Coronary artery wall shear stress is associated with progression and transformation of atherosclerotic plaque and arterial remodeling in patients with coronary artery disease.* Circulation, 2011. **124**(7): p. 779-788.

201. Trepel, M., W. Arap, and R. Pasqualini, *In vivo phage display and vascular heterogeneity: implications for targeted medicine.* Current Opinion in Chemical Biology, 2002. **6**(3): p. 399-404.
202. Arap, W., M.G. Kolonin, M. Trepel, J. Lahdenranta, M. Cardo-Vila, R.J. Giordano, . . . R. Pasqualini, *Steps toward mapping the human vasculature by phage display.* Nature Medicine, 2002. **8**(2): p. 121-127.
203. Ruoslahti, E., S.N. Bhatia, and M.J. Sailor, *Targeting of drugs and nanoparticles to tumors.* Journal of Cell Biology, 2010. **188**(6): p. 759-768.
204. Smith, G.P. and J.K. Scott, *Libraries of Peptides and Proteins Displayed on Filamentous Phage.* Methods in Enzymology, 1993. **217**: p. 228-257.
205. Doorbar, J. and G. Winter, *Isolation of a Peptide Antagonist to the Thrombin Receptor Using Phage Display.* Journal of Molecular Biology, 1994. **244**(4): p. 361-369.
206. Szardenings, M., S. Tornroth, F. Mutulis, R. Muceniece, K. Keinanen, A. Kuusinen, and J.E.S. Wikberg, *Phage display selection on whole cells yields a peptide specific for melanocortin receptor 1.* Journal of Biological Chemistry, 1997. **272**(44): p. 27943-27948.
207. Kelly, K.A., M. Nahrendorf, A.M. Yu, F. Reynolds, and R. Weissleder, *In vivo phage display selection yields atherosclerotic plaque targeted peptides for imaging.* Molecular imaging and biology : MIB : the official publication of the Academy of Molecular Imaging, 2006. **8**(4): p. 201-207.
208. Sanger, F., S. Nicklen, and A.R. Coulson, *DNA Sequencing with Chain-Terminating Inhibitors.* Proceedings of the National Academy of Sciences of the United States of America, 1977. **74**(12): p. 5463-5467.
209. Levesque, M.J. and R.M. Nerem, *The Elongation and Orientation of Cultured Endothelial-Cells in Response to Shear-Stress.* Journal of Biomechanical Engineering-Transactions of the Asme, 1985. **107**(4): p. 341-347.
210. Adey, N.B., A.H. Mataragnon, J.E. Rider, J.M. Carter, and B.K. Kay, *Characterization of phage that bind plastic from phage-displayed random peptide libraries.* Gene, 1995. **156**(1): p. 27-31.
211. Son, D.J., S. Kumar, W. Takabe, C.W. Kim, C.W. Ni, N. Alberts-Grill, . . . H. Jo, *The atypical mechanosensitive microRNA-712 derived from pre-ribosomal RNA induces endothelial inflammation and atherosclerosis.* Nature communications, 2013. **4**: p. 3000.
212. Bernatchez, P.N., L. Acevedo, C. Fernandez-Hernando, T. Murata, C. Chalouni, J. Kim, . . . W.C. Sessa, *Myoferlin regulates vascular endothelial growth factor receptor-2 stability and function.* Journal of Biological Chemistry, 2007. **282**(42): p. 30745-30753.
213. Bernatchez, P.N., A. Sharma, P. Kodaman, and W.C. Sessa, *Myoferlin is critical for endocytosis in endothelial cells.* American Journal of Physiology-Cell Physiology, 2009. **297**(3): p. C484-C492.
214. Sharma, A., C. Yu, C. Leung, A. Trane, M. Lau, S. Utokaparch, . . . P. Bernatchez, *A New Role for the Muscle Repair Protein Dysferlin in Endothelial Cell Adhesion and Angiogenesis.* Arteriosclerosis Thrombosis and Vascular Biology, 2010. **30**(11): p. 2196-U2397.
215. Chidlow, J.H., Jr. and W.C. Sessa, *Caveolae, caveolins, and cavins: complex control of cellular signalling and inflammation.* Cardiovascular research, 2010. **86**(2): p. 219-225.
216. Fernandez-Hernando, C., J. Yu, Y. Suarez, C. Rahner, A. Davalos, M.A. Lasuncion, and W.C. Sessa, *Genetic evidence supporting a critical role of endothelial caveolin-1 during the progression of atherosclerosis.* Cell metabolism, 2009. **10**(1): p. 48-54.
217. Conway, D.E., M.T. Breckenridge, E. Hinde, E. Gratton, C.S. Chen, and M.A. Schwartz, *Fluid shear stress on endothelial cells modulates mechanical tension across VE-cadherin and PECAM-1.* Curr Biol, 2013. **23**(11): p. 1024-1030.
218. Orr, A.W., J.M. Sanders, M. Bevard, E. Coleman, I.J. Sarembock, and M.A. Schwartz, *The subendothelial extracellular matrix modulates NF-kappaB activation by flow: a potential role in atherosclerosis.* J Cell Biol, 2005. **169**(1): p. 191-202.

219. Orr, A.W., M.H. Ginsberg, S.J. Shattil, H. Deckmyn, and M.A. Schwartz, *Matrix-specific suppression of integrin activation in shear stress signaling.* Mol Biol Cell, 2006. **17**(11): p. 4686-4697.
220. Modarres, H.P. and M.R. Mofradt, *Filamin: a structural and functional biomolecule with important roles in cell biology, signaling and mechanics.* Mol Cell Biomech, 2014. **11**(1): p. 39-65.
221. Schiller, C., K.N. Diakopoulos, I. Rohwedder, E. Kremmer, C. von Toerne, M. Ueffing, . . . E.H. Weiss, *LST1 promotes the assembly of a molecular machinery responsible for tunneling nanotube formation.* Journal of Cell Science, 2013. **126**(3): p. 767-777.
222. Stahlhut, M. and B. van Deurs, *Identification of filamin as a novel ligand for caveolin-1: Evidence for the organization of caveolin-1-associated membrane domains by the actin cytoskeleton.* Molecular Biology of the Cell, 2000. **11**(1): p. 325-337.
223. Bachmann, A.S., J.P. Howard, and C.W. Vogel, *Actin-binding protein filamin A is displayed on the surface of human neuroblastoma cells.* Cancer Science, 2006. **97**(12): p. 1359-1365.
224. Sykes, M.C., *Regulation of endothelial gene transcription by shear stress in a manner dependent on p47phox-based NADPH oxidases*, in *Biomedical Engineering*2008, Georgia Institute of Technology: Available from ProQuest Dissertations & Theses Full Text; ProQuest Dissertations & Theses Global.
225. Glogauer, M., P. Arora, D. Chou, P.A. Janmey, G.P. Downey, and C.A. McCulloch, *The role of actin-binding protein 280 in integrin-dependent mechanoprotection.* J Biol Chem, 1998. **273**(3): p. 1689-1698.
226. Byfield, F.J., Q. Wen, I. Levental, K. Nordstrom, P.E. Arratia, R.T. Miller, and P.A. Janmey, *Absence of filamin A prevents cells from responding to stiffness gradients on gels coated with collagen but not fibronectin.* Biophys J, 2009. **96**(12): p. 5095-5102.
227. Psarros, C., R. Lee, M. Margaritis, and C. Antoniades, *Nanomedicine for the prevention, treatment and imaging of atherosclerosis.* Nanomedicine : nanotechnology, biology, and medicine, 2012. **8 Suppl 1**: p. S59-68.
228. Babincova, M., D. Leszczynska, P. Sourivong, and P. Babinec, *Selective treatment of neoplastic cells using ferritin-mediated electromagnetic hyperthermia.* Medical hypotheses, 2000. **54**(2): p. 177-179.
229. Decuzzi, P., R. Pasqualini, W. Arap, and M. Ferrari, *Intravascular Delivery of Particulate Systems: Does Geometry Really Matter?* Pharmaceutical Research, 2009. **26**(1): p. 235-243.
230. Decuzzi, P., F. Gentile, C. Chiappini, D. Fine, R.C. Bhavane, M.S. Peluccio, . . . M. Ferrari, *The effect of shape on the margination dynamics of non-neutrally buoyant particles in two-dimensional shear flows.* Journal of Biomechanics, 2008. **41**(10): p. 2312-2318.
231. Decuzzi, P. and M. Ferrari, *Design maps for nanoparticles targeting the diseased microvasculature.* Biomaterials, 2008. **29**(3): p. 377-384.
232. Schlachter, E.K., H.R. Widmer, A. Bregy, T. Lonnfors-Weitzel, I. Vajtai, N. Corazza, . . . M. Reinert, *Metabolic pathway and distribution of superparamagnetic iron oxide nanoparticles: in vivo study.* International journal of nanomedicine, 2011. **6**: p. 1793-1800.
233. Weissleder, R., D.D. Stark, B.L. Engelstad, B.R. Bacon, C.C. Compton, D.L. White, . . . J. Lewis, *Superparamagnetic iron oxide: pharmacokinetics and toxicity.* AJR. American journal of roentgenology, 1989. **152**(1): p. 167-173.
234. Weinmann, H.J., W. Ebert, B. Misselwitz, and H. Schmitt-Willich, *Tissue-specific MR contrast agents.* European journal of radiology, 2003. **46**(1): p. 33-44.
235. Gore, J.C., T.E. Yankeelov, T.E. Peterson, and M.J. Avison, *Molecular Imaging Without Radiopharmaceuticals?* Journal of Nuclear Medicine, 2009. **50**(6): p. 999-1007.
236. Yu, S.S., R.L. Scherer, R.A. Ortega, C.S. Bell, C.P. O'Neil, J.A. Hubbell, and T.D. Giorgio, *Enzymatic- and temperature-sensitive controlled release of ultrasmall superparamagnetic iron oxides (USPIOs).* Journal of nanobiotechnology, 2011. **9**: p. 7.

237. Duvall, C.L., A.J. Convertine, D.S. Benoit, A.S. Hoffman, and P.S. Stayton, *Intracellular delivery of a proapoptotic peptide via conjugation to a RAFT synthesized endosomolytic polymer.* Mol Pharm, 2010. **7**(2): p. 468-476.
238. Convertine, A.J., D.S.W. Benoit, C.L. Duvall, A.S. Hoffman, and P.S. Stayton, *Development of a novel endosomolytic diblock copolymer for siRNA delivery* J Control Release. 2009; 133(3):221-229.
239. Schiener, M., M. Hossann, J.R. Viola, A. Ortega-Gomez, C. Weber, K. Lauber, . . . O. Soehnlein, *Nanomedicine-based strategies for treatment of atherosclerosis.* Trends in molecular medicine, 2014. **20**(5): p. 271-281.
240. Gupta, A.S., *Nanomedicine approaches in vascular disease: a review.* Nanomedicine : nanotechnology, biology, and medicine, 2011. **7**(6): p. 763-779.
241. Eraso, L.H., M.P. Reilly, C. Sehgal, and E.R. Mohler, 3rd, *Emerging diagnostic and therapeutic molecular imaging applications in vascular disease.* Vascular medicine, 2011. **16**(2): p. 145-156.
242. Jaffer, F.A., P. Libby, and R. Weissleder, *Optical and multimodality molecular imaging: insights into atherosclerosis.* Arteriosclerosis, thrombosis, and vascular biology, 2009. **29**(7): p. 1017-1024.
243. Yu SS, L.C., Thomas SN, Jerome WG, Maron DJ, Dickerson JH, Hubbell JA, Giorgio TD, *Size- and Charge- Dependent Non-Specific Uptake of PEGylated Nanoparticles by Macrophages.* International Journal of Nanomedicine, 2012.
244. Nelson, C.E., J.R. Kintzing, A. Hanna, J.M. Shannon, M.K. Gupta, and C.L. Duvall, *Balancing cationic and hydrophobic content of PEGylated siRNA polyplexes enhances endosome escape, stability, blood circulation time, and bioactivity in vivo.* ACS nano, 2013. **7**(10): p. 8870-8880.
245. Passman, J.N., X.R. Dong, S.P. Wu, C.T. Maguire, K.A. Hogan, V.L. Bautch, and M.W. Majesky, *A sonic hedgehog signaling domain in the arterial adventitia supports resident Sca1+ smooth muscle progenitor cells.* Proceedings of the National Academy of Sciences of the United States of America, 2008. **105**(27): p. 9349-9354.
246. Albanese, A., P.S. Tang, and W.C. Chan, *The effect of nanoparticle size, shape, and surface chemistry on biological systems.* Annual review of biomedical engineering, 2012. **14**: p. 1-16.
247. Yu, S.S., R.A. Ortega, B.W. Reagan, J.A. McPherson, H.J. Sung, and T.D. Giorgio, *Emerging applications of nanotechnology for the diagnosis and management of vulnerable atherosclerotic plaques.* Wiley interdisciplinary reviews. Nanomedicine and nanobiotechnology, 2011.
248. Sykes, E.A., J. Chen, G. Zheng, and W.C.W. Chan, *Investigating the Impact of Nanoparticle Size on Active and Passive Tumor Targeting Efficiency.* ACS nano, 2014. **8**(6): p. 5696-5706.
249. Gabizon, A. and D. Papahadjopoulos, *Liposome Formulations with Prolonged Circulation Time in Blood and Enhanced Uptake by Tumors.* Proceedings of the National Academy of Sciences of the United States of America, 1988. **85**(18): p. 6949-6953.
250. Lanio, M.E., M.C. Luzardo, C. Alvarez, Y. Martinez, L. Calderon, M.E. Alonso, . . . A. Disalvo, *Humoral immune response against epidermal growth factor encapsulated in dehydration rehydration vesicles of different phospholipid composition.* J Liposome Res, 2008. **18**(1): p. 1-19.
251. Fukushima, T. and J.C. Nixon, *Analysis of reduced forms of biopterin in biological tissues and fluids.* Anal Biochem, 1980. **102**(1): p. 176-188.
252. Fink, B., K. Laude, L. McCann, A. Doughan, D.G. Harrison, and S. Dikalov, *Detection of intracellular superoxide formation in endothelial cells and intact tissues using dihydroethidium and an HPLC-based assay.* Am J Physiol Cell Physiol, 2004. **287**(4): p. C895-902.
253. Plump, A.S., J.D. Smith, T. Hayek, K. Aaltosetala, A. Walsh, J.G. Verstuyft, . . . J.L. Breslow, *Severe Hypercholesterolemia and Atherosclerosis in Apolipoprotein-E-Deficient Mice Created by Homologous Recombination in Es Cells.* Cell, 1992. **71**(2): p. 343-353.
254. McCormack, B. and G. Gregoriadis, *Entrapment of cyclodextrin-drug complexes into liposomes: potential advantages in drug delivery.* J Drug Target, 1994. **2**(5): p. 449-454.
255. Gregoriadis, G., *Drug entrapment in liposomes.* FEBS Lett, 1973. **36**(3): p. 292-296.

256. Piedrahita, J.A., S.H. Zhang, J.R. Hagaman, P.M. Oliver, and N. Maeda, *Generation of Mice Carrying a Mutant Apolipoprotein-E Gene Inactivated by Gene Targeting in Embryonic Stem-Cells.* Proceedings of the National Academy of Sciences of the United States of America, 1992. **89**(10): p. 4471-4475.
257. Hopkins, A.L. and C.R. Groom, *The druggable genome.* Nat Rev Drug Discov, 2002. **1**(9): p. 727-730.
258. Curtis, M.J., *Emerging druggable targets for cardiovascular disease.* Curr Opin Pharmacol, 2009. **9**(2): p. 81-83.
259. Miller, E.R., L.J. Appel, E. Guallar, and R. Pastor-Barriuso, *High-dosage vitamin E supplementation and all-cause mortality - Response.* Annals of Internal Medicine, 2005. **143**(2): p. 156-158.
260. Miller, E.R., R. Pastor-Barriuso, D. Dalal, R.A. Riemersma, L.J. Appel, and E. Guallar, *Meta-analysis: High-dosage vitamin E supplementation may increase all-cause mortality.* Annals of Internal Medicine, 2005. **142**(1): p. 37-46.
261. Milman, U., S. Blum, C. Shapira, D. Aronson, R. Miller-Lotan, Y. Anbinder, . . . A.P. Levy, *Vitamin e supplementation reduces cardiovascular events in a subgroup of middle-aged individuals with both type 2 diabetes mellitus and the haptoglobin 2-2 genotype - A prospective double-blinded clinical trial.* Arteriosclerosis Thrombosis and Vascular Biology, 2008. **28**(2): p. 341-347.
262. Li, H., C.E. Nelson, B.C. Evans, and C.L. Duvall, *Delivery of intracellular-acting biologics in pro-apoptotic therapies.* Curr Pharm Des, 2011. **17**(3): p. 293-319.
263. Foster, S., C.L. Duvall, E.F. Crownover, A.S. Hoffman, and P.S. Stayton, *Intracellular delivery of a protein antigen with an endosomal-releasing polymer enhances CD8 T-cell production and prophylactic vaccine efficacy.* Bioconjug Chem, 2010. **21**(12): p. 2205-2212.
264. Vickers, K.C., B.T. Palmisano, B.M. Shoucri, R.D. Shamburek, and A.T. Remaley, *MicroRNAs are transported in plasma and delivered to recipient cells by high-density lipoproteins.* Nat Cell Biol, 2011. **13**(4): p. 423-433.
265. Caravan, P., J.J. Ellison, T.J. McMurry, and R.B. Lauffer, *Gadolinium(III) Chelates as MRI Contrast Agents: Structure, Dynamics, and Applications.* Chem Rev, 1999. **99**(9): p. 2293-2352.
266. Mulder, W.J., G.J. Strijkers, G.A. van Tilborg, A.W. Griffioen, and K. Nicolay, *Lipid-based nanoparticles for contrast-enhanced MRI and molecular imaging.* NMR Biomed, 2006. **19**(1): p. 142-164.
267. Lindner, J.R., J. Song, J. Christiansen, A.L. Klibanov, F. Xu, and K. Ley, *Ultrasound assessment of inflammation and renal tissue injury with microbubbles targeted to P-selectin.* Circulation, 2001. **104**(17): p. 2107-2112.
268. Duivenvoorden, R., J. Tang, D.P. Cormode, A.J. Mieszawska, D. Izquierdo-Garcia, C. Ozcan, . . . W.J. Mulder, *A statin-loaded reconstituted high-density lipoprotein nanoparticle inhibits atherosclerotic plaque inflammation.* Nat Commun, 2014. **5**: p. 3065.
269. Kim, Y., F. Fay, D.P. Cormode, B.L. Sanchez-Gaytan, J. Tang, E.J. Hennessy, . . . Z.A. Fayad, *Single step reconstitution of multifunctional high-density lipoprotein-derived nanomaterials using microfluidics.* ACS Nano, 2013. **7**(11): p. 9975-9983.
270. Rui, M., W. Guo, Q. Ding, X. Wei, J. Xu, and Y. Xu, *Recombinant high-density lipoprotein nanoparticles containing gadolinium-labeled cholesterol for morphologic and functional magnetic resonance imaging of the liver.* Int J Nanomedicine, 2012. **7**: p. 3751-3768.
271. von Eckardstein, A. and G. Assmann, *Clinical implications of elevated lipoprotein(a).* Curr Atheroscler Rep, 2001. **3**(4): p. 267-270.